Dipole moment determination of large chromophores in solution

Inaugural-Dissertation

for the attainment of the title of doctor
in the Faculty of Mathematics and Natural Sciences
at the Heinrich-Heine-University Düsseldorf

presented by

Mirko Matthias Lindic

from Langenfeld

Düsseldorf, August 2021

from the Institute for Physical Chemistry 1
at the Heinrich-Heine-University Düsseldorf

Printed by permission of the
Faculty of Mathematics and Natural sciences at
Heinrich-Heine-University Düsseldorf

Supervisor: Prof. Dr. Michael Schmitt

Co-Supervisor: Prof. Dr. Peter Gilch

Date of the oral examination: 07.12.2021

Contents

Declaration of Authorship

I declare under oath that I have produced my thesis independently and without any undue assistance by third parties under consideration of the ‚Principles for the Safeguarding of Good Scientific Practice‘ at Heinrich Heine University Düsseldorf. All direct or indirect sources used are acknowledged as references.

The presented dissertation has not been submitted in this or in a similar form to any other institution. No prior unsuccessful attempts have taken place so far.

Mirko Matthias Lindic

Düsseldorf, December 13, 2021

Acknowledgements

First of all, I want to thank my supervisor Michael Schmitt for his ongoing support through all steps of my academic process. The continuous and outraging effort he takes to give all his students the best possible foundation for a stress-free and positive working and learning climate is far beyond the limits of what is to be expected from a supervisor in science. There is no way I could feel more gratitude for all the opportunities I enjoyed during my time under his supervision. He gave me the chance to travel to Mexico and learn the way of scientific work at the other end of the world at the beginning of my Ph.D time and now in the end I had the possibility to arrange a good balance between work and family life even in times of the COVID-19 pandemic without high pressure. I hope a lot of future students will be able to profit from this wonderful teacher and his commitment for scientific innovation, people who want to learn and last but not least the climate and social equality.

Also I want to thank Prof. Dr. Peter Gilch, who agreed to review my thesis as second supervisor.

My colleagues in the group of Michael Schmitt and also the others of the institute for physical chemistry 1 have been like a second family for me in the last few years. I have to thank you all for nice teamwork, productive inspirational conversations and excellent parties through all of the years.

To the people which were mandatory for the success of my research: Sonja Schiller and Corell Spöringer from the workshop of chemistry and pharmaceutics who built the heart of the spectrometer and helped with many aspects in planning and construction and were always present to help with small repairs and support, thank you very much. Klaus Kelbert for the help with every electrical issue I had to solve and devices I had to built, thank you very much. Andrea Lotzwick for help with all issues in administration and financial issues, as well as many interesting conversations during coffee brakes, thank you very much. And Martin Kleinschmidt for several advices in theoretical chemistry and calculations, thank you very much. Big thanks also to Annabel Lohmeyer for proofreading this work.

No long academic work is done without the supports of good friends. I want to thank my three best buddies who all go the same way with me and gave support to me and to each other, no matter if with scientific advice and conversations or a nice evening with soulfood and too much whisky while discussing the matter of life, thank you Bernd Günter Kosper, Peter Brüggemann and Angelo Altavilla, the chaotic quartett for just being what you are. Besides of this, there can be generated some friends by sharing days in the office and in the laboratory, spending time with observing measurements and discussing or just listening to musik all day long, big thanks to Carolin Borbeck, Tim Oberkirch, Rami Kalfouni and the wonderful and glorious ginger, my favourite biologist and one of the best friends I gained in the last years, Patricia Blum.

Behind every student there should stand a supporting and loving family who can carry at least some of the weight, may it be financially, emotional or in other aspects. I am one very lucky guy to have exactly this type of family behind me and can profit from their love. Thanks to my mother Doris, my father Georg, my sister Sonja and her partner Tobias. Thanks to my grandmother Wanda, my aunt and genetically second mother Petra and her partner Rainer and all the other aunts and uncles, cousins and their families.

In the end I have to mention the persons, who changed my life in the last two years. It was kind of unexpected but still developed with insane celerity and now where I am about to finish my academic education there is a woman in my life which I can call my loving wife with two wonderful daughters who accept me better than I could have ever wished and additionally I can look forward to my unborn child which will see the light of day approximately in November of 2021. Thanks for your love, Michaela, Cecilia, Melina and our little sweet fortune cookie. I love you more than the world.

Abstract

The behaviour of fluorescent organic substances in solution is of increasing scientific interest in the fields of biological, chemical as well as interdisciplinary research. In some areas, technical applications have already grown out of research. As an example, results from solution measurements are used to develop dyes for the application in organic light emitting diodes (OLED). Molecular dyes polarity in all involved electronic states is an important aspect in the knowledge of interactions between the dye and solvent. The polarity is represented by the molecular electric dipole moment. Since the beginning or rather the middle of the 20^{th} century, dipole moments in the electronic ground and lowest excited states have been investigated intensely by many scientists. This thesis mainly touches the experimental determination of the first excited singlet states dipole moment of molecules in solution via thermochromic UV/Vis absorption and fluorescence spectroscopy and gives a critical analysis of the limitations of the method.

Known methods in this field are based on solvatochromic spectroscopic measurements in different solvents to analyse the behaviour of a molecular dye in a varying dielectric surrounding [1–3]. The major deficiencies of this initial approach are, on the one hand, the underestimation of the number of properties which change with substitution of the solvent and on the other hand, the utilisation of the so called Onsager radius [4], which is an estimation of the volume occupied solely by the dissolved molecule without present solvent. This approximation defines one fix radius depending only on the dye molecule, which is used as constant parameter in the evaluation. Ongoing research in this field has led to the idea of changing the temperature instead of the solvent [5, 6] which drastically reduces the approximations made for the solvent-solute interactions. Independently, the concept of a universal Onsager radius was challenged by experimental determination of the molecular cavity volume [7] which gives the opportunity of determining the exact cavity volume for each solvent and temperature. The fusion of both innovative ideas is the basis of the thermochromic method, presented in this work. Studies with smaller building blocks like anisole, 1-methylindole and 2,3-benzofuran were performed to examine the validity of the method and for supporting investigations in other areas. The molecules were mainly chosen

for their ability to be evaporated into a vacuum which grants the possibility of electronic Stark measurements for the accurate determination of excited state dipole moments [8]. Finally, a large bichromophoric dye molecule composed of a disubstituted quinoxaline has been investigated. Through comparisons with reference methods in the gas phase and quantum chemical calculations, the benefit of the method has been proven. This knowledge can be useful for research upon complex systems which are of present scientific interest.

Nevertheless, the results of the presented studies show the limitation of the applicability of solution methods for the dipole moment determination in solution. Indications have found that the behaviour of polar molecules in solution is far more complex and uncharted than assumed in most methods. After interpretation of the results compared with theoretical studies it becomes clear that without comparison of one or more valid reference methods, no result of an experiment in the basic method of solvatochromic and thermochromic UV/Vis absorption and fluorescence spectroscopy can be taken for granted. It can not be clearly said only from solution methods to which state the observed dipole moment belongs as the tremendous impact of the reaction field of the solvent can mix state properties.

Übersicht

Das Verhalten fluoreszierender organischer Substanzen in Lösung gewinnt immer mehr wissenschaftliches Interesse seitens der biologischen, chemischen sowie interdisziplinärer Forschung. In einigen Bereichen ist hierbei schon technische Anwendung aus der Forschung erwachsen, als Beispiel seien an dieser Stelle organische Licht emittierende Dioden genannt, sogenannte OLEDs. Ein wichtiger Aspekt zur Kenntnis der Wechselwirkungen zwischen einem Farbstoff und dem Lösemittel, welches ihn umgibt, ist die Polarität des betrachteten Farbstoffmoleküls in allen am Prozess beteiligten elektronischen Zuständen, repräsentiert durch das molekulare elektrische Dipolmoment. Die Bestimmung der Dipolmomente des elektronischen Grundzustands und ersten elektronisch angeregten Singulettzustands werden seit dem Anfang bzw. Mitte des 20. Jahrhunderts von vielen Wissenschaftlern intensiv erforscht. Diese Arbeit befasst sich hauptsächlich mit der Bestimmung des ersten elektronisch angeregten Singulettzustands in Lösung durch thermochrome UV/Vis Absorptions- und Fluoreszenzspektroskopie, woraus ein kritisches Gutachten über die Grenzen der Methodik resultiert. Bekannte Methoden auf diesem Gebiet basieren auf solvatochromer Spektroskopie in verschiedenen Lösungsmitteln zur Untersuchung des Verhaltens von Farbstoffmolekülen in wechselnder dielektrischer Umgebung [1–3]. Die größten Schwächen dieses ursprünglichen Ansatzes liegen einerseits darin, dass die Zahl der Eigenschaften, welche sich durch ein Austauschen des Lösungsmittels ändern, drastisch unterschätzt wird. Andererseits birgt die Nutzung des sogenannten Onsagerradius [4], welcher den ausschließlich vom gelösten Molekül eingenommenen Raum in einer Lösung beschreibt, den Fehler, einen allgemeingültigen Radius für ein Farbstoffmolekül zu bestimmen, welcher in jeder Umgebung identisch sein soll. Anhaltende Studien in diesen Bereichen zeigen führten zur Erkenntnis, dass die Änderung der Temperatur anstatt des Lösungsmittel die Zahl der Näherungen zur Solvens-Solvat Wechselwirkung und damit die Fehler in der Auswertung drastisch reduziert [5, 6]. Unabhängig davon wurde das Konzept eines allgemeingültigen Onsagerradius in Frage gestellt und als Gegenvorschlag die experimentelle Bestimmung des Kavitätsvolumen eines Moleküls in Lösung eingebracht [7], was die Bestimmung eines individuellen Radius in jedem Lösungsmittel und bei jeder Temperatur erlaubt. Die Zusammenführung der beiden genannten

innovativen Ansätze bildet das Fundament für diein dieser Arbeit präsentierte thermochrome Methode. Zum Test der Methode sowie unterstützender Forschung in anderen Bereichen wurden Studien an kleineren Bausteinen wie Anisol, 1-Methylindol sowie 2,3-Benzofuran durchgeführt sowie ein großes Farbstoffmolekül auf Basis eines zweifach substituierten Chinoxalins untersucht. Diese Stoffe wurden hauptsächlich deshalb ausgewählt, weil sie in ein Vakuum vaporisiert werden können, was die exakte Bestimmung des Dipolmoments im angeregten Zustand mittels elektronischer Stark Spektroskopie erlaubt [8]. In vielerlei Hinsicht wurden bei diesen Studien die Vorteile der entwickelten Methode durch direkte Vergleiche mit Referenzmethoden aus der Gasphase sowie quantenchemischen Rechnungen bestätigt, was in weiteren Forschungen zu Erkenntnis über komplexe Systeme des aktuellen wissenschaftlichen Interesses von Nutzen ist. Ebenso zeigten jedoch einige Ergebnisse die Grenzen der Anwendbarkeit von Methoden zur Dipolmomentsbestimmung in Lösung auf, da Hinweise darauf zu finden sind, dass das Verhalten polarer Moleküle in Lösung durchaus vielschichtiger und unerforschter ist, als in den meisten Modellen angenommen. Durch die Interpretation der Ergebnisse mit dem Vergleich theoretischer Studien, die zu diesem Zwecke angestellt wurden, wird klar, dass ohne den Vergleich zu einer oder mehrerer valider Methoden bei keinem Ergebnis eines Experiments in der Grundmethodik der solvatochromen und thermochromen UV/Vis Absorptions- und Fluoreszenzspektroskopie sicher sein kann, zu welchem angeregten Zustand das gemessene Dipolmoment gehört, da der starke Einfluss des Lösemittel-Reaktionsfelds die Eigenschaften nahegelegener Zustände vermischen kann.

Part I.

Introduction

1. Introduction and Motivation

Natural sciences aim to describe the phenomena which can be observed in the universe and generally are classified into five main branches

- Physics
- Chemistry
- Biology
- Astronomy
- Geology.

The tools and language used to translate the phenomena of nature into mentally conceivable explanations is the science of mathematics. For its connective role between natural sciences and humanities, mathematics cannot be considered in any way inferior to any of the general fields.

This thesis is concerned with the thermally dependent UV/Vis absorption and emission spectra of dye molecules in a solution of liquid state. It can be categorized as being both in the fields of physics and chemistry, because molecules are investigated by using physical methods and the tools of mathematics, in order to gain information about them which then determines parts of their chemical behaviour. As the main focus of interest lies on information regarding chemical behaviour, the scientific field is called physical chemistry.

Thermochromic absorption and fluorescence spectroscopy is initially used to determine the difference of the dipole moments between the first electronically excited singlet state and the electronic ground state. Here, as shown in Chapter 3, electronic spectroscopy is performed dependent on the solution's temperature. By this, the primary dielectric influence of the solvent on transition energies of the molecular dye is measured quantitatively. Taking into account the polarity parameters of the solvent-solute system on the ground state dipole moment, an evaluation of the spectral data yields the magnitude of the excited state dipole

moment. Resulting from this evaluation, the comparison to gas phase experiments and quantum chemical results, conclusions can be made regarding the influence of the polar ambience on the behaviour of excited states.

Knowledge about the difference between excited state and ground state dipole moments is of great interest for several branches in chemical and physicochemical investigation both for basic science and applications. The significance of dipole moment determination and investigations of the influence of the ambient medium for [**F**luorescence or **F**örster] **R**esonance **E**nergy **T**ransfer ([F]RET) falls primarily into the area of basic science. RET describes the transfer of (excitation) energy between separated molecules over a range without the emission of visible light. The physical distance where RET can occur lies in the range of protein sequences or, for example, biological membrane sizes [9]. As the rate of energy transfer is dependent on the range which is specific for a donor-acceptor pair, it can be used to determine distances in the chosen biological system such as proteins. The application of the RET process ranges from artificial light harvesting to biomedical sensing, quantum computation, fluorescence microscopy and nano-emitters [9, 10]. While RET-based biosensors are used to investigate cells, their behaviour and interactions, scientists try to construct the ideal artificial light harvesting device by imitating the photosynthesis in plants, where natural RET is used to guide the energy from the light antenna to the reactive centre with an efficiency near $100\,\%$. RET can be observed by including two chromophores in one sample, while the fluorescence emission of one chromophore overlaps with the absorption of the other one. The specific observation is that if both chromophores are present, excitation of the one with higher absorption frequency leads to the detection of the emission spectrum of the chromophore with the energetically lower first excited singlet state. Concluding from this observation, the mechanism of RET was found to include a chromophore in the first excited singlet state (donor) and one in the electronic ground state (acceptor) which interact with each other through a long range dipole-dipole interaction of the transition dipole moments known as Coulomb coupling [10]. For further investigation and understanding of the RET mechanism, leading to a wider range of applications and more accurate manipulation, a detailed knowledge about the involved dipole moments of donor and acceptor moieties is of inherent importance. Of special interest is the influence of polar ambience on the donor and acceptor dipole moments and the effect on RET rate and efficiency.

Another field where accurate determination of excited state dipole moments in solution is part of every discussion is the investigation on molecules which can perform **T**hermally **A**ctivated **D**elayed **F**luorescence (TADF) which is also seen in combination with the formation of **I**ntramolecular **C**harge **T**ransfer (ICT) states [11, 12]. The construction of molecules in the

focus of TADF investigation is based on the spatial separation of an electron-donating (D) and an electron accepting (A) moiety which interact with each other by forming an ICT state after electronic excitation. An ICT state can either be directly adressed with excitation, which is preferred for TADF, or occur after the electronic excitation of a molecule with D and A moieties to the locally excited state (LE) and is formed by the transfer of electron density between the mentioned subunits. The electron density transfer creates a state with a larger dipole moment which can be stabilized further in a polar ambience resulting in a reduction of the excited state's energy. It could be shown that in organic molecules both the LE and the ICT states can show fluorescence, while the identification of the emission bands is indicated by the relative position of the local maxima. The longer wavelength maximum is said to belong to the ICT state because it should be stabilized further when using a polar solvent[13]. Molecules of this type also can show nonlinear optical (NLO) properties [12]. Substances which can form ICT states and perform TADF are of high interest in different fields of basic research and technical applications, e.g. OFET (Organic field-effect transistors), OLED (Organic light emitting diodes), NLO materials, biological sensing, single molecule spectroscopy, cell imaging, laser dyes, biomarkers, solar cells and artificial photosynthesis [11, 12, 14–16]. Thermally activated delayed fluorescence is a process which can occur in molecules with a remarkably small energy gap between the lowest triplet state and the first excited singlet state. Through the small energy gap, thermal energy is sufficient to engage the triplet state's energy to a suitable level for the enabling of intersystem crossing (ISC) to the fluorescing singlet state [17]. The possibility to convert triplet states into fluorescing singlet states by the simple use of thermal energy is of greatest interest for usage in commercial high-performance OLEDs. In OLED devices, the molecules are excited via an electrical current enabling all transitions including only one electron. Statistically, all four different excited states have the same probability while three of them belong to a degenerated set of states forming a triplet. The result is that in the first place, a maximum $25\,\%$ of the energy input can be emitted as fluorescent light. The usage of molecules which can perform TADF opens the door to a theoretical efficiency of $100\,\%$ in OLED devices. To achieve this performance, chemists try to design molecules which fulfil the criteria of a small energy gap between low lying singlet and triplet states as well as a good ISC rate constant lacking heavy elements and additionally a high quantum yield for the fluorescence process. These characteristics are hardly ever found in combination. The knowledge about the excited singlet state dipole moment and its interactions with the ambience is crucial for further investigation and deeper understanding of the processes and properties of ICT states and the TADF process. Detailed knowledge about the influence of a polar surrounding on the excited states of a molecule is of high interest especially because in most applications the ambience of a molecular dye will be of a polar

nature.

Regarding the effects a molecule in an excited state can undergo with polar solvents there have been some results on this for indole in the past [18, 19]. One observation of these studies has been an apparent inversion of the excited state order.

In a non-polar solvent, emission from the ^1L_b state can be observed while emission from the ^1L_a state can be seen with increasing solvent polarity. The same effect on a smaller scale can be seen in the absorption spectra [20–22]. Chapter 12 and 13 of this work will go into detail regarding the effect of a polar solvent on the excited states of indole-type molecules. The results of these studies support the theory of excited states mixing with each other under a high electric field perturbation, leading to an alteration of excited state order between an isolated molecule and a molecule in a polar solvent environment where the more polar state is stabilized [23]. This finding and methods to investigate its outcomes can have tremendous impact on all of the above mentioned fields. Generally, all applications and investigations where polar fluorescence dyes are used in a mainly polar ambience can profit from new perceptions about excited state behaviour. As an example, for its natural appearance in tryptophane as a building block for proteins, indole is often used for FRET studies and other techniques, but indole especially shows a strong excited state reaction to polar influences which have an impact on the models used to describe the observations. The models are then used to design predictions for other experiments, where the knowledge about the reaction to polar influences could be crucial. Organic chemists try to develop new fluorescent dye molecules which satisfy the demands for TADF emitters in OLEDs and to do this, theoretical studies are performed in an attempt to predict the behaviour of chromophores in their technical application. Every piece of knowledge about the emitters and their behaviour in the ambience of the technical application, including detailed information about the excited state behaviour in polar solutions, is a step forward for precise models and successful development in this area of chemistry.

As mentioned at the beginning, the method of determining the dipole moments of electronically excited singlet states in solution via thermochromic UV/Vis absorption and fluorescence spectroscopy combined with *ab initio* methods ranges between the scientific fields of chemistry and physics. But a closer view of the applications both for scientific and commercial purposes has shown that the range of impact the method has also includes other fields of science. Results from this method can have an important influence at least in biological investigations. Finally moving on to commercial interest, the development of new technology in electronic devices like OLED screens is directly linked to information about excited state behaviour and polarity.

2. Historical Context

In the year 1913, the shifting and splitting of rotational and rovibrational lines in the spectra of molecules which are interacting with an external electric field was discovered independently by J. Stark [24] and A. Lo Surdo [25]. The direct relation between an external electric field and the molecule's dipole moments allows an accurate determination of the latter via gas phase rotational spectroscopy in a defined electric field. With modern high resolution methods, an electric field can be applied to high resolution laser induced fluorescence spectroscopy which gives access to the excited state dipole moment. By dissolving a molecule into a polar solvent, an electric field is created by the arrangement of the solvent molecules around the solute. Consequently, the Stark effect of this reaction field can be used for the determination of excited state dipole moments in solution.

The method of determining electronically excited state dipole moments of dye molecules in solution using the manipulation of the dielectrical parameters of the solvent has a history which dates back to the 1950s. Starting from a perturbation theory second order calculation by Ooshika in 1954, [26] describing the mathematical background for absorption spectra of dyes in solution, Lippert and Mataga both enhanced this theory for fluorescence spectra.[1, 2] By combining both calculations they derived a method to calculate the dipole moment of a dye molecule in its fluorescing excited state from spectral measurements of the dyes absorption and fluorescence in different solvents.

This so-called solvatochromic method uses the observable effect that the position of spectral curves of molecules in absorption and fluorescence spectroscopy are dependent on the used solvent. When a polar molecule enters a polar solvent, the vectorial dipole moments of the solvent molecules will rearrange themselves along the vectorial dipole moment of the solute. This rearrangement creates an electric field that stabilizes the solute depending on its dipole moment. For most molecules, the dipole moment of the first electronically excited state has a higher magnitude than in the ground state leading to a better stabilization in the excited state. Compared to the free molecule, the excitation energy is therefore generally lower for a molecule in solution and gets even lower with increasing solvent polarity. The same effect, but

stronger, can be observed in the fluorescence spectra which can be explained by taking into account the relaxation process of an excited state after excitation. By measuring electronic spectra in different solvents and tracing back the effects of stabilization, the difference between the ground and excited state dipole moment can be determined. If the ground state dipole moment is known, which is often the case, the absolute value of the excited state dipole moment can be determined. [1, 2, 27]

Although Lippert and Mataga created a revolutionary method to tap into new areas of dipole moment determination, both of them mentioned drawbacks of the method, problems which can occur and matters which have to be taken into account of, further development in this field. The results of using this the method will always be more reasonable when a highly polar sample molecule is combined with lowly polar solvents. Both highly polar and non polar solvents would not suit the approximation which is made in the theory. They also stated not to use solvents which tend to interact via hydrogen bonds to avoid wrong interpretation of the results regarding the impact of the different solvent-solute interactions. Common solvents like water or alcohols therefore would not be appropriate for the method.

After the publications of Lippert and Mataga, other scientists started investigations in the field of the determination of excited state dipole moments in solution. Probably the most successful work came from Bilot and Kawski [3, 28, 29] who also derived their theory from a perturbation theory calculation. Contrary to Lippert and Matage, they took into account the polarizability of the solute, which leads to equations that converge into the theory of Lippert and Mataga if the polarizability is ignored. In their work, [3] Bilot and Kawski controlled their derivation of the perturbation theory by comparison with the results of Lippert and a completely different method by Czekalla [30] using dichroism techniques. The conclusion is that their values fit well with the results of Czekalla, while Lippert obtained much higher dipole moments. In some important conclusions, Bilot and Lippert agree with each other regarding the choice of solvents to use for the spectral measurements: neither non polar solvents nor those which tend to build hydrogen bonds are suited for these methods. In Bilot and Kawski [29], additionally the possibility of calculating the angle between ground and excited state dipole moments is given.

Due to the known disadvantages of the developed methods, namely the problems with the solubility in less polar solvents and uncontrollable interactions with a variety of solvents like alcohols, Gryczyński and Kawski [5] in 1975 and later Suppan and Tsiamis [31] introduced the first experiments with thermochromic absorption and fluorescence spectra. Both declared that thermochromic measurements generally give reasonable results which are in agree well with the solvatochromic method. Additionally, Suppan stated that the thermochromic shifts

are significantly smaller than solvatochromic shifts and therefore their usage in the calculation of excited state dipole moments would be difficult.

About 20 years later, Kawski began to publish the first articles about successful determination of the excited state dipole moment in solution via thermochromic absorption and fluorescence spectroscopy measurements[6, 32–38]. The method he used was based on the formalism he worked out for solvatochromic shifts, but he replaced the dependence of the polarity function from the solvent by a dependence on the temperature. The greatest difficulties he had to overcome were the accurate and precise determination of the exact spectral maxima. As stated by Suppan, the temperature dependent changes in spectra are much smaller than when changing the solvent and to achieve reasonable results the determination of maxima positions has to be very exact and reproducible [31]. Kawski used a method based on Bezier splines to determine the accurate maxima positions [6]. In addition, the temperature range which is used in the experiment should be as wide as possible, to compensate for the very small changes on the spectral shift. But with using the pressure cell from [5], a quite large number of different temperatures were available.

One of the heavily discussed topics throughout the history of solvatochromic and thermochromic spectroscopy for determining dipole moments of electronically excited states, is the usage of the so-called Onsager radius, which defines the radius of a spherical cavity occupied by a dissolved molecule. The Onsager radius hardly ever is determined by a reasonable measurement or quantum chemical method. Some publications only use estimation methods, for example, summing up all atomic radii in the molecule [1, 6, 33, 35] and sometimes where the values come from is not even mentioned [28]. While the approximation of spherical solute cavities can not be eliminated from the theory without major changes in the mathematical expressions, Demissie et al. [7] presented a method for determining the cavity volume of a solved molecule directly via weight fraction dependent density measurements of the solute/solvent system. With this step, the rough estimation of molecular radii is eliminated from the theory and substituted by experimental values. Following this substitution, the cavity volume can be moved from the main equation to the solvent polarity function thus leading to a simplification of the evaluation.

Parallel to the progress made in solvatochromic studies, a different method was developed and investigated by Liptay in the 1960s, which is built on the same basic effect. The mentioned basic effect is the Stark effect, discovered by Stark in 1913 [39] and describes the splitting of transitions in an electric field due to degeneration loss. The loss of degeneration is observable in a change of the absorption coefficient in a spectroscopic experiment in solution, where the maximum of the absorption spectrum or the shape of the curve in general, is manipulated.

The method of solvatochromism uses the electric field which results from the interaction between solvent and solute and the changes in the electric field by using different solvents. Liptay focused on the effect he called electrochromism which describes the manipulation of a spectrum in a single solvent by applying an external electric field [27]. The influences of the external electric field on the absorption spectra can be categorized by three effects:

1. The orientation effect, which describes the response of polar solute molecules towards the external electric field via orientation. The absorption coefficient of the solute is dependent on the angle between the transition moment of the molecules and the direction of light polarization. According to this, the orientation effect can be observed by taking spectra with polarized light of a solution in an electric field. The orientation effect can be utilized to approximate the direction of the transition moment vector of a spectral transition.

2. The band shift effects result from the direct interactions between the ground and excited state dipole moments with the electric field vector of the applied field which forces the molecule into partial orientation. The angle between the dipole moment vector and the electric field vector impacts on the transition energy and therefore on the position of the absorption band and its maximum. This enables the possibility of determining the dipole moment of the unrelaxed excited state.

3. The direct field-dependence of the transition moment plays an additional role to the orientation effect. Not only the angle between the transition moment and the polarisation of the light can affect the extinction coefficient, but the transition moment is directly proportional to the external electric field strength. The field strength is linked with a transition polarizability tensor, whilst the magnitude of this effect is mainly determined by the initial value of the transition moment. A very strong initial transition moment is practically unaffected by changes in the electric field, whilst a weak transition moment is affected in a higher manner. The extinction coefficient however, is directly dependent on the transition moment and so this effect can have a magnitude equivalent to the former.

The performance and evaluation of electrochromic measurements according to Liptay's work may be more complicated than the method of solvatochromism or thermochromism, but has still been used successfully up to the present day. One of the most recent works was performed by Nemkovich et al. in 2019 on crown ethers [40]. This method will not be further discussed,

but should be recognized for the sake of comparison.

The last step of evolution in the family of solvatochromic/thermochromic models has been the foundation of this thesis. In order to improve the general method, it was the aim to collect the benefits of contemporary published approaches and merge them to result in a reasonable modern approach of excited state dipole moment determination in solution. Based on the method of Kawski, which gave decent results in the first decade of 2000 using thermochromic absorption and fluorescence spectroscopy[6, 35–37], the idea of determining the Onsager radii from density measurements like Demissie [7] instead of assuming or estimating it from calculations was included as the first step of enhancement. In direct consequence the temperature dependence of the Onsager radius was taken into account and the density measurements were performed in a wide temperature range. To improve data for the temperature dependence of permittivity and refractive index of ethyl acetate, which is the mainly used solvent for all spectroscopic measurements in this work, the measurements were performed again using modern, more accurate instruments in order to benefit from the evolution and improvement in measurement technology. To finally remove of the necessity of using literature data, the method of ground state dipole moment determination in solution based on works of Hedestrand, Guggenheim and Smith was included [41–45]. Thankfully, fitting perfectly into the experimental setup. Finally, no variation to an existing method nor the development of a new method can reasonably be made without verifying the results through comparison with renowned methods. To accomplish this, all achieved results for ground and excited state dipole moments are compared, if possible, with at least one of either gas phase stark spectroscopy or quantum chemical calculations.

3. Theoretical Background

In general, spectroscopy is the observation of interactions between light and matter under very specific circumstances. The aim of spectroscopy in most of its uses, is the determination of one aspect in the molecular behaviour that characterizes the chosen sample in the chosen environment. Which properties of the sample should be addressed, can be controlled by the choice of the lights frequency, i.e. the alternation rate of the electromagnetic field. If the light frequency matches the frequency of a molecular, atomic or electronic transition, the energy of light is absorbed and the decrease of light intensity can be observed in the spectrum. Looking at organic molecules, spectroscopy using UV/Vis light mainly addresses the transitions of electrons in molecules with an electronic π-system in unoccupied orbitals. If the electron resumes back into the initial orbital, light can be emitted as well. This process is called fluorescence and can also be analysed spectroscopically.

The depth of detail which can be observed in molecular spectroscopy depends strongly on the surrounding of the molecule under investigation. Any influence which leads the system further away from the isolated situation lowers the resolution of the spectrum and therefore also the complexity of information, which could be evaluated. Whilst for a quasi isolated molecule even rotational transitions can be measured in microwave [46], rotationally resolved infrared [47] or HRLIF spectroscopy[48, 49], information on rotational levels gets lost in most cases, while vibrational information has a reduced resolution in electronic spectroscopy, when a polar molecule is dissolved in a polar solvent.

Polar (fluorescence dye) molecules in solution are exposed to a various number of different influences. On the one hand, there may be direct chemical interactions like proton transfers in acid-base reactions, which both exclusively occur with highly active groups on the dissolved molecule and/or protic solvents, whereas, on the other hand, there are physical interactions like dipolar interactions or van-der-Waals forces. H-bonds are a special case of interactions, because they originate from dipolar interactions but are considered to be chemical interactions (cf. Nomenclature H-**bond**) because of the strength they can reach. Whilst spectrochemists try to avoid the appearance of chemical interactions during absorption and fluorescence

spectroscopy, which can possibly influence the molecule in its electronic structure, physical interactions are unavoidable and can even be used to investigate molecular properties. The dipolar interactions between solvent and solvate molecule and their influence on UV/Vis absorption and fluorescence spectra can be investigated further in order to draw conclusions about the magnitude of the electric dipole moment alteration among electronic excitation of a dye molecule[1, 2].

3.1. The electric dipole moment

Molecules which are investigated in UV/Vis absorption and fluorescence spectroscopy are generally charge neutral, but partial charges can be distributed inhomogeneously throughout the molecule due to the effect of electronegativity. The exact mathematical description of a molecules charge distribution in the approximation of large distances is a multipole expansion, where the first term is the overall charge, the second term is the vectorial distribution (the dipole moment), the third term is the distribution defined with a two dimensional tensor (the quadrupole moment) etc.. According to Debye [50], the easiest way to describe a charge neutral molecule regarding its electrical characteristics, is the electric dipole moment, which represents the second term of the multipole expansion. Mathematically, the dipole moments magnitude μ can be described as the product of the distance r between two charges and the difference of the magnitude of both charges q (cf. 3.1).

$$\mu = q \cdot r \tag{3.1}$$

For molecules the dipole moment is a vector, pointing from the positive centre of charge to the negative centre of charge[1]. Inter alia, the concept of molecular dipole moments gained popularity because it is possible to construct them using only the bond dipole moments and the given geometry[51].

Through transition to an electronically excited state, the electronic distribution of a molecule changes. The geometry, representing the angles and bond lengths of the atoms, also alters to reach a maximal stabilization of the new electronic situation. This redistribution of charge carriers in most cases leads to a different dipole moment than in the stable ground state. In

[1] This is the definition in chemistry. In physics the direction of the dipole moment is defined in the exact opposite direction.

general, this excited state dipole moment will have a greater magnitude than the ground state dipole moment.

3.2. Electronic spectroscopy in solution

The interactions between different dipolar molecules in a solution has a high level of influence on the electronic energies of a dye molecule. If a polar dye molecule is dissolved in a polar solvent, the solvent molecules will arrange themselves around the dye and create a cavity. Through dipole interactions, the solvent molecules will rotate so that their charges oppose the solute in a contrary manner to its charge. The facing charges around the cavity now create an electric field which stabilizes the electronic energy of the dye molecule. One effect the solvent electric field has on the dye molecule is the fast relaxation to the vibrational ground state of the first electronically excited state after excitation [9]. To go into the detail of solvent effects in electronic spectroscopy, it is useful to follow the path of one excitation in Figure 3.1.

When a photon hits the solvent stabilized molecule (cf. Fig. 3.1 bottom left state), an electron is transferred to a higher orbital and the molecule is lifted up in energy to the so called Franck-Condon (FC) state [9] on a time scale of 10^{-15} seconds. This FC state represents a vibrationally excited state of the first electronically excited state, which is not yet stabilized by the electric field of the solvent (cf. Fig. 3.1 top left state). The lifetime of the excited state for strongly fluorescent organic molecules is in the range of 10^{-9} seconds. During this time, the geometry of the molecule relaxes and the surrounding solvent molecules rearrange to the new polarity of the excited state within a timescale of 10^{-12} to 10^{-10} seconds[53]. The result is a stabilization into a relaxed excited state (cf. Fig. 3.1 top right state) which is energetically lower than the FC excited state. The energy gap depends on the magnitude of the dipole moment. From the relaxed excited state the electron can again transfer to its orbital of origin leading the molecule in a FC ground state (cf. Fig. 3.1 bottom right state). This FC ground state again is energetically higher because the electron transfer itself is on an identical time scale to the absorption. The solvent molecules do not stabilize the state yet. Additionally, according to the Franck-Condon principle, the transition will lead to a vibrationally excited state which will relax together with the solvent. The solvent molecules will now rearrange similarly to the process before, leading to the relaxed ground state and a stabilized molecule. To sum up the process which is described here: The Stokes shift of a dye molecule in a polar solvent, which is the difference in average photon energy between ground and excited state and is represented by the spectral maxima, directly depends on the interaction forces between the dipole moment of the ground state and the excited state of the dye molecule and the

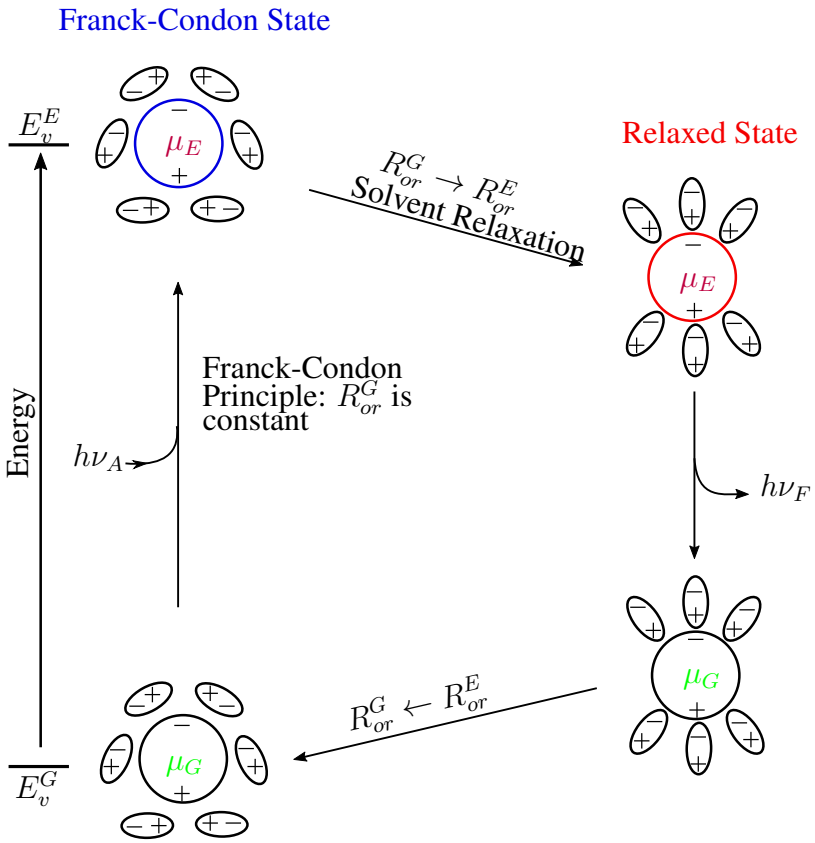

Figure 3.1.: Interactions between solvent and solute during a full fluorescence cycle of a single dye molecule. The vertical position of the states represent the electronic energy they are at. $R_{or}^{E/G}$ is the electric field of the solvent orientation. From Ref. [52]

polarity and mobility of the surrounding solvent molecules. Because of the determination of the Stokes shift in dependency of the solvent polarity parameters, the difference now, between ground and excited state dipole moment should be accessible experimentally. The solvent polarity parameters which are generally available for solvents are the permittivity (dielectrical constant) and the index of refraction. The permittivity describes the reaction of an entire molecule to an electric field with a low frequency and the index of refraction refers to the reaction only of the electrons in a molecule to an electric field with a high frequency [9]. In terms of the process in Fig. 3.1, the refractive index, regarding only electronic movements, leads to an immediate stabilization of the electrons in a FC state within the timescale of the excitation. The permittivity now, including all reactions of a molecule to an electric field, is responsible for the solvent relaxation. To isolate the information about the excited state dipole moment, the terms regarding the refractive index always have to be subtracted from the terms of permittivity.

3.3. Derivation of the solvatochromic and thermochromic method

3.3.1. A comment on systems of units

The original publications of Lippert and Mataga, as wella s Bilot and Kawski, are from the middle of the 20^{th} century where the CGS-unit system was commonly used. To convert eq. 3.12 for usage with the SI-unit system, which is primarily used today in 2021, the factor $\frac{1}{4\pi\varepsilon_0}$ has to be included in the definitions of the reaction fields. In the CGS-unit system the so called Coulomb constant had the value 1 and therefore did not visually appear in the equation.

In this chapter the original derivations from the last century are given, where the CGS-unit system is used. Later in the experimental section, all equations will be written in the SI-unit system.

3.3.2. The Lippert-Mataga-Theory

Lippert [1] and Mataga [2] first published an approach for the determination of excited state dipole moments using alterations of the Stokes shift due to variations in solvent polarity parameters, i.e. measurements in different solvents. Both of their studies are based on a calculation of perturbation theory published by Ooshika [26], which initially only addressed absorption spectra. A number of approximations have to be made to break complex processes,

such as the interactions of a polar molecule which is dissolved in a polar solvent, into an applicable equation with the intention to solve it via linear regression, as was usual for a long time in physics. First, the molecular dye in this theory is replaced by a point dipole in a spherical cavity which is surrounded by a continuous dielectric medium. Any specific interactions with the solvent are neglected, as well as the polarizability of the dye molecule. Additionally, a change in direction of the dipole moment upon excitation which certainly has influence on solvent reorientation is not respected in the theory. Regarding the solvent relaxation, it is assumed, that the lifetime of the excited state is long enough in order to guarantee a complete solvent relaxation prior to the emission of a photon. However, it has to be taken into account, that the excited state lifetime, as well as the solvent reorientation can be represented by exponential decays. Taking this into account, there can still occur an influence of non-relaxed solvent on the fluorescence spectrum, creating a systematic error in the evaluation [9, 52]. Errors of this type may be caused by factors such as changes in temperature, viscosity and the excited state lifetime of the molecular dye.

Deriving the Lippert-Mataga equation mathematically can be performed for example, by using Figure 3.1. The aim is, to subtract the emitted photons energy from the absorbed photons energy, resulting in a simple use of the energy difference ΔE between the involved states as measurable parameter. A dipole in solution is described by the absolute energy

$$E_{dipole} = -\mu \cdot R_i^j, \tag{3.2}$$

with μ as magnitude of the dipole and R_i^j as reactive electric field which is induced in the dielectric continuum by the dipole. R_i^j is defined in equation 3.3 using the cavity radius a and the polarizability f of the solvent.

$$R_i^j = \frac{2\mu}{a^3} f \tag{3.3}$$

The indices i and j are introduced to separate between electronic/orientational contribution and ground/excited state, respectively. The polarizability of the solvent can, in a common approximation, be separated into the electronic contribution $f(n)$ (cf. eq. 3.4), defined as the high frequency polarizability, and the low frequency polarizability $f(\varepsilon)$ (cf. eq 3.5), which also includes the molecular orientation.

$$f(n) = \frac{n^2 - 1}{2n^2 + 1} \tag{3.4}$$

$$f(\varepsilon) = \frac{\varepsilon - 1}{2\varepsilon + 1} \tag{3.5}$$

$$\Delta f = \frac{\varepsilon - 1}{2\varepsilon + 1} - \frac{n^2 - 1}{2n^2 + 1} \tag{3.6}$$

To extract the contribution which originates from orientation only, the high frequency polarization has to be subtracted from the low frequency polarization to exclude the electronic contribution. This results in the so called orientation polarizability shown in equation 3.6.

In the example used, a solvent which fulfils $\varepsilon \backsimeq n^2$, equation 3.6 solves to $\Delta f \approx 0$. Therefore, no spectral shifts can arise from solvent reorientation for solvents without a permanent dipole moment. Contrary to this, any polar solvent will lead to $\Delta f > 0$ and induce a detectable Stokes shift. All interactions between fluorophore and solvent can be, without extending the hereby given parameters, separated into ground- and excited state dipole moment interactions with the solvent reaction fields. The reaction fields, according to eq. 3.3 now have to be separated, not only regarding the states dipole moment, but concerning the contribution of electronic or orientational polarizability, additionally.

$$\begin{aligned} R^g_{el} &= \frac{2\mu_g}{a^3} f(n) \\ R^e_{el} &= \frac{2\mu_e}{a^3} f(n) \\ R^g_{or} &= \frac{2\mu_g}{a^3} \Delta f \\ R^e_{or} &= \frac{2\mu_e}{a^3} \Delta f \end{aligned} \tag{3.7}$$

In equations 3.7, the involved reaction fields which are partially already presented in Fig. 3.1 are shown. Now, to obtain the energies of the ground- and excited states, which are involved in the absorption process E^j_A, the active dipole energies (cf. eq.3.2) for the reactive fields have to be subtracted from the vapor phase energy of the state E^j_v. The state energies of the absorption process of Fig. 3.1 are shown in eq. 3.8.

$$\begin{aligned} E_A^E &= E_v^E - \mu_E R_{or}^G - \mu_E R_{el}^E \\ E_A^G &= E_v^G - \mu_G R_{or}^G - \mu_G R_{el}^G \end{aligned} \tag{3.8}$$

To include the time scales and the delayed solvent relaxation, only the ground state orientational field is active in this case, but due to the much faster electron movement, the active electronic field is always equal to the present electronic state. The fluorescence processes' state energies can be calculated the same way (cf. eq 3.9), while it is important that in this case the excited state orientational field is used, for both involved electronic states.

$$\begin{aligned} E_F^E &= E_v^E - \mu_E R_{or}^E - \mu_E R_{el}^E \\ E_F^G &= E_v^G - \mu_G R_{or}^E - \mu_G R_{el}^G \end{aligned} \tag{3.9}$$

If both in eq. 3.8 and 3.9 the ground state energy is subtracted from the excited state energy, the transition energies for the absorption and emission process can be calculated as shown in equations 3.10 and 3.11

$$hc\tilde{\nu}_A = hc(\tilde{\nu}_A)_v - (\mu_E - \mu_G)\left(R_{or}^G\right) - \mu_E R_{el}^E + \mu_G R_{el}^G \tag{3.10}$$

$$hc\tilde{\nu}_F = hc(\tilde{\nu}_F)_v - (\mu_E - \mu_G)\left(R_{or}^E\right) - \mu_E R_{el}^E + \mu_G R_{el}^G, \tag{3.11}$$

with $\tilde{\nu} \cdot hc = \Delta E$ representing the transition energy and $\tilde{\nu}_{A/F}$ the maxima of the absorption or fluorescence spectra. The index v shows the vapour state behaviour. A subtraction of eq. 3.11 from eq. 3.10 results in an expression which can be evaluated by linear regression. Through substitution of the reactive field parameters according to eq. 3.7 the known Lippert-Mataga equation is formed (cf. 3.12) [9].

$$\tilde{\nu}_A - \tilde{\nu}_F = \frac{2\left(\mu_E - \mu_G\right)^2}{hca^3}\Delta f + const \tag{3.12}$$

3.3.3. The Bilot-Kawski Theory

To overcome at least one of the approximations, which are made in the Lippert-Mataga equation, Bilot and Kawski derived a different theory, considering the fact that the fluorophore has a polarizability [3, 28]. The theory of Bilot and Kawski is also based on the Onsager model [4], meaning that the general approximations of a spherical solvent cavity with isotropic polarizability cannot be eliminated. In general, the derivation of the Bilot-Kawski theory is identical as aforementioned. The major difference can be found in the calculation of the state energies (cf. eg. 3.8 and 3.9), where Lippert and Mataga only used the first term of the row expansion, including the permanent dipole moment and the reaction field according to the first order Stark effect. On the other hand, Bilot and Kawski expanded the row to the second term regarding the static electron polarizability α and the squared reaction field according to the second order Stark effect as shown in eq. 3.13 for the ground state.

$$E_G = E_0 - \mu_G R_G - \frac{1}{2}\alpha R_G^2 \tag{3.13}$$

Even though the terms for the second order Stark effect are neglected in the final equation (cf. Bilot and Kawski [3], eq. (19)), the initial dipole moments used in eq. 3.7, 3.8 and 3.9 are derivatives of the state energy given by eq. 3.14

$$\mu_G = -\frac{\partial E_G}{\partial R_G}. \tag{3.14}$$

Therefore, even in the first order Stark effect term there are influences of the static electron polarizability remaining through the definition of the dipole moments. Bilot and Kawski propose their final equation as shown in eq. 3.15

$$\tilde{\nu}_A - \tilde{\nu}_F = \frac{2(\mu_E - \mu_G)^2}{hca^3} \frac{\left(\frac{\varepsilon-1}{2\varepsilon+1} - \frac{n^2-1}{2n^2+1}\right)}{\left(1 - \frac{2\alpha}{a^3}\frac{n^2-1}{2n^2+1}\right)^2 \left(1 - \frac{2\alpha}{a^3}\frac{\varepsilon-1}{2\varepsilon+1}\right)} + const. \tag{3.15}$$

If the polarizability α is considered to be zero, eq. 3.15 becomes identical to the original Lippert-Mataga equation eq. 3.12. In Bilot and Kawski [28], also the addition of the transition energies $\tilde{\nu}_A + \tilde{\nu}_F$ is proposed, leading to eq. 3.16 which has been mainly used in this work

for method development.

$$\tilde{\nu}_A + \tilde{\nu}_F = -\frac{2(\mu_E^2 - \mu_G^2)}{hca^3}\left[\frac{\left(\frac{\varepsilon-1}{2\varepsilon+1} - \frac{n^2-1}{2n^2+1}\right)}{\left(1 - \frac{2\alpha}{a^3}\frac{n^2-1}{2n^2+1}\right)^2\left(1 - \frac{2\alpha}{a^3}\frac{\varepsilon-1}{2\varepsilon+1}\right)} + 2\frac{\frac{n^2-1}{2n^2+1}\left(1 - \frac{\alpha}{a^3}\cdot\frac{n^2-1}{2n^2+1}\right)}{\left(1 - \frac{2\alpha}{a^3}\cdot\frac{n^2-1}{2n^2+1}\right)^2}\right] + const. \tag{3.16}$$

For most fluorophores, the polarizability is unknown but according to Kawski et al. [6], the approximation $\frac{\alpha}{a^3} = 0,5$ is acceptable for most molecules and eq. 3.16 simplifies to

$$\tilde{\nu}_A + \tilde{\nu}_F = -\frac{2(\mu_E^2 - \mu_G^2)}{hca^3}\left[\frac{2n^2+1}{n^2+2}\left(\frac{\varepsilon-1}{\varepsilon+2} - \frac{n^2-1}{n^2+2}\right) + 3\frac{(n^4-1)}{(n^2+2)^2}\right] + const.\ . \tag{3.17}$$

3.3.4. Thermochromy

Initially, both of the theories which are presented above were derived to be used with the results of solvatochromic absorption and fluorescence spectroscopy. But both Lippert [1] and Bilot and Kawski [28] included comments explaining the possible negative influence of changing the solvent to the spectroscopic maxima. They agreed to the fact that solvents with a very small permittivity induce a systematic deviation. For example, even a small amount of water in a non polar solvent can accumulate around the fluorophore. This effect can strongly influence the reaction field of the fluorophore. Also highly polar solvents come with strong deviations from the theory because the approximation of isotropic polarizabilities is no longer acceptable under their influence. Alcohols or other solvents with the ability to form H-bonds can even influence the integrity of the fluorophore and are therefore not recommended. Only aprotic solvents with a medium polarity seem to be a proper choice for the methods and even there some deviations can be observed [1, 7, 54].

Beginning with the work of Gryczynski and Kawski [5], the idea of utilizing the variation of the solution's temperature to manipulate the permittivity and refractive index joined the theory. The first results were published by Kawski at the beginning of the 21^{st} century [6, 32–35]. The advantage of thermochromic measurements is the nearly exclusive change of permittivity and index of refraction upon temperature variation in the solvent. A drawback of this method is the very small variation in Stokes shift upon temperature change which makes an accurate

evaluation of the spectral maxima mandatory. Overall, the studies of Kawski have shown that thermochromism is an eminent improvement in the means of precision for the relation between Stokes shift and solvent polarity function.

3.3.5. The Spectral Maxima

All theories which are presented above, technically, are meant to be used on the $0-0$ transitions of the involved states in molecules. Unfortunately, solution spectra show the distribution around the vertical excitation which is the maximum of the spectral curve. Therefore, experimental spectra do not contain exact information on both of the $0-0$ transitions in a dissolved molecule. A problem with recording electronic spectra in solution is the broadening and mixing of spectral peaks from vibrational or rotational transitions, leading to a broad absorption band which contains only low information on the substance which is interacting with the used light. Regularly, the shape of an UV/Vis absorption or fluorescence emission spectrum recorded in solution can be described with a sum of Gaussian functions [55]. The problem which now occurs for the practical execution of the methods is to choose a point in the spectrum which represents the theoretical $0-0$ transition in a proper way and can be observed to investigate the reaction of the ambient manipulation. It is common sense [1–3, 6] to use the local maximum with the lowest energy of the absorption spectrum and the overall maximum of the fluorescence spectrum as these representative points for the evaluation. In the general behaviour of these type of spectral curves, maxima are the only points where the position of different spectra can be compared reasonably. The lowest energy absorption maximum is used because it is not uncommon that higher electronic states can also be seen in one spectrum (cf. Fig. 6.9). Nevertheless, the lowest excited singlet state should always be represented by the lowest energy maximum because usually represents the lowest allowed transition and the fluorescent state, accordingly. According to the rule of Kasha [56], fluorescence only occurs from the vibrational ground state of the lowest excited singlet state which should imply that any substance obeying this rule should only show a single maximum in the fluorescence spectrum, which makes the usage of the overall maximum as a measurement for the spectral position reasonable.

Even though reference points in the spectra have now been introduced and justified, there still is more to discuss. The solvatochromic shifts of polar molecules' spectra usually are quite large and the maxima are clearly separated from each other, making small errors in the determination of the maximum position less important. With the step into thermochromic measurements, the increment in solvent polarity change and therefore the alteration of the maxima positions become substantially smaller. In fact, sometimes the change in the max-

imum position is in the range of the spectral resolution, so the noise in the spectral curves becomes a problem when determining the maximum positions. At this point it is crucial to introduce a fitting technique to the recorded spectra, that gives one definite maximum position whilst including the information of the complete spectrum into the fitting procedure. The fitting of spectra using a sum of Gaussian functions and the Fast-Fourier-Transformation filtering technique, which are both used at several points of this work, are presented in Chapter 6.

Part II.

Experimental

4. Overview

One main topic of the work for this thesis was the development of a complete experimental method for determining dipole moments in ground and electronically excited states of fluorescing dye molecules in solution on the base of thermochromic UV/Vis absorption and fluorescence emission spectroscopy. This part of the manuscript presents the evolution of the experimental setup and the first tests with small molecules. The three following publications cover the major part of experimental development, including the construction of a spectroscopic heatable and coolable vacuum chamber and details of the evaluation process.

First, Chapter 6 contains an article, published in the journal MethodsX [55], that describes the complete basic method which was developed for the determination of excited state dipole moments in solution.

Chapter 7 contains a publication on methoxybenzene (anisole) which was chosen as a sample molecule for the first test of the thermochromic method in direct comparison to an experimental reference method [8]. The experimental data recorded on anisole were published additionally in the journal Data in Brief [57] and are shown here in Chapter 9 in order to give other scientists the opportunity of reusing the original data.

Detailed information about the process of development of the experimental setup is given in Chapter 10. It contains the planning and construction of the spectroscopic vacuum chamber and additionally explanations on a method for determining ground state dipole moments experimentally.

5. Comments on the MethodsX Article

The following chapter contains the article titled ¨Determination of excited state dipole moments in solution via thermochromic methods˝ which is published in the journal MethodsX. Unfortunately, the article was published whilst still containing a number of mistakes. These mistakes have not been eliminated by the production office in the proofs. Here, the mistakes are listed and corrected to satisfy the scientific aspiration of this thesis.

Firstly, nearly all absolute Kelvin temperatures are missing the 0.15 addition representing round Celsius temperatures which were used in the experiments and calculations.

There are two equations with the numeration 3 in the article. Even if the first equation number 3 is mentioned in the text directly before its appearance, the pdf-hyperlink only works for the second one. All equations after the first number 3 should be counted +1 to be displyed correctly.

The section ¨Determination of the ground state dipole moment from permittivity measurements˝ is titled incorrectly. The correct title is ¨Determination of the ground- and excited state dipole moment from thermochromic absorption and fluorescence emission spectroscopy˝.

The first paragraph of the subsection ¨Evaluation of the spectral shifts˝ contains incorrect citations. The two citations numbered 8 and 9 refer to the publications of da Luz de Sousa [58] and Budzák [59] whilst the correct citation for this paragraph should be number 19 and 20. These refer to two articles of Lindic et al. regarding anisole [8, 57]. The citation numeration is different in this thesis than in the original publication.

In the subsection ¨Evaluation of the dipole moment˝ the introduction of the parameters for Equations 6.8 - 6.11 are missing some blank spaces. Correctly written, the sentence would be ¨Here, m_x ($x = LM$, BK, A, E) are the slopes of the diagrams according to Eqs. 6.5, 6.6 and 6.7, respectively, ε_0 is the permittivity of the vacuum, h is Planck's constant, c is light speed in vacuum and μ_x ($x = g$, e) are the dipole moments of ground (g) and excited state (e). ˝.

The method article [55] originally should have been published directly after the article about anisole [8]. Unfortunately, the reviewing process met with several problems and delays. Therefore, the method article has been rewritten with more input from the article about the substituted quinoxaline [60], which was published in between. According to this, some techniques mentioned in Chapter 6 will not be found in Chapter 7 as they have been introduced into the method afterwards.

6. Method Article

Determination of excited state dipole moments in solution via thermochromic methods

Mirko Matthias Lindic[a], Matthias Zajonz[a], Marie-Luise Hebestreit[a], Michael Schneider[a], W. Leo Meerts[b], Michael Schmitt[a,*]

[a] Heinrich-Heine-Universität, Institut für Physikalische Chemie I, D-40225 Düsseldorf, Germany [b] Radboud University, Institute for Molecules and Materials, Felix Laboratory, Toernooiveld 7c, 6525 ED Nijmegen, the Netherlands

6.1. Abstract

The method basically combines the existing ideas of excited state dipole moment determination via thermochromic fluorescence spectroscopy with the determination of the solvent cavity volume via concentration dependent density measurements of the solution densities at different weight fractions. Additionally, the determination of the cavity volume in dependence of the solvent temperature is included here, which provides a better accuracy of the excited state dipole moment determination. With this step two major sources of errors are eliminated: the use of the very imprecise Onsager radius and the assumption, that the cavity size is temperature independent.

- Thermochromic absorption and fluorescence spectroscopy.
- Cavity volume determination by density measurements.
- Temperature dependent cavity volume determination.

6.2. Method details

This section will give a step-by-step instruction for performing the method of thermochromic shifts for determination of excited state dipole moments.

6.3. Introduction

Although the determination of excited state dipole moments using solvatochromic shifts of absorption/emission spectra in different solvents has many shortcomings, that are well-documented [54, 61–64], it is still widely applied experimentally [58, 59, 65, 66] and investigated theoretically [67], due to its conceptual and experimental simplicity. Recently, dipole moment changes upon electronic excitation, even of different conformers, could be resolved in solution by a combination of stationary and time-resolved fluorescence measurements and ultraviolet-visible transient absorption spectroscopy [68]. A recent review on excited state dipole moments compares the different methods that are used for the determination of dipole moments of molecules in their electronically excited states [48]. These methods comprise solvatochromism [69], electrochromism [27], thermochromism [32] (in solution) and direct Stark effect measurements [70, 71] (in the gas phase).

Some of the problems that are connected with the solvatochromic method can be solved, if one makes use of the fact, that variation of the solvent polarity function might as well be reached by variation of the temperature of the solution in spite of the solvent. This is due to the fact that both index of refraction and permittivity, which make up the solvent polarity function, depend on the temperature of the solvent. However, spectral shifts, which are induced by temperature variations are smaller than those, originating from variation of the solvent. Therefore, a good temperature stability and a reproducible determination of absorption and emission maxima are crucial for the success of the method. One of the major problems of the methods of solvatochromic shifts, the differing interactions of the solute with different solvents can be avoided by the use of thermochromic shifts. Apart from the use of thermochromic shifts in spite of solvatochromic shifts, replacement of the original Onsager radius [4] for description of the cavity size by the experimentally determined cavity volume greatly improves the method. In the following we describe, how the method can be employed reliably.

We have chosen two different systems to describe the method in detail. Anisole [8, 57] and 2-((4-methoxyphenyl)ethynyl)-3-(1-methyl-1H-indol-3-yl)quinoxaline (Q1) [60], both in ethyl acetate solution have been chosen as examples for medium size dipole moment and

dipole moment change (anisole) and large dipole moment and dipole moment change upon excitation for Q1.

6.4. Density Measurement

Accurate density measurements of the solution as function of the temperature have been performed, using a high precision density meter with temperature control (Anton Paar DMA4500M). Concentration (weight fraction) dependent density measurements in a wide temperature range are necessary. The weight fractions are chosen to match the accuracy of the density meter, but should be as low as possible for the concentration used in spectral measurements. Representative results can be produced using eleven different weight fractions between 0.0013 and 0.0129 for anisole and between 0.0004 and 0.004 for Q1 and temperatures between $263\,\mathrm{K}$ and $343\,\mathrm{K}$ with an increment of $2\,\mathrm{K}$. To minimize concentration fluctuation and maximize precision, the measurements are performed starting at low temperatures.

6.5. Evaluation of the cavity volume from density measurements

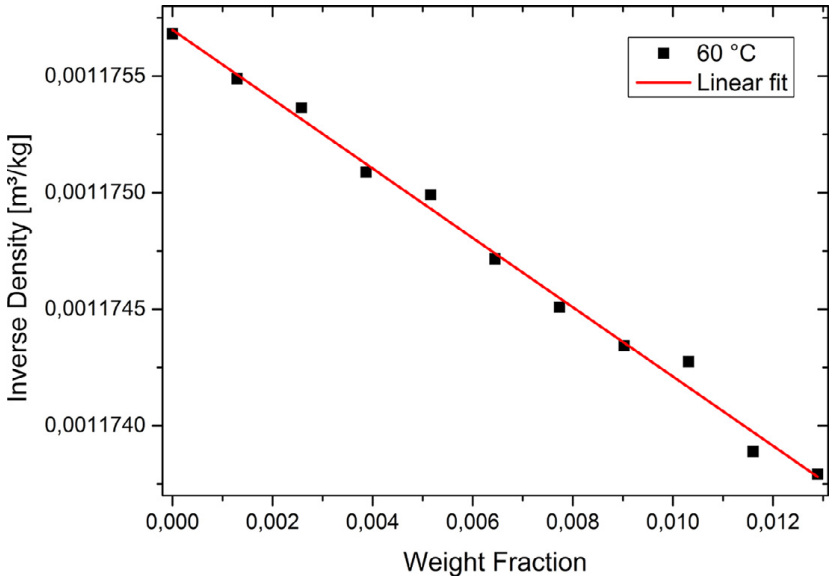

Figure 6.1.: Plot and fit of inverse density vs. weight fraction of anisole in ethyl acetate at $333\,\mathrm{K}$.

According to Eqs. 6.1 and 6.2 the cavity volume is calculated from the slope of the linear regression of the inverse density versus weight fraction w of the solute at each temperature.

$$\frac{1}{\rho} = \frac{1}{\rho^*} + \left(\frac{V_m}{M_W} - \frac{1}{\rho^*}\right) \cdot w \tag{6.1}$$

$$V_m = \left(S + \frac{1}{\rho^*}\right) \cdot M_W \tag{6.2}$$

Here, ρ is the actual density of the solution, ρ^* is the density of the pure solvent, V_m is the molar cavity volume, M_W is the molecular weight, w is the weight fraction and S is the slope of the linear regression of $\frac{1}{\rho}$ vs. w. An example diagram at a temperature of $60\,°\mathrm{C}$ including the linear fit is given in Fig. 6.1. From the measured cavity volume at each temperature the function $V(T)$ is generated, which is the linear regression of the molecular cavity volume versus the temperature, shown in Fig. 6.2.

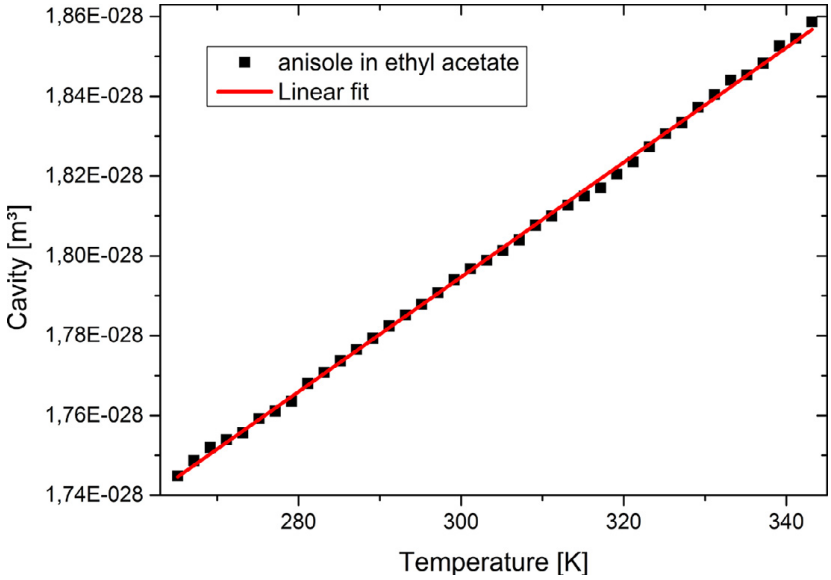

Figure 6.2.: Plot and fit of cavity volume versus temperature for anisole in ethyl acetate.

6.6. Permittivity measurements

The permittivity of the solvent which is needed for the solvent polarity function, has to be determined in a temperature range, as large as possible. To provide precise measurements, the capacity of a liquid test fixture (Keysight 16452A) is measured with an E4990A impedance analyzer. Temperature dependent measurements are performed by placing the fixture in an oil tank, which is temperature controlled via an external liquid cooling. For determination of the permittivity of a solvent its capacity is measured in a temperature range between $277\,\mathrm{K}$ and $323\,\mathrm{K}$ with intervals of $2\,\mathrm{K}$ using the Keysight 16452A liquid test fixture. Finally, the

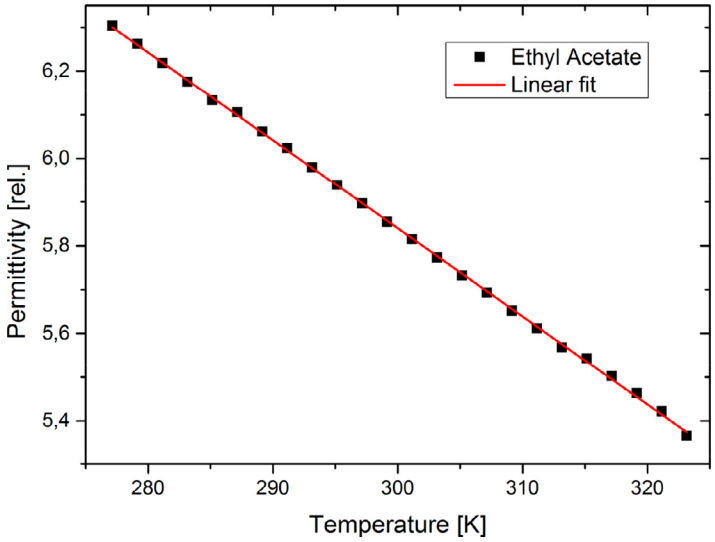

Figure 6.3.: Temperature dependent permittivity of ethyl acetate including linear fit of the measurement data.

measured capacity is divided by the air capacity of the capacitor according to Eq. 6.3.

$$\varepsilon_r = \frac{C_p}{C_p^0} (3)$$

Fig. 6.3 shows the temperature dependent permittivity of ethyl acetate in a temperature range of $277\,\mathrm{K}$ to $323\,\mathrm{K}$. The data were fitted to a linear function which can be extrapolated for later evaluation.

6.7. Determination of the index of refraction

Additionally to the temperature dependent cavity volume and the temperature dependent permittivity, the temperature dependent index of refraction of the chosen solvent is essential to calculate the solvent polarity function. For precise measurements of the temperature dependent index of refraction, we used an Anton Paar Abbemat MW refractometer, which provides good temperature control in a range of $283\,\mathrm{K}$ to $343\,\mathrm{K}$. Fig. 6.4 shows the values of the index of refraction of ethyl acetate at a wavelength of $589.6\,\mathrm{nm}$ including a third order polynomial fit of the data.

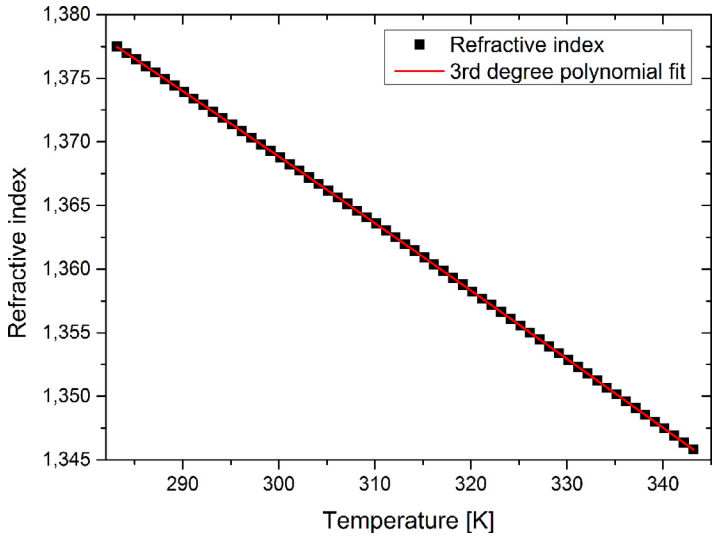

Figure 6.4.: Temperature dependent index of refraction of ethyl acetate including polynomial fit.

6.8. Determination of the ground state dipole moment from permittivity measurements

6.8.1. Spectral measurements

The absorption and fluorescence spectra should be measured in a large temperature range within the limits given by freezing and boiling points of solvent and to provide better evaluation the interval should be about $2\,\mathrm{K}$. For measurements below $273\,\mathrm{K}$, water vapor condensation has to be prevented on the transmitting surfaces. In order to minimize temperature fluctuations and condensation on the surface, a vacuum chamber was built around the temperature controlled parts of the apparatus. The vacuum chamber contains the cuvette, which is insulated to the lid of the chamber on the top and placed inside a copper frame which conducts the heat to a double-stage Peltier unit. It's hot side is cooled by a liquid cooling cycle. The set-up is shown in Fig. 6.5. The stainless-steel vacuum chamber is supplied with feedthroughs for the liquid cooling and the electric connections as well as with three Suprasil I windows for light transmission. The lid of the chamber gives direct access to the cuvette for an easy handling of the sample without necessity to break the vacuum. Two perspectives of the chambers outside are given in Figs.6.6 and 6.7. The vacuum chamber is equipped with an adapter to fit it both in the absorption as well as in the fluorescence emission spectrometer. As in the density measurements, the data are collected, starting from the lowest temperature and heating up the sample step by step. A PID control of the Peltier unit is used to stabilize the temperature during the measurement of the spectra to an accuracy better than $0.1\,\mathrm{K}$.

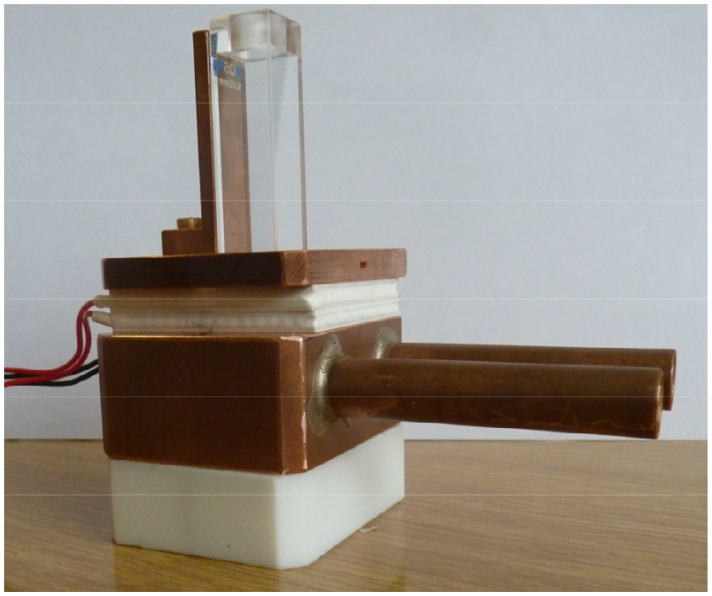

Figure 6.5.: Cooling and heating unit, including cuvette, Peltier elements and liquid cooling inside of copper block.

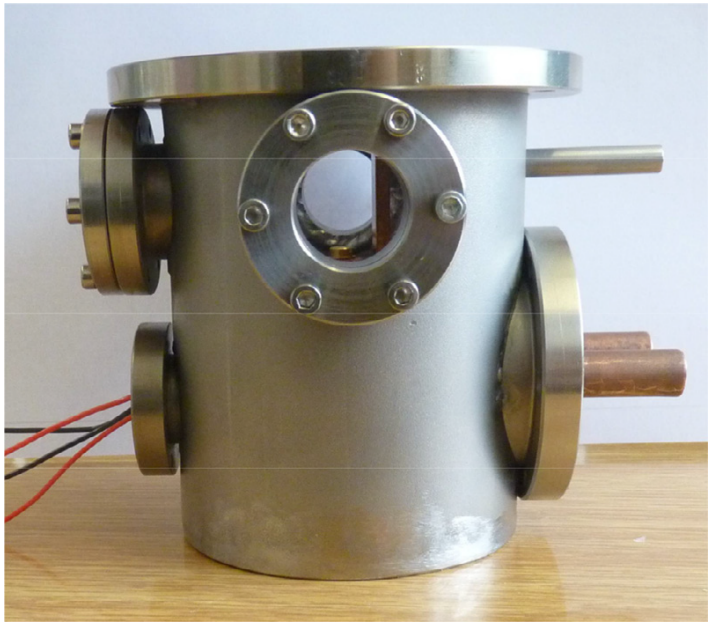

Figure 6.6.: Housing of the spectroscopy chamber with view through the transmission spectroscopy windows.

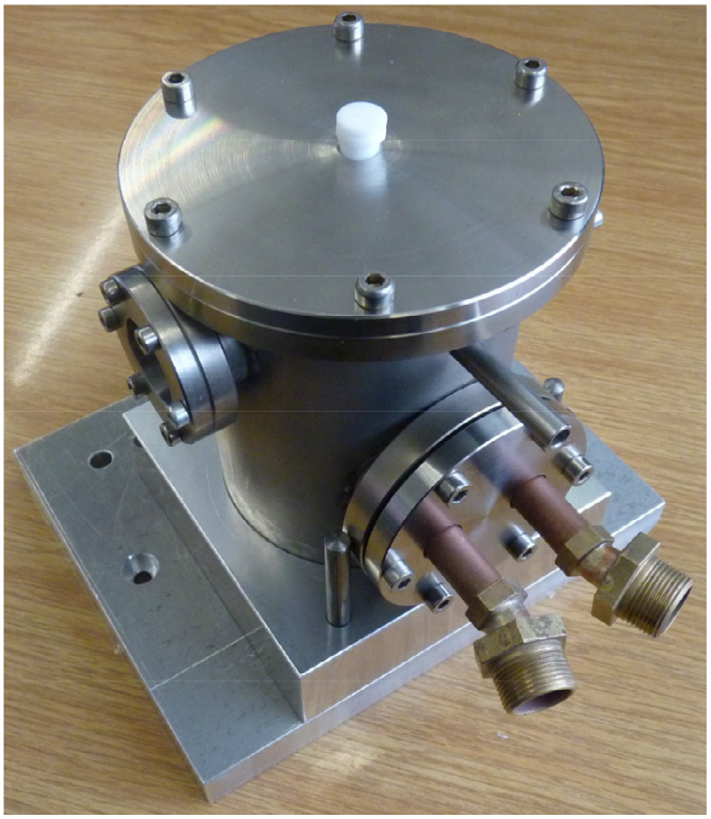

Figure 6.7.: Housing of the measurement chamber with closed lid and liquid cooling connectors. The sample can be manipulated without breaking the vacuum.

6.8.2. Evaluation of the spectral shifts

Since thermochromic shifts are smaller, than solvatochromic shifts, the evaluation of the maximum of the absorption and emission bands is crucial. The unfitted absorption and fluorescence spectra of Q1 are shown in Fig. 6.8, additional data for anisole can be found in [58, 59]. It is necessary to apply a good fit to the measured data, to avoid measurement artifacts or noise that could lead to an artificially shifted band. The best results have been found using either a fit function, which is constructed from multiple Gauss functions or a fast Fourier transformation (FFT) filter to the raw data. Both methods can give good results, but the FFT-Filter is easier to apply. Both methods are described in the following. The maximum position of the spectra can be determined from fits to a sum of several Gauss functions, whose number have to be determined manually. Examples for the fit-function applied to the data and the construction of one fit-function are given in Fig. 6.9. The maxima of the functions can either be found with a peak-picking tool or by using the fit-function and finding the analytical solution. For the evaluation, the longest wavelength maximum of the absorption spectrum and the overall maximum of the fluorescence spectrum is needed. The second method for determination of the maximum of the intensities in the absorption and emission spectra is the usage of a Fast Fourier Transformation (FFT) Filter. With this method the high frequency noise is eliminated and a smoothened graph without change in positions and intensities is obtained. An example of FFT-filtered maximum of the absorption is given in Fig. 6.10. For anisole, both of the fit methods agreed within $0.2\,\mathrm{cm}^{-1}$. However, for a different molecule, 1-methylindole, we found a mean deviation of about $9\,\mathrm{cm}^{-1}$ but a maximum deviation of more than $100\,\mathrm{cm}^{-1}$ for both methods, which is a large difference. The overall influence of the fit on the final dipole moment results in a deviation of $0.15\,\mathrm{D}$, which is, regarding the accuracy of the method, not a big difference. On the other hand, the precision of the method can in no case be better, more likely be worse, than $0.15\,\mathrm{D}$, even if the statistical error may be smaller.

6.8.3. Evaluation of the dipole moment

First, the solvent polarity functions of Lippert-Mataga [1, 2] and Bilot-Kawski [3, 6], given in Eqs. 6.3 and 6.4 , which include the experimentally determined cavity volume function $V(T)$, refractive index $n(T)$ data and permittivity $\varepsilon_r(T)$ of the solvent have to be determined.

$$F_{LM}(T) = \frac{1}{V(T)} \left[\frac{\varepsilon_r(T) - 1}{2\varepsilon_r(T) + 2} - \frac{1}{2} \left(\frac{n(t)^2 - 1}{2n(T)^2 + 1} \right) \right] \tag{6.3}$$

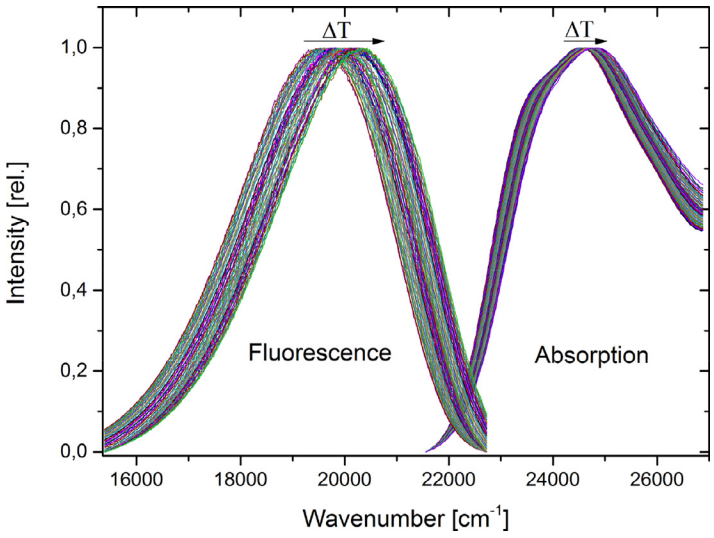

Figure 6.8.: Absorption and emission spectra of Q1, measured is ethyl acetate. Temperature shift is indicated by text and arrows. Spectra are normalized but not fitted.

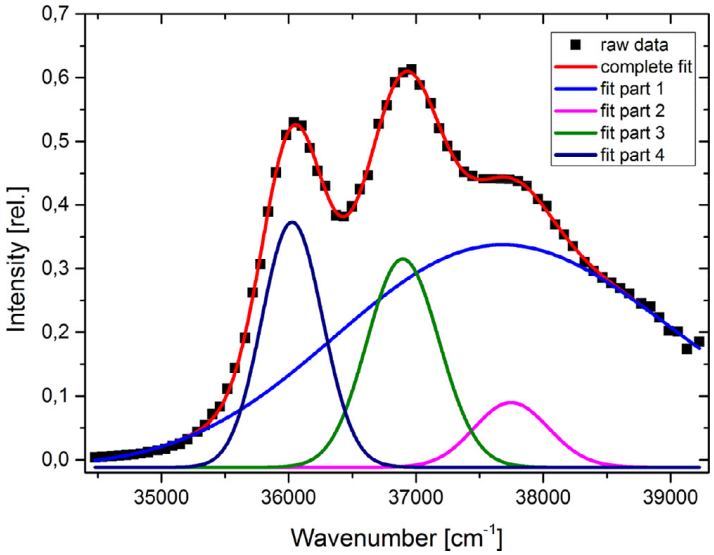

Figure 6.9.: Construction of a fit-function (red trace) consisting of 4 Gauss-functions applied to the raw absorption spectrum of anisole in ethyl acetate at 293.15 K.

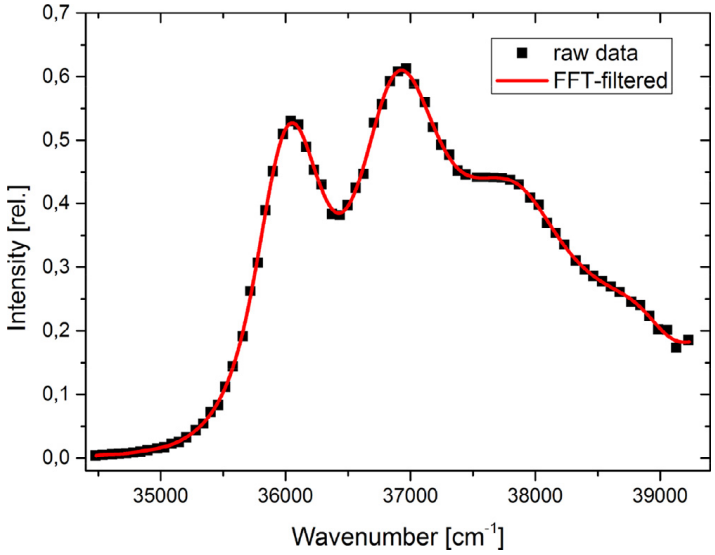

Figure 6.10.: Absorption spectrum of anisole (black squares) and the smoothened function (red trace) using a low bandpass Fourier filter with a cut-offfrequency of $0.35\,\mathrm{nm}^{-1}$.

$$F_{BK}(T) = \frac{1}{V(T)}\left(\frac{2n(T)^2+1}{n(T)^2+2}\left(\frac{\varepsilon_r(T)-1}{\varepsilon_r(T)+1}-\frac{n(T)^2-1}{n(T)^2+2}\right)+\frac{3\left(n(T)^4-1\right)}{\left(n(T)^2+2\right)^2}\right) \tag{6.4}$$

Plots of the sum and of the difference of the wavenumber maxima vs. the different solvent polarity functions, according to Eqs. 6.5, 6.6 and 6.7 have to be prepared. For Eq. 6.7, which was introduced by Demissie et al. [7], it is possible to apply several solvent polarity functions F_X for the evaluation.

$$\tilde{\nu}_A(T)+\tilde{\nu}_F(T) = -\frac{2(\mu_e^2-\mu_g^2)}{3\varepsilon_0 hc}\cdot F_{BK}(T)+const. \tag{6.5}$$

$$\tilde{\nu}_A(T)-\tilde{\nu}_F(T) = -\frac{2(\mu_e-\mu_g)^2}{3\varepsilon_0 hc}\cdot F_{LM}(T)+const. \tag{6.6}$$

$$\tilde{\nu}_{A/E}(T) = \tilde{\nu}^0_{A/E}(T)-\frac{2\mu_{g/e}\left(\mu_e-\mu_g\right)}{3\varepsilon_0 hc}\cdot F_X(T) \tag{6.7}$$

From the slope of the linear regression of the data, the dipole moments can be calculated according to Eqs. 6.8, 6.9, 6.10 and 6.11.

$$\mu_e = \sqrt{\mu_g^2+\frac{3\varepsilon_0\cdot h\cdot c\cdot m_{BK}}{2}} \tag{6.8}$$

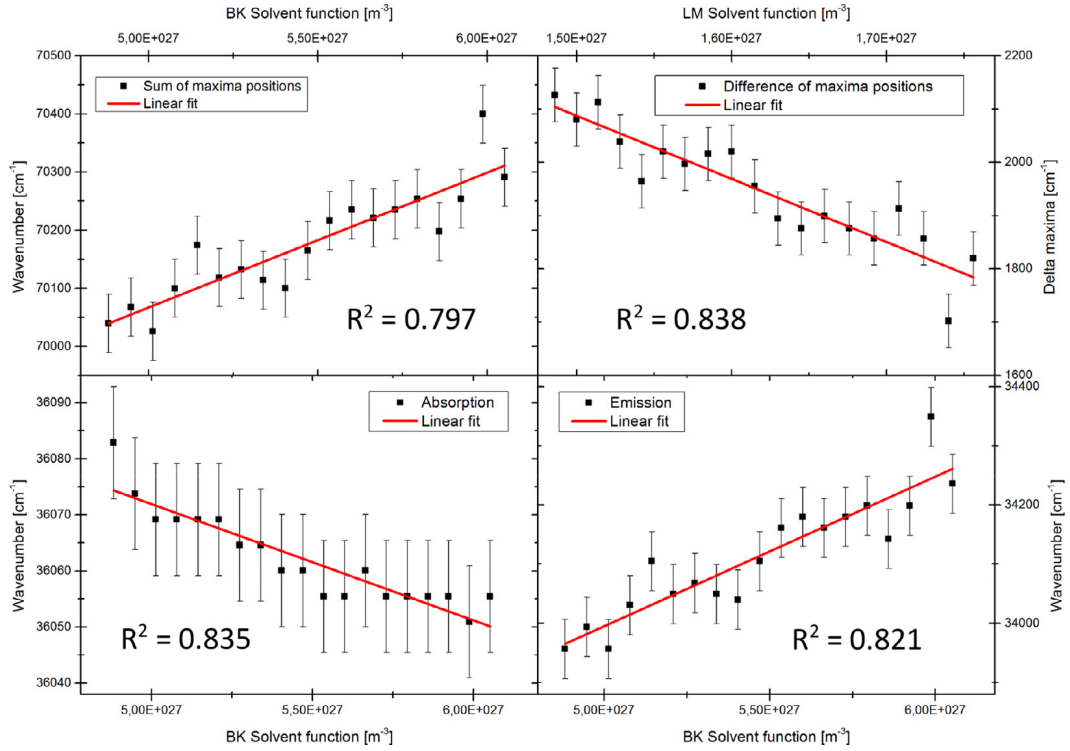

Figure 6.11.: Plots of maxima wavenumbers versus solvent polarity functions of Bilot-Kawski and Lippert-Mataga. The sample molecule is anisole with solvent ethyl acetate. R^2 for the goodness of the individual fits is shown in each graph.

$$\Delta\mu = \sqrt{\frac{3\varepsilon_0 \cdot h \cdot c \cdot m_{LM}}{2}} \tag{6.9}$$

$$\mu_g = \sqrt{\frac{3\varepsilon_0 hcm_A^2}{2(m_E - m_A)}} \tag{6.10}$$

$$\mu_1 = \sqrt{\frac{3\varepsilon_0 hcm_E^2}{2(m_E - m_A)}} \tag{6.11}$$

Here, m_x ($x = LM$, BK, A, E) are the slopes of the diagrams according to Eqs. 6.5, 6.6 and 6.7, respectively, $\varepsilon_0$is the permittivity of the vacuum, $h$is Planck's constant, $c$is light speed in vacuum and μ_x ($x = g$, e) are the dipole moments of ground (g) and excited state (e). Examples for plots, according to Eqs. 6.5, 6.6 and 6.7, are shown in Figs. 6.11 and 6.12.

Since the dipole moment changes upon excitation are larger for Q1 compared to anisole, the fits perform better for the former and show a much better R^2. The resulting changes of dipole moments of anisole and Q1 upon electronic excitation from the plots of Figs. 6.11 and 6.12 and Eqs. 6.8, 6.9, 6.10 and 6.11 are summarized in Tab. 6.1 along with calculated dipole moment changes from ab initio calculations and the gas phase value (for anisole) from

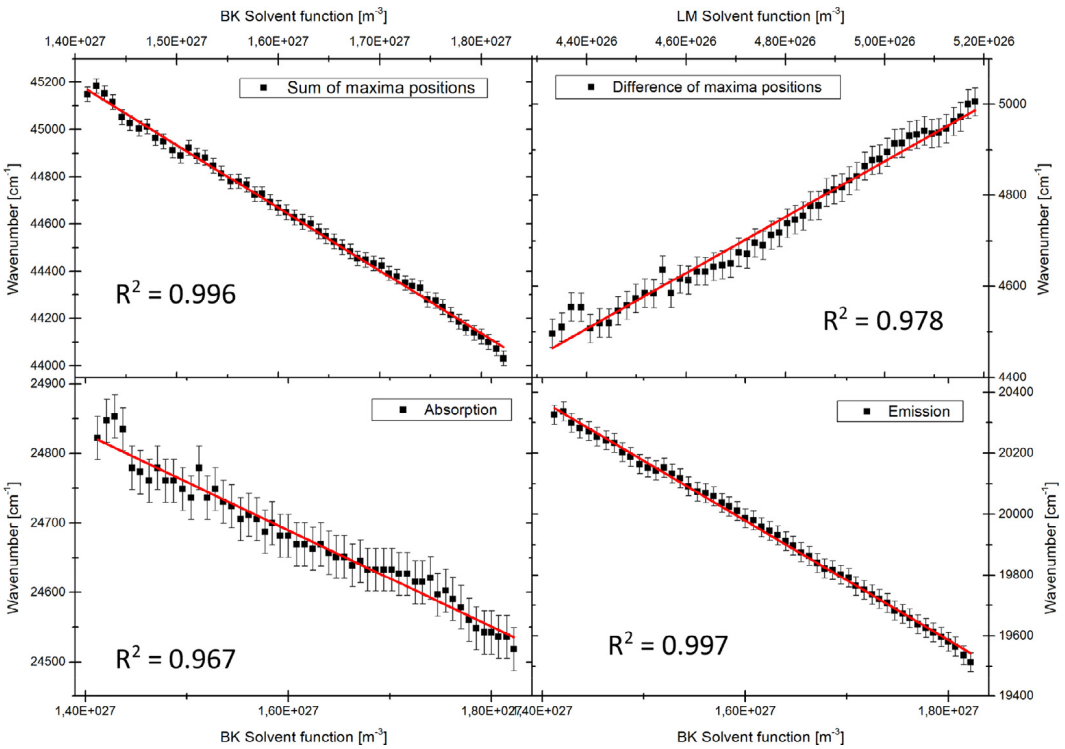

Figure 6.12.: Plots of maxima's wavenumbers versus solvent polarity functions of Bilot-Kawski and Lippert-Mataga. The sample molecule is 2-((4-methoxyphenyl)ethynyl)-3-(1-methyl-1H-indol-3-yl)quinoxaline with solvent ethyl acetate. R^2 for the goodness of the individual fits is shown in each graph.

Table 6.1.: Changes of the permanent dipole moments of anisole and Q1 upon electronic excitation in Debye according to the evaluations discussed in the main text. Although Demissie's method allows for an independent determination of the ground state dipole moment, we evaluated the change of dipole moment for anisole using the much more exact value from microwave Stark spectroscopy [46].

	Bilot-Kawski	Demissie (BK)	Demissie (LM)	Lippert-Mataga	CC2/cc-pVTZ	Gas phase
Anisole	1.5(3)	1.2(3)	3.2(6)	5.4(4)	0.97	0.93(1)
Q1	5.27(3)	5.49(11)	8.3(5)	12.1(2)	6.48	-

rotationally resolved electronic Stark spectroscopy [8].

Considering the large difference of both molecular systems, we see a quite uniform pattern emerging: Evaluation of the dipole moment changes using Bilot-Kawski's or Demissie's methods yields good results if the Bilot-Kawski solvent polarity function is used. Evaluation of dipole moment changes using Lippert-Mataga's plots, either in the original version, or as solvent polarity function in Demissie's method exaggerates the dipole moment change considerably. The remaining discrepancies between the results from the referencing methods, CC2/cc-pVTZ and gas phase measurement, and the results from thermochromic spectroscopy can be traced back to the expectable change of the dipole angle during electronic excitation. The change of the dipole orientation is by now not considered in the applied theories.

However, measuring thermochromic absorption and emission spectra, combined with exact determination of all necessary temperature dependent parameters, yields results, which show a clean linear trend with small deviations. Therefore, a reasonable evaluation can be facilitated for the dipole moments, depending on the used evaluation method. By comparison to linear plots from solvatochromic measurements from the literature the improvement of the dipole determination from thermochromic rather than solvatochromic shifts is obvious. Also the accuracy of results, compared with *ab initio* calculations or reasonable reference methods, is increased compared to different works from the past.

Supplementary material and/or Additional information: M. M. Lindic, M. Zajonz, M.-L. Hebestreit, M. Schneider, W. L. Meerts and M. Schmitt, Data in Brief 21 (2018) 313–315

6.9. Acknowledgements

Financial support of the Deutsche Forschungsgemeinschaft via grants SCHM1043/12-3 and SCHM1043/16-1 is gratefully acknowledged.

6.10. Own share in the publication

The content of this chapter has already been published in the journal *MethodsX*, **7**, 101101, 2020 under the title *Determination of excited state dipole moments in solution via thermochromic methods* written by Mirko Matthias Lindic, Matthias Zajonz, Marie-Luise Hebestreit, Michael Schneider, W. Leo Meerts and Michael Schmitt.

My own share in the publication sums up to $70\,\%$ and consists of formal analysis, software, investigation, methodology, writing - original draft, writing - review and editing.

7. Article - Anisole

Excited state dipole moments of anisole in gas phase and solution

Mirko Matthias Lindic,[a] Matthias Zajonz,[a] Marie-Luise Hebestreit,[a] Michael Schneider,[a] W. Leo Meerts,[b] and Michael Schmitt[1a]

[a] Heinrich-Heine-Universität, Institut für Physikalische Chemie I, D-40225 Düsseldorf, Germany, E-mail:mschmitt@hhu.de.
[b] Radboud University, Institute for Molecules and Materials,
Felix Laboratory, Toernooiveld 7c, 6525 ED Nijmegen, The Netherlands.

7.1. Abstract

The excited state dipole moment of anisole has been determined in the gas phase from electronic Stark spectroscopy and in solution using thermochromic shifts in ethyl acetate. Electronic excitation increases the anisole dipole moment in the gas phase from 1.26 Debye in the ground state to 2.19 Debye in the electronically excited singlet state, leaving the orientation of the dipole moment practically unchanged. These values are compared to solution phase dipole moments. From variation of the fluorescence emission and absorption maxima with temperature, an excited state dipole moment of 2.7 Debye was determined. Several solvent polarity functions have been used in combination with experimentally determined cavity volumes at the respective temperatures. Both gas phase and condensed phase experimental dipole moments are compared to the results of *ab initio* calculations at the CC2 level of theory, using the cc-pVTZ basis set for the isolated molecule and using the COnductor-like Screening MOdel (COSMO), implemented in Turbomole, for the solvated anisole molecule.

[1] mschmitt@hhu.de

7.2. Introduction

The use of dipole moments as measures for the distribution of electrons in molecules has successfully be applied for more than 100 years. The earliest designation of the concept of molecular dipoles goes back to Debye's paper of 1912 on a kinetic theory of insulators.[72] However, this concept is not uncontroversial, since for larger molecules higher terms of the multipole expansion may be needed to properly describe molecular electronic properties. The success of the model can be traced back to the fact, that the overall dipole moment can be constructed from atomic dipoles, which are centered at the atomic positions and point along the chemical bonds, the so called bond dipoles.[51] The main problem concerning the molecular dipole moments, however, results from the fact, that their experimental determination should preferably be performed in the vapor phase to avoid interaction with the surrounding solvent. Many substances of interest decompose thermally, before their vapor pressure is high enough to allow for the experimental determination of the dipole. In these cases determination of the molecular dipole in dilute solutions is the only possibility. For the ground state several schemes exist, to obtain vapor-phase dipole moments from solution measurements.[73] They can be applied to strongly dilute solutions with nonpolar solvents. For the excited state, the situation is much more complex, since mutual solvent-solute interactions are a prerequisite in many techniques used for the determination of excited state dipole moments in solution.[74]

The knowledge of excited state dipole moments of molecules and of transition dipole moments connecting ground and excited states are important prerequisites for the understanding of resonance energy transfer processes like Förster Resonant Energy Transfer (FRET)[9, 75] and for molecular excitonic interactions.[76] While determination of permanent dipole moments in the electronic ground state of molecules is straightforward using microwave spectroscopy, exact dipole moments in electronically excited states are much more difficult to be determined. The probably most exact method is rotationally resolved electronic Stark spectroscopy.[77–81] This method has the advantage to yield both the ground and excited state dipole moments with an accuracy of about 1 %. The applied field strengths in these experiments are -depending on the size of the dipole moment- in the range of 100 - 1000 V/cm, what allows to treat the electric field induced changes to the rotational Hamiltonian as perturbations. However, this method can only be applied to isolated molecules in the gas phase at considerably low temperatures as obtained in molecular beams.

Historically, excited-state dipole moments in solution have been determined from solvatochromic shifts in solvents of different dielectric constants [61, 69] or from electro-optical absorption measurements[27, 82]. The evaluation of excited state dipole moments from solvatochromic shifts applies the so called Lippert-Mataga equation[1, 2]. The derivation

of this equation is based on Onsager's reaction field[4], which assumes the fluorophore to be a point dipole, which is located in the center of a spherical cavity. The cavity of radius a is formed by the homogeneous and isotropic solvent with the permittivity ϵ. The molecular dipole moment of the solute induces a dipole in the homogeneous solvent. This (reaction) dipole is the source of an electric field, which interacts with the molecular dipole, leading to an energetic stabilization. In the case of anisole, the cavity volume is about $1.79{\cdot}10^{-28}$ m^3 equivalent to a cavity radius of $4.2{\cdot}10^{-10}$ m. With a reaction dipole of 1.3 Debye, a field strength in the cavity of $5{\cdot}10^8$ V/m is reached. This field strength is more than 1000 times higher than the fields used in gas phase Stark spectroscopy.

This model already defines the limits of the method, since the original Lippert-Mataga theory does not account for non-spherical cavities, expanded dipoles in the cavity, specific interactions between the solute and the solvent like hydrogen bonds etc., and reorientation of the molecular dipole upon electronic excitation. Numerous improvements to the basic Lippert-Mataga theory have been introduced over the years, like the utilization of multi-parameter solvent polarity scales, which quantitatively reproduce solvent-solute interactions. These interactions are modulated through linear solvation energy relationships [83, 84]. An improved model by Abe also allows for a determination of the angle θ between the ground and excited state dipole moments[85]. All improvements add several new parameters, which are mainly empirical, like scaling factors for the solvent hydrogen solvent bond donor acidities and basicities, empirical polarity parameters of the solvents, and the volume variation of cavity with solvent polarity to account for non-spherical cavities.[7] Apart from improvements of the solvent functions used, Kawski introduced the method of thermochromic shifts in spite of solvatochromic shifts, in order to minimize the effect of different solvents on the Onsager radius. [6]

The structures of the anisole chromophore in the ground and lowest excited singlet states have been studied by high resolution spectroscopy before using rotationally resolved fluorescence excitation spectroscopy in the groups of Becucci[86] and Pratt. [87] Also, triply deuterated anisole (deuterated at the methoxy group OCD_3) was studied in high resolution by Pasquini *et al.*. [88] However, exact dipole data of anisole are available only for the ground state from a microwave Stark experiment. [46]

In the present study, excited state dipole moments of anisole from electronic Stark spectroscopy in the gas phase are compared to those measured in solution using thermochromic shifts. Anisole was chosen as test molecule, because it combines several advantages for this comparison. First, it is small enough to facilitate evaporation and gas phase spectroscopic investigations. Secondly, the angle of the dipole moment of anisole in the molecular frame

stays nearly constants upon electronic excitation. Third, it dissolves well in aprotic solvents, to minimize effects due to hydrogen bond formation between solute and solvent. The final goal is to extend and calibrate methods for the determination of dipole moments of large molecules in solution to the limit in which they cannot be determined anymore by means of gas phase spectroscopy.

7.3. Computational Methods

7.3.1. Quantum chemical calculations

Structure optimizations were performed employing Dunning's correlation consistent polarized valence triple zeta (cc-pVTZ) basis set from the TURBOMOLE library. [89, 90] The equilibrium geometries of the electronic ground and the lowest excited singlet states were optimized using the second order approximate coupled cluster model (CC2) employing the resolution-of-the-identity (RI) approximation. [91–93] Dipole moments are calculated as first derivatives of the respective energy with respect to an external field at the CC2 level of theory. The Conductor-like Screening Model (COSMO)[94], which is implemented in the ricc2 module of the TURBOMOLE package, was used for the calculation of ground and excited state dipole moments in solution.

7.3.2. Fits of the rovibronic spectra using evolutionary algorithms

Evolutionary algorithms have proven to be perfect tools for the automated fit of rotationally resolved spectra, even for large molecules and dense spectra. [95–98] Beside a correct Hamiltonian to describe the spectrum and reliable intensities inside the spectrum, an appropriate search method is needed. Evolutionary strategies are powerful tools to handle complex multi-parameter optimizations and find the global optimum. For the analysis of the presented high-resolution spectra we used the covariance matrix adaptation evolution strategy (CMA-ES), which is described in detail elsewhere. [99, 100] In this variant of global optimizers mutations are adapted via a covariance matrix adaptation (CMA) mechanism to find the global minimum even on rugged search landscapes that are additionally complicated due to noise, local minima and/or sharp bends. The analysis of the rotationally resolved electronic Stark spectra is described in detail in ref. [71] The fit of the rovibronic Stark spectra with $\Delta M = 0$ and $\Delta M = \pm 1$ selection rules can be fit simultaneously, improving both the accuracy and reducing the correlation between the fitted parameters. Additionally, we implemented the use of boundary conditions in the simultaneous fits of Stark spectra of

different isotopologues. Since the absolute values of the dipole moments $|\mu|$ in the ground and excited state depend only weakly on the different isotopologues, the parameters $|\mu^g|$ and $|\mu^e|^2$ can be set equal leaving only the components $|\mu_a^{g,e}|$(isotopologue 1), $|\mu_a^{g,e}|$(isotopologue 2), $|\mu_b^{g,e}|$(isotopologue 1) and $|\mu_b^{g,e}|$(isotopologue 2) to be fit.

7.3.3. Evaluation of excited state dipole moments from thermochromic shifts

The limitations utilizing solvatochromic shifts for determination of excited state dipole moments have been discussed thoroughly.[1–3, 6, 7, 85, 101] To circumvent the problems of non-constant cavity sizes when using different solvents, Kawski proposed to use the influence of the temperature on the permittivity and index of refraction of the solvent to induce the spectral shifts of the solutions. Still, the problem remains, that small variations of the Onsager radius result in large errors of the excited state dipole moments, since the Cavity radius enters the Lippert-Mataga [1, 2] and the Bilot-Kawski [3, 6] equations in the third power. Therefore, Demissie[7] proposed using the real cavity volume instead of a spherical cavity calculated from Onsager radius.[4] The real cavity volume is determined experimentally from concentration dependent density measurements which are evaluated using eq. 7.1.

$$\frac{1}{\rho} = \frac{1}{\rho^*} + \left(\frac{V_m}{M} - \frac{1}{\rho^*}\right) \cdot w \tag{7.1}$$

ρ is the measured density of the solution, ρ^* is the density of the pure solvent and w is the mass fraction of the solvate. The slope of the graph $\frac{1}{\rho}(w)$ gives the cavity volume per mole V_m of the solvate. This procedure has been applied at all temperatures, for which spectral shift data were obtained.

The original equation for solvatochromic shifts according to Lippert-Mataga can be used for thermochromic shifts as well, when the temperature dependence of ϵ and n is known:

$$\tilde{\nu}_A - \tilde{\nu}_F = -\frac{2(\mu_e - \mu_g)^2}{4\pi\varepsilon_0 hca^3} \cdot F_{LM} + const. \tag{7.2}$$

where ε_0 is the vacuum permittivity, h the Planck constant, c the lights speed, a the Onsager

[2]The superscript "g" and "e" refer to the electronic ground and excited state, respectively.

cavity radius, and F_{LM} the solvent polarity function according to Lippert and Mataga[1, 2]:

$$F_{LM} = \frac{\varepsilon - 1}{2\varepsilon + 1} - \frac{1}{2}\left(\frac{n^2 - 1}{2n^2 + 1}\right) \tag{7.3}$$

The modified equation from Kawski [6] has also been used:

$$\tilde{\nu}_A + \tilde{\nu}_F = -\frac{2(\mu_e^2 - \mu_g^2)}{4\pi\varepsilon_0 hca^3} \cdot F_{BK} + const. \tag{7.4}$$

where F_{BK} the solvent polarity function according to Bilot and Kawski F_{BK} [3]:

$$F_{BK} = \left[\frac{\varepsilon - 1}{\varepsilon + 2} - \frac{n^2 - 1}{n^2 + 2}\right]\frac{2n^2 + 1}{2(n^2 + 2)} + \frac{3}{2}\left[\frac{(n^4 - 1)}{(n^2 + 2)^2}\right] \tag{7.5}$$

with ε as solvent permittivity and n as refractive index of the solvent.

Using the cavity volume per mole V_m, equations (7.4) and (7.5) can be rearranged to include the single molecule cavity volume $V = 4/3\pi a^3 = V_m/N_A$ into the solvent polarity function:

$$F_{BKD} = \frac{1}{V}\left(\frac{2n^2 + 1}{n^2 + 2}\left(\frac{\varepsilon - 1}{\varepsilon + 1} - \frac{n^2 - 1}{n^2 + 2}\right) + \frac{3(n^4 - 1)}{(n^2 + 2)^2}\right) \tag{7.6}$$

The modified thermochromic equation, which will be used in the evaluation of the dipole moments according to Demissie[7] is:

$$\tilde{\nu}_{A/E}(T) = \tilde{\nu}^0_{A/E}(T) - \frac{2\mu_{g/e}\,(\mu_e - \mu_g)}{3\varepsilon_0 hc} \cdot F_{BKD}(T) \tag{7.7}$$

with

$$F_{BKD}(T) = \frac{1}{V}\left(\frac{2n(T)^2 + 1}{n(T)^2 + 2}\left(\frac{\varepsilon(T) - 1}{\varepsilon(T) + 1} - \frac{n(T)^2 - 1}{n(T)^2 + 2}\right) + \frac{3(n(T)^4 - 1)}{(n(T)^2 + 2)^2}\right) \tag{7.8}$$

The temperature dependent values of ε and n were determined by Gryczyński and Kawski [5]. The slope m of $(\tilde{\nu}_A + \tilde{\nu}_F)$ versus F_{BK} using the experimentally determined ground state dipole moment now gives the excited state dipole moment (from equation 7.4 and 7.5):

$$\mu_e = \sqrt{\mu_g^2 + \frac{3\varepsilon_0 \cdot h \cdot c \cdot m}{2}} \tag{7.9}$$

Using equations (7.7) and (7.8), the slopes m_A and m_F of the respective plots of $\tilde{\nu}_A(T)$ and $\tilde{\nu}_E(T)$ vs. the solvent polarity functions $F_{BK}(T)$ or $F_{BKD}(T)$ yield the dipole moments of ground and excited state independently:

$$\mu_g = \sqrt{\frac{3\varepsilon_0 hcm_A^2}{2(m_F - m_A)}} \tag{7.10}$$

$$\mu_e = \sqrt{\frac{3\varepsilon_0 hcm_F^2}{2(m_F - m_A)}} \tag{7.11}$$

7.4. Experimental Methods

7.4.1. Electronic Stark spectroscopy

Anisole ($\geq 98\%$) and d_3-anisole were purchased from Sigma-Aldrich and used without further purification. The sample was heated to 40°C and co-expanded with 200 - 300 mbar of argon into the vacuum through a 200 μm nozzle. After the expansion a molecular beam was formed using two skimmers (1 mm and 3 mm, 330 mm apart) linearly aligned inside a differentially pumped vacuum system consisting of three vacuum chambers. The molecular beam was crossed at right angles with the laser beam 360 mm downstream of the nozzle. To create the excitation beam, 10 W of the 532 nm line of a diode pumped solid state laser (Spectra-Physics Millennia eV) pumped a single frequency ring dye laser (Sirah Matisse DS) operated with Rhodamine 110. The light of the dye laser was frequency doubled in an external folded ring cavity (Spectra Physics Wavetrain) with a resulting power of about 25 mW. The fluorescence of the samples was collected perpendicular to the plane defined by laser and molecular beam using an imaging optics setup consisting of a concave mirror and two plano-convex lenses onto the photocathode of a UV enhanced photomultiplier tube (Thorn EMI 9863QB). The signal output was then discriminated and digitized by a photon counter and transmitted to a

PC for data recording and processing. The relative frequency was determined with a *quasi* confocal Fabry-Perot interferometer. The absolute frequency was obtained by comparing the recorded spectrum to the tabulated lines in the iodine absorption spectrum.[102] A detailed description of the experimental setup for the rotationally resolved laser induced fluorescence spectroscopy has been given previously. [103, 104]

To record rotationally resolved electronic Stark spectra, a parallel pair of electro-formed nickel wire grids (18 mesh per mm, 50 mm diameter) with a transmission of 95% in the UV was placed inside the detection volume, one above and one below the molecular beam - laser beam crossing with an effective distance of 23.49 $\pm$ 0.05 mm. [71] In this setup the electric field is parallel to the polarization of the laser radiation. With an achromatic $\lambda/2$ plate (Bernhard Halle, 240-380nm), mounted on a linear motion vacuum feedthrough, the polarization of the incoming laser beam can be rotated by 90° inside the vacuum.

7.4.2. Thermochromic shifts

The density ρ of the solution of anisole in ethyl acetate was measured at different mass fractions w in a temperature range of -10 °C and $+70$ °C with 2 ° C increment using a density meter (Anton Paar DMA4500M). The cavity volume is determined from the slope of the graph of $\frac{1}{\rho}$ vs. the mole fraction w at each temperature. A plot of the inverse density of the solution of anisole in ethyl acetate versus the weight fraction of anisole along with the linear fit of the data is shown in Figure S1 of the Ref.[57]

Absorption spectra of anisole, dissolved in ethyl acetate have been recorded in a temperature range of -10 °C and $+70$ °C with 5 °C increment using a Varian Cary 50 Scan UV spectrometer. A custom built coolable and heatable cell holder has been constructed using a pair of Peltier elements from Uwe Electronics GmbH. The hot side was cooled using a Julabo Corio 600F cooler with Thermal G as cooling liquid. The cell holder is mounted in a vacuum chamber to avoid condensation of water on the windows at low temperatures. Fluorescence emission spectra were recorded in a Varian Cary Eclipse spectrometer using the same cell holder as for the absorption measurements.

7.5. Results

7.5.1. Computational Results

The structures of anisole in the electronic ground and excited states have been optimized at the CC2/cc-pVTZ level of theory. The Cartesian coordinates of all optimized structures are given in Tables S5 and S6 of the Ref.[57]. Table 7.1 summarizes the results on structures and dipole moments of anisole along with the experimental results. The rotational constants as measures of the quality of the CC2/cc-pVTZ optimized structures in the ground and first electronically excited state agree well with the experimentally determined ones, cf. Table 7.1. The absolute permanent dipole moment of the isolated anisole molecule in the electronic ground state was calculated to 1.33 D. The projections of the dipole moment onto the inertial a and b-axes (cf. Figure 7.1) are calculated to be 0.64 D and 1.17 D, respectively.

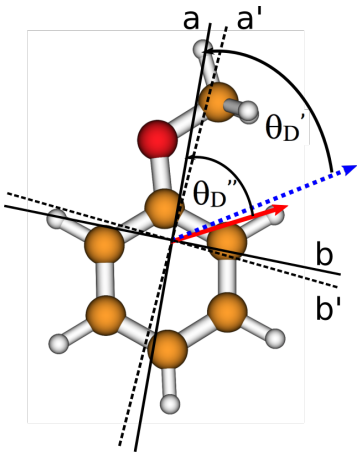

Figure 7.1.: Structure, inertial axis system and dipole moment in ground (red, straight) and first electronically excited singlet state (blue, dotted) of anisole. The dipole vector is drawn from negative to positive. The primed coordinate system (black, dashed) refers to the d_3 isotopologue. The positive direction of the dipole moment angle θ''_D in the ground state and θ'_D in the excited state are shown.

From these projections an angle θ''_D of $+61°$ of the dipole moment with the inertial a-axis is obtained in the electronic ground state. A positive sign of this angle means an anticlockwise rotation of the dipole moment vector onto the main inertial a-axis for the molecular orientation, shown in Figure 7.1. For the lowest electronically excited singlet state of anisole, dipole moment components of 1.20 and 1.95 D with respect to the inertial a and b-axes are calculated, corresponding to an angle θ'_D of $+58°$. Thus, the angle of the dipole moment within the molecular frame stays nearly constant upon electronic excitation.

Table 7.1 also reports the results for the triply deuterated d_3-anisole. In first order, the dipole moment of the deuterated compound will be the same as of the undeuterated one. However, due to the larger mass of the -CD_3 group, the inertial a axis is rotated towards the -CD_3

group. This opens the possibility to determine the absolute orientation of the dipole moment experimentally. Dipole moment components from Stark measurements have an indeterminacy of the sign of the components, since only the projections onto the inertial axes are obtained. Tilting the axis via isotopic substitution removes the indeterminacy partially, since for both signs of μ_a and μ_b positive, the angle between the dipole moment vector and the a axis decreases, while for different signs of μ_a and μ_b it increases. Thus, the dipole moment points from the origin to the first or third quadrant, if the angle gets smaller upon deuteration.

7.5.2. Experimental Results

Permanent dipole moments of anisole from Stark spectra

The rotationally resolved electronic spectrum of anisole has been presented and analyzed before in the groups of Becucci and Pratt.[86, 87] However, no Stark measurements have been performed until now, and the dipole moment in the excited singlet state of the isolated molecule is not known experimentally. We measured and analyzed the electronic Stark spectrum of anisole shown in Figure 7.2.

The dipole moments have been obtained from a combined fit to the Stark spectra in parallel as well as in perpendicular arrangement of laser polarization and electric field.[71] The fit using the CMA-ES algorithm yielded the parameters given in Table 7.1. The ground state dipole components, which have been obtained by Desyatnyk *et al.* [46] using microwave Stark spectroscopy, have been kept fixed in our fit, due to the inherently larger accuracy of the MW values. Experimental rotational constants and dipole moments of both electronic states are in good agreement with the results for the CC2//cc-pVTZ optimized structure. From the ratio of intensities of the a and the b lines of anisole, the angle of the excited state dipole moment with the inertial a axis can be determined to be 56.7° in reasonable agreement with the theoretical value from CC2/cc-pVTZ calculations of 61°. The results of the fits are compiled in Table 7.1.

Electronic Stark spectra of d_3-anisole

Electronic Stark spectroscopy yields the projections of the dipole moments in both electronic states onto the inertial axes. No information however, is obtained regarding the sign of the dipole components. The calculated permanent dipole moment of anisole in the electronic ground state, shown in Figure 7.1 has both dipole components (μ_a and μ_b) positive. i.e. the dipole moment vector points to the first quadrant in the chosen orientation of Figure

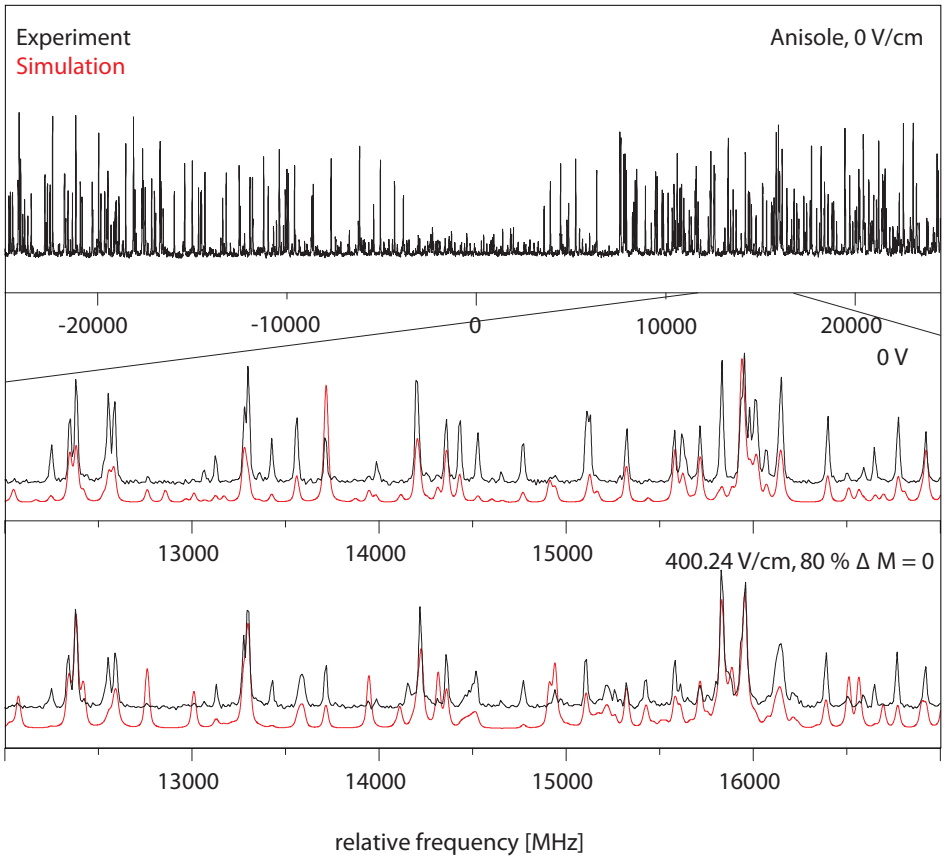

Figure 7.2.: Rotationally resolved electronic Stark spectrum of the electronic origin of anisole at 36384.07 cm^{-1}. The upper trace shows the experimental spectrum at zero-field. The second trace shows a zoomed in portion of the spectrum along with the simulated spectrum, using the molecular parameters from Table 7.1. The lowest trace contains the Stark spectrum at a field strength of 400.24 V/cm with electric field direction and electromagnetic field parallel to each other, hence with $\Delta M = 0$ selection rules.

Table 7.1.: Calculated rotational constants, permanent electric dipole moments μ and their components μ_i along the main inertial axes i=a, b, c of anisole compared to the respective experimental values. Doubly primed parameters belong to the electronic ground and single primed to the excited state. θ_D is the angle of the dipole moment vector with the main inertial a-axis. A positive sign of this angle means a clockwise rotation of the dipole moment vector onto the main inertial a-axis.
[1] Set to the microwave values from Ref. [46].
[2] Adiabatic excitation energy, including ZPE corrections.
[3] From Ref. [105]
[4] [1] = Kawski; [2] = Lippert-Mataga; [3] = Demissie with Bilot-Kawski polarity function; [4] = Demissie with Lippert-Mataga polarity function. For details see text.

	theory			experiment					
	isolated		COSMO	gas phase		thermochromic shifts[4]			
	h_3	d_3	h_3	h_3	d_3	[1]	[2]	[3]	[4]
A'' / MHz	5023	4846	-	5028.84414(19)[1]	4850.68(8)	-	-	-	-
B'' / MHz	1579	1448	-	1569.364308(68)[1]	1438.81(2)	-	-	-	-
C'' / MHz	1211	1131	-	1205.825614(41)[1]	1126.03(2)	-	-	-	-
μ_a'' / D	+0.64	+0.66	-	±0.6937[1]	±0.79(6)	-	-	-	-
μ_b'' / D	+1.17	+1.15	-	±1.0547[1]	±0.98(3)	-	-	-	-
μ'' / D	1.33	1.33	1.12	1.2623[1]	1.2623	1.17[3]	1.17[3]	0.19(3)	0.40(5)
θ_D'' / °	+61	+60	-	±56.7	±51.3	-	-	-	-
A' / MHz	4777	4621	-	4795.17(13)	4636.82(11)	-	-	-	-
B' / MHz	1567	1436	-	1555.68(4)	1310.97(3)	-	-	-	-
C' / MHz	1189	1111	-	1184.45(3)	934.39(3)	-	-	-	-
μ_a' / D	+1.20	+1.23	-	±1.59(3)	±1.76(1)	-	-	-	-
μ_b' / D	+1.95	+1.94	-	±1.50(3)	±1.30(2)	-	-	-	-
μ' / D	2.30	2.30	2.01	2.19(4)	2.19	2.7(2)	6.6(3)	2.4(2)	4.9(3)
θ_D' / °	+58	+57	-	±43.4	±36.5	-	-	-	-
ν_0 / cm^{-1}	37179[2]	37184[2]	-	36384.07(1)	36387.31(1)	-	-	-	-

7.1. The sign however, can be obtained from the evaluation of Stark spectra of isotopically substituted anisole. We chose the methoxy-deuterated isotopologue, since the effect of hydrogen-deuterium exchange gives the largest possible isotopic ratio and the effect on the inertial axes of the parent molecule will be large enough to be measured reliably. The d_3-anisole spectrum has been fit together with the h_3-anisole under the constraint of equal absolute values of the dipole moment $|\mu|$ in both states. This assumption seems to be justified, since in medium sized molecules dipole moment changes of 0.001 to 0.01 D are found upon hydrogen−deuterium exchange are reported.[106] The so determined dipole moment components μ_a and μ_b in the ground state are equivalent to an angle of the dipole moment with the inertial a-axis of 51.3°. This decrease compared to the value of the h_3 isotopologue matches the predicted change from the *ab initio* calculations. Inspection of Figure 7.1 shows, that the inertial axes will be rotated towards the dipole moment vector upon H↔D interchange, leading to the observed decrease of the angle θ_D. The experimentally determined decrease is considerably larger, than the predicted ones, using the CC2 optimized structures, what is probably due to the limitations of the above model.

Permanent dipole moments of anisole from thermochromic shifts

In a first step, we determined the cavity volume of anisole in ethyl acetate from equation 7.1. Figure S1 of the Ref.[57] shows the plot of the inverse density of the solution of anisole in ethyl acetate versus the weight fraction of the solute at 293 K. From the slope of the graph, a cavity volume of $1.79{\cdot}10^{-28}$ m^3 at 293 K could be determined. Subsequently, the cavity volume was determined at all temperatures, for which absorption and emission spectra have been taken. The plot of the molar volumes vs. the temperature is shown in Figure 7.3.

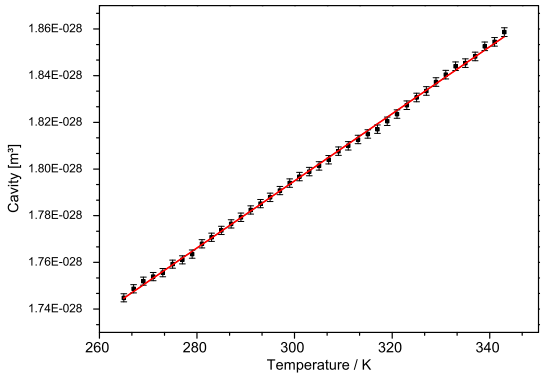

Figure 7.3.: Plot of the cavity volumes versus temperature of anisole in ethyl acetate along with the linear fit of the data.

The absorption and fluorescence emission spectra of anisole, dissolved in ethyl acetate at temperatures between 258 K and 348 K are shown in Figure 7.4. For the evaluation of the maxima of the absorption spectra, they were fit with a set of multiple Gauss functions. We used the lowest energy local maximum of the absorption spectra as $\tilde{\nu}_A$ and the overall maximum of the emission spectra as $\tilde{\nu}_F$ (see Fig. 7.4).

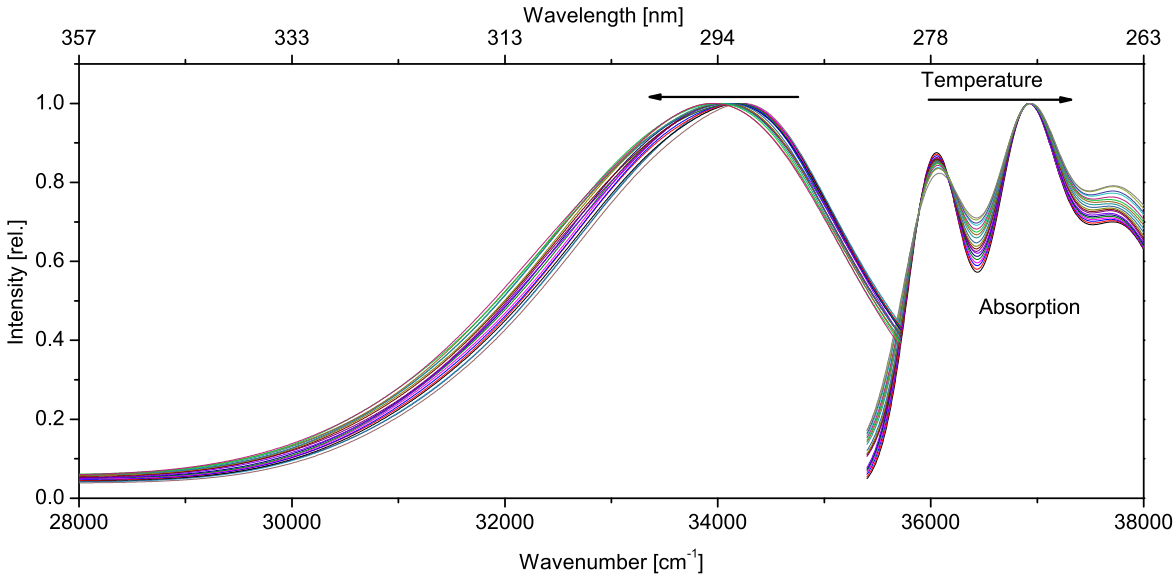

Figure 7.4.: Absorption and emission spectra of anisole in ethyl acetate between 258 K and 348 K. The inset shows an enlarged portion of the emission spectra

Several approaches to the changes of the dipole moments upon electronic excitation have been tested. Following equation 7.4, the sum of wavenumbers $\tilde{\nu}_A + \tilde{\nu}_F$ is plotted versus calculated solvent polarity function F_{BK}, as shown in Figure 7.5. The excited state dipole moment can be calculated from its slope m of this plot, using the known ground state dipole moment as shown in equation 7.9. Using the experimentally determined ground state dipole moment of 1.17 D, the excited state dipole moment is determined to be 2.7(2) D using the experimental molar cavity volume and the solvent polarity function of Bilot and Kawski (equation 7.6) ([1] in Table 7.1).

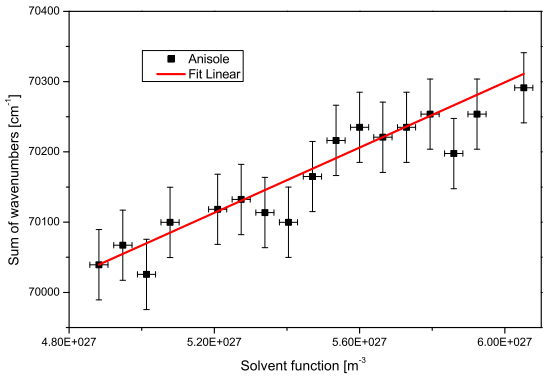

Figure 7.5.: Plot of $\tilde{\nu}_A + \tilde{\nu}_F$ versus calculated polarity function F_{BK}

Application of the original Lippert-Mataga-Plot ([2] in Table 7.1), an excited state dipole moment of 6.6(3) D is obtained. The modified thermochromic equation according to Demissie

with the Bilot-Kawski solvent polarity function ([3] in Table 7.1) allows for an independent determination of the ground and excited state dipole moments. It yields 0.19(3) D for the ground state and 2.4(2) D for the electronically excited state. The same equation, but with the Lippert-Mataga solvent polarity function ([4] in Table 7.1) values of 0.40(4) D and 4.9(3) D for ground and excited state, respectively are obtained.

7.6. Discussion

The excited state dipole moment of anisole has been determined from Stark spectroscopy of anisole and its triply (methyl group) deuterated isotopologue. The absolute value 2.30 D shows that the dipole moment increases by more than 1 D upon electronic excitation. The direction of the dipole changes only slightly upon electronic excitation as can be seen from the experimentally determined dipole components.

The comparison of the experimentally determined excited state dipole moments from electronic Stark measurements and from thermochromic shifts shows best agreement between the gas and condensed phase experimental values using the equations from Demissie's equation along with the Bilot and Kawski solvent function (model [3] in Table 7.1). However, the ground state dipole moment in solution, which is determined independently using these equations is completely wrong, when compared to the gas phase value from MW spectroscopy. The original Lippert-Mataga model fails completely in describing the excited state dipole moment correctly (model [2] in Table 7.1). The reason for this large discrepancy concerning the original Lippert-Mataga equation is described nicely by Kawski.[54] For a polarizability of the solute $\alpha = 0$ the solvent polarity function of Bilot and Kawski (ref. [3, 6]) passes over to the original Lippert-Mataga equation. It can thus safely be stated that it is the neglect of solvent polarizability in Lippert and Mataga's equation, which causes the deviations to the experiment.

Good agreement for the excited state is also obtained using Kawski's equations with the Bilot and Kawski solvent function (model [1] in Table 7.1). This method yields only changes of the dipole moment upon electronic excitation. The ground state dipole from solution measurements of Ref. [105] has been used.

The last test was performed in order to check, if the Lippert-Mataga solvent function gives reliable results using Demissie's modified equations (model [4] in Table 7.1). Clearly, in this case ground and excited state dipole moments deviate strongly from the gas phase values.

The cavity volume, which is calculated from the COSMO model, implemented in the ricc2

module of turbomole is determined to be $1.42 \cdot 10^{-28}$ m^3 while the experimental value from the measurement of the solution density as function of the weight fraction of anisole is $1.79 \cdot 10^{-28}$ m^3. The deviation of 21% might seem small, but since the cavity radius enters in the third power in the original Lippert-Mataga plots, its effect on the excited dipole moment is crucial.

Overall, the Bilot-Kawski method[3, 6], modified by Demissie[7] using real cavity volumes is the most promising method for determination of excited state dipole moments in solution. Furthermore it must be emphasized that this method yields through the extrapolation technique of the linear fit to the experimental data values, which correspond to the gas phase. This dipole moment, free from solute-solvent interactions, is the only which can be compared to the gas phase data and to ab initio calculations of the isolated molecule.[65] This work will be extended to molecules, which have a larger difference of the orientation of the dipole moments in ground and excited state. Since most molecules of interest will have arbitrary orientations, the extension of the Bilot-Kawski method in order to include the change of the angle of the dipole moment upon electronic excitation, like in the model of Abe.[85]

7.7. Conclusions

The exact determination of dipole moments of molecules in their excited states from rotationally resolved Stark experiments can only be performed with small and/or volatile molecules. Conceptionally and experimentally straightforward approaches like solvatochromic shifts in different solvents with a large variety of different solvent polarity functions have been used in numerous investigations over many decades. However, large deviations between vapor and condensed phase dipole moments have been found in the few thorough comparisons of molecules for which exact gas phase data are available. [63, 64]

Several reasons for the discrepancy between excited state dipole moments from Stark experiments in the gas phase and solvatochromic shifts have been identified. (i) Many theories, based on the original Onsager and Lippert-Mataga equations use the Onsager radius as free parameter. This radius is neither well known nor well defined, but enters the respective equations in cubic power, causing a large error. (ii) The inherently low resolution in solution makes the determination of spectral shifts cumbersome. (iii) Changing the solvent causes inevitably also changes in the interaction between solvent and solute and results in changes of the cavity radius of cavity volume. (iv) The large field strengths in solution lead to perturbative state mixing with nearby electronic states of different dipole moment. (v) For some molecules, the direction of the dipole moment changes upon electronic excitation what causes additional sources of errors.

The current scheme of thermochromic shifts with solvent polarity functions, that contain experimentally determined cavity volumes at each temperature, eliminates some of the above errors. Figure 7.3 clearly shows that the cavity volume (and therefore also the cavity radius, assuming a spherical cavity) is a linear function of the temperature. Correct application of the equations describing the thermochromic shifts, therefore demands for the consideration of the temperature dependence of the cavity volume.

Other sources of error have been minimized in the current study by choosing the molecule carefully. The direction of the dipole moment in anisole is only slightly altered upon electronic excitation. Furthermore, the energetically following excited singlet state (S_2) is 9200 cm^{-1} apart,[107] minimizing the problem of perturbative state mixing. In subsequent studies, we will systematically vary the molecules according to these limitations in order to allow for more exact dipole moment determinations of excited state in the condensed phase.

7.8. Acknowledgements

Financial support of the Deutsche Forschungsgemeinschaft via grant SCHM1043 12-3 is gratefully acknowledged. Computational support and infrastructure was provided by the "Center for Information and Media Technology" (ZIM) at the Heinrich-Heine-University Düsseldorf. We furthermore thank the Regional Computing Center of the University of Cologne (RRZK) for providing computing time on the DFG-funded High Performance Computing (HPC) system CHEOPS as well as support.

7.9. Own share in the publication

The content of this chapter has already been published in the *Journal of Photochemistry and Photobiology A: Chemistry*, **365**, 213-219, 2018 under the title *Excited state dipole moments of anisole in gas phase and solution* written by Mirko Matthias Lindic, Matthias Zajonz, Marie-Luise Hebestreit, Michael Schneider, W. Leo Meerts and Michael Schmitt.

My own share in the publication sums up to $50\,\%$ and consists of formal analysis, software, investigation, methodology, writing - original draft.

8. Comments on the article published in the Data in Brief journal

Unfortunately, the following article which was published in the Data in Brief journal again contains some mistakes. Firstly, in Tables S2 and S3 the measurement temperatures are not displayed correctly: The temperatures should originally increase by about $5\,\mathrm{K}$ per step, but all temperatures between $323\,\mathrm{K}$ and $348\,\mathrm{K}$ are exactly $100\,\mathrm{K}$ below the correct data. This could be considered a typo but should be mentioned anyway. Secondly, the promised data sources for Table S4 are completely missing in the online publication. In this thesis, the data are included as mentioned in the article.

To maintain the integrity of the article, the mentioned data are shown separately in the appendix / supplementary material.

9. Data in Brief

Additional data for evaluation of the excited state dipole moments of anisole

Mirko Matthias Lindic[a], Matthias Zajonz[a],Marie-Luise Hebestreit[a], Michael Schneider[a], W. Leo Meerts[b], Michael Schmitt[a,1]

[a] Heinrich-Heine-Universität, Institut für Physikalische Chemie I, D-40225 Düsseldorf, Germany [b] Radboud University, Institute for Molecules and Materials, Felix Laboratory, Toernooiveld 7c, 6525 ED Nijmegen, the Netherlands

Abstract

We present the temperature dependent density, fluorescence emission and absorption spectroscopic data, that are needed for an evaluation of the excited state dipole moment of anisole in ethyl acetate via the methods of thermochromic shifts. Furthermore, the rotationally resolved electronic Stark spectrum of anisole in the molecular beam is presented. Finally, the Cartesian coordinates of the CC2/cc-pVTZ optimized structures of anisole are given in bohr units. For details about the evaluation of the dipole moments from the given data, see the connected research article: Lindic et al. (2018)[8].

[1]Corresponding author, E-Mail: mschmitt@hhu.de

Specifications table

Subject area	*Physics, Chemistry*
More specific subject area	*Molecular Spectroscopy, Physical Chemistry*
Type of data	*Table, text file, graph, figure*
How data was acquired	*High resolution electronic Stark spectroscopy. (Home-built apparatus)* *Determination of the cavity size using a density meter (Anton Paar DMA4500M)* *Thermochromic shifts of emission (Varian Vary Eclipse) and absorption spectra (Varian Cary 50 Scan UV spectrometer)*
Data format	*Raw and analyzed*
Experimental factors	*The chemicals used were of spectroscopic grade*
Experimental features	*Gas phase excited state dipole moments on anisole are obtained from CW rotationally resolved electronic Stark spectra in a molecular beam.* *Solution values are obtained from thermochromic shifts of the fluorescence emission and absorption spectra of anisole in ethyl acetate*
Data source location	*Data might be obtained in electronic form from the authors*
Data accessibility	*Data are contained in this article*

Value of the data

- Temperature dependent absorption and emission data can be used for alternative evaluation schemes for dipole moments etc.
- The temperature dependent density data can be used for own determinations of cavity sizes.
- The ab initio structures give the optimized structures at CC2/cc-pVTZ level of theory and can be used as good starting geometried for other levels of theory.

9.1. Data

- Fig. S1: Plot of the inverse density of the solution of anisole in ethyl acetate versus the weight fraction of anisole at $293\,\mathrm{K}$ along with the linear fit of the data.
- Fig. S2: Rotationally resolved electronic Stark spectrum had been obtained before of d3-anisole at $36\,387.31\,\mathrm{cm}^{-1}$. The field free spectrum had been obtained before by

Pasquini et al. [88].

- Table S1: Measured density of the solution of anisole in ethyl acetate versus the weight fraction between 0 and 0.013 of the solute between $258\,\mathrm{K}$ and $348\,\mathrm{K}$. The densities are given as $\mathrm{kg\,m^{-3}}$.
- Table S2: Absorption spectra (in wavenumber) of anisole in ethyl acetate between $258\,\mathrm{K}$ and $348\,\mathrm{K}$ in steps of $5\,\mathrm{K}$. These data are available as Table S2.doc and Table S2.csv. The raw data (in nm) are available as Table 2.dat
- Table S3: Emission spectra (in wavenumber) of anisole in ethyl acetate between $258\,\mathrm{K}$ and $348\,\mathrm{K}$ in steps of $5\,\mathrm{K}$. These data are available as Table S3.doc and Table S3.csv. The raw data (in nm) are available as Table 3.dat
- Table S4: Linearized laser induced fluroescence Stark spectrum of anisole at an electric field strength of $819.09\,\mathrm{V\,cm^{-1}}$. The first column gives the relative frequeny in $1\,\mathrm{MHz}$ increment, the second column the relative intensities.
- Table S5: Cartesian coordinates of anisole S_0 in Bohr units from the CC2/cc-pVTZ calculations using the Turbomole program package [89–93].
- Table S6: Cartesian coordinates of anisole S_1 in Bohr units from the CC2/cc-pVTZ calculations using the Turbomole program package [89–93].

9.2. Experimental design, materials and methods

The density ρ of the solution of anisole in ethyl acetate was measured at different mass fractions w in a temperature range of $263\,\mathrm{K}$ and $343\,\mathrm{K}$ with an increment of $2\,\mathrm{K}$ using a density meter (Anton Paar DMA4500M). The cavity volume is determined from the slope of the graph of ρ^{-1} vs. the mole fraction w at each temperature [8]. A plot of the inverse density of the solution of anisole in ethyl acetate versus the weight fraction of anisole along with the linear fit of the data is shown in Fig. S1.

Absorption spectra of anisole, dissolved in ethyl acetate have been recorded in a temperature range of $-10\,^{\circ}\mathrm{C}$ and $70\,^{\circ}\mathrm{C}$ with $5\,^{\circ}\mathrm{C}$ increment using a Varian Cary 50 Scan UV spectrometer [8]. A custom built coolable and heatable cell holder has been constructed using a pair of Peltier elements from Uwe Electronics GmbH. The hot side was cooled using a Julabo Corio 600F cooler with Thermal G, as cooling liquid. The cell holder is mounted in a vacuum chamber to avoid condensation of water on the windows at low temperatures. Fluorescence

emission spectra were recorded in a Varian Cary Eclipse spectrometer using the same cell holder as for the absorption measurements.

Acknowledgements

Financial support of the Deutsche Forschungsgemeinschaft via Grant SCHM1043 12-3 is gratefully acknowledged. Computational support and infrastructure was provided by the "Center for Information and Media Technology" (ZIM) at the Heinrich-Heine-University Düsseldorf. We furthermore thank the Regional Computing Center of the University of Cologne (RRZK) for providing computing time on the DFG-funded High Performance Computing (HPC) system CHEOPS as well as support.

Transparency document. Supplementary material

Transparency document associated with this article can be found in the online version at https://doi.org/10.1016/j.dib.2018.09.110.

9.3. Own share in the publication

The content of this chapter has already been published in the journal *Data in Brief*, **21**, 313-315, 2018 under the title *Additional data for evaluation of the excited state dipole moments of anisole* written by Mirko Matthias Lindic, Matthias Zajonz, Marie-Luise Hebestreit, Michael Schneider, W. Leo Meerts and Michael Schmitt.

My own share in the publication sums up to $70\,\%$ and consists of formal analysis, software, investigation, writing - original draft.

10. Additional information for the experimental setup and basic methods

10.1. The spectroscopic vacuum chamber

The thermochromic shifts of the maxima in absorption and fluorescence emission spectra are, compared to the quite common solvatochromic shifts, of a relatively small magnitude. To determine the dipole moment of a molecule in its first electronically excited singlet state with a low uncertainty, the overall investigated shift of maxima positions should aim to be as high as possible. To accomplish this aim, carrying out measurements in a large temperature range is mandatory. With the choice of ethyl acetate as solvent, which has proven to give good results in previous works [6], the accessible temperature range, spans between its melting point at about $190\,\mathrm{K}$ [108] and the boiling point at about $350\,\mathrm{K}$ [109] if no pressure cell is used. In order to reach a maximal temperature range, as mentioned before, the usage of temperatures below the melting point of water is inevitable. A problem which occurs immediately when temperatures below $273.15\,\mathrm{K}$ are applied to a glass cuvette, is that the humidity in the surrounding air starts freezing on the glass surface making it opaque.

Avoiding the freezing of humidity while cooling a cuvette can be achieved in several ways, but here the decision was made to fully insulate the cuvette surfaces by placing it in a vacuum chamber. The planning and construction of a vacuum cell with active heating and cooling technology presents a few challenges:

- insulating the cuvette in the vacuum without exposing the sample to the vacuum
- The demand for accurate and precise heating and cooling down to temperatures far below ambient temperature requires double stack Peltier cooling which is countered by an additional liquid cooling system.

- Vacuum tight feedthroughs for liquid cooling and electric supplies have to be constructed.
- The vacuum chamber needs to fit in all used spectrometers.
- Windows of high quality have to be included which are insulated from metal and must be protected from breaking.
- For easy control during the measurement, the cuvettes inside should be accessible with active vacuum and a temperature sensor has to measure the temperature of the sample directly.

The results of the ideas depicted here have already been mentioned in Chapter 6, but for more detail, the schematic construction of the vacuum cell is shown in Figure 10.1.

In detail, the chamber was planned on the basis of a steel tube (1) with a sealed bottom to fit the spatial needs and provide access from all sides. The lid of the chamber (2) has a hole in its middle for granting access to the sample inside of the cuvette without breaking the vacuum. The sealing of the lid works with o-rings on the rim of the cuvette and the chamber. For light input and output for both absorption and fluorescence emission spectroscopy, three windows (3) are attached to the upper half of the chamber. One window is for letting light in, one is attached at a $180\,^\circ$ angle to the first for transmission measurements and one at a $90\,^\circ$ angle to the first for emission measurements. The quartz windows from HEBO Spezialglas are mounted with customized window flanges, sealing the windows with o-rings from both sides while securing the outer ring of the flange with six screws.

The base of the cooling stack inside the chamber is a PTFE (PolyTetraFluoroEthylene) block for both insulation and height adjustment. The second part is a cavernous copper block (8) for the application of a liquid cooling cycle of a Julabo Corio 600F into the system. In the first version, the copper block was a simple hollow block with two tubes (cf. Fig. 10.2a) for input and output but experiments have shown, that the cooling is not efficient enough for the expected result. To overcome this problem, the copper block was rebuilt as shown in Fig. 10.2b. It now includes a number of copper rods inside the cavity which increase the heat exchanging surface area. This modification lead to an increase in performance which satisfied the demands on cooling.

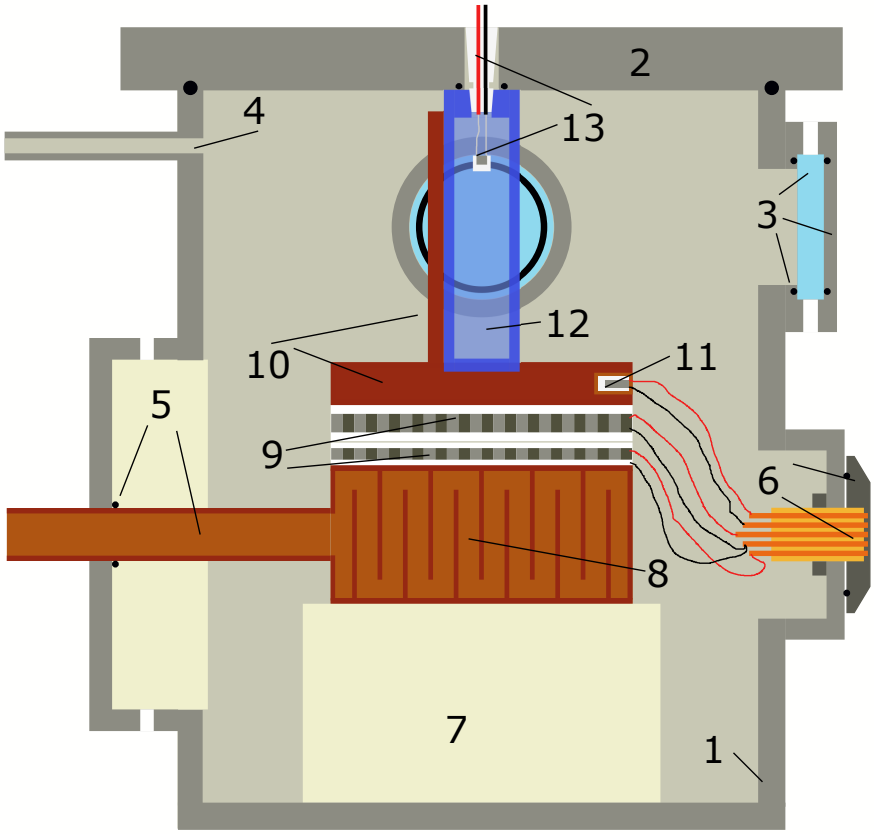

Figure 10.1.: Schematic construction of the spectroscopic vacuum cell including heating and cooling technology. With 1. the outer shell, 2. the flanged lid, 3. one of three flanged windows, 4. tube for applying a vacuum pump, 5. PTFE feedthrough for liquid input and output of the cooling block, 6. electronic socket from LEMO Elektronik GmbH, sealed with an o-ring, 7. PTFE block for insulating the liquid cooling block from the outer shell, 8. liquid cooling block, 9. double stack Peltier element, 10. Cuvette holder, 11. temperature sensor, 12. Cuvette, 13. Cuvette plug with electric feedthrough and temperature sensor.

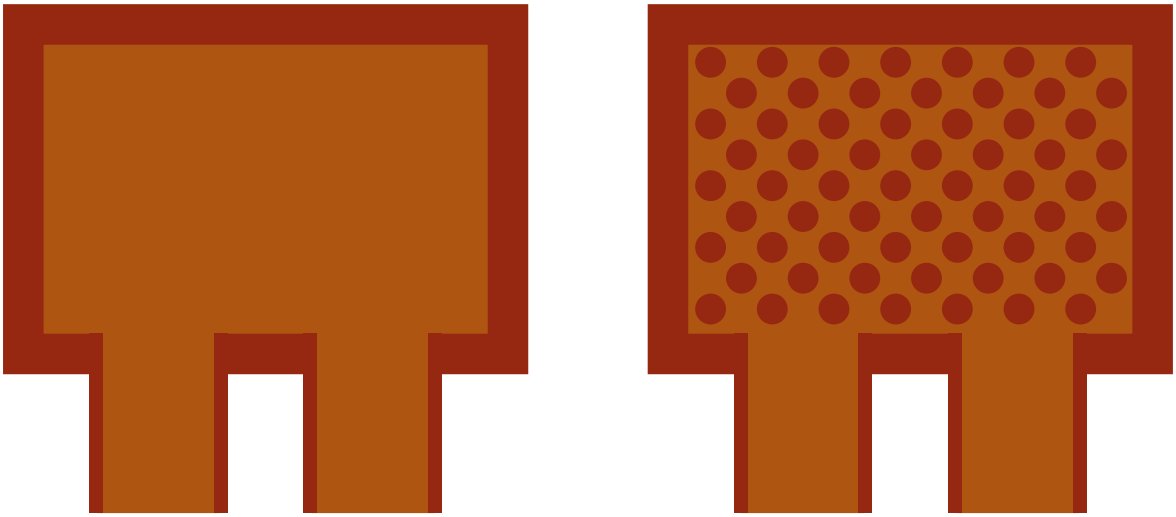

Figure 10.2.: The copper cooling block for the application of liquid cooling inside of the vacuum chamber in two stages of evolution. (a) simple hollow copper block. (b) copper block with a number of copper rods which increase the heat exchanging surface.

A feedthrough for the two copper tubes of the cooling block had to fulfil two requirements: vacuum tightness and insulation of the outer shell from the tubes. To achieve insulation, the copper tubes are surrounded by a massive PTFE block with o-rings at the meeting point of tube and the outer ring of the flange to supply a vacuum tight connection. Additionally, the PTFE itself generates a vacuum tight connection to the metal parts due to the deformation under pressure when the flange is closed tightly. The design of this construction means that there is no direct metal-metal contact between copper and the steel of the casing, therefore only slow heat transfer can be observed.

On top of the copper block two stacked Peltier elements (9) for electric heating and cooling, purchased from Uwe Electronics GmbH, are positioned. Peltier elements can change temperature much faster than the liquid cooling supply and also expand the temperature limits of the experiment in both directions. The combination of two Peltier elements is important especially for cooling, as the weaker element cools the sample and the stronger element can cool the hot side of the weaker element. The hot side of the stronger element then is cooled by the copper block and the result is a high precision, intense cooling of the sample. A small PT100 temperature sensor (11) which is included in the base plate of the cuvette holder (10) is used to control the work of the Peltier elements. The controls are provided by a Omron E5CC PID controller from Uwe Electronics GmbH. The electronic supplies are connected to a LEMO Elektronik GmbH socket, which seals vacuum tight to a customised flange and provides very easy to handle connection options on the outside.

The cuvette holder (10) consists of the base plate which conducts the applied heating and cooling of the Peltier elements and includes the temperature sensor (11). An orthogonal upright copper plate transfers the heating and cooling to the only unused side of the cuvette (12). The whole construction is made to hold Hellma cuvettes type 111 with $10\,\mathrm{mm}$ square ground area, $3500\,\mu\mathrm{L}$ volume and a round tight PTFE lid. A PTFE cable plug which also includes cables for another PT100 sensor is passed through the chamber lid into the cuvette opening. This plug is used for the monitoring of the current sample temperature. In addition, it seals the cuvette from the atmosphere and gives the chamber lid a final positon.

10.2. Experimental determination of the ground state dipole moment

The method shown in Chapter 6 in its present form, is more or less independent of the literature data, except in regards to the ground state dipole moment, which at the present time, still needs to be taken from other scientific publications or even quantum chemical calculations. The measurement of the solvent permittivity was already introduced in Chapter 6. With the knowledge that the dipole moment is directly linked to the permittivity of an isolated substance [50], it seems logical to take the next step and also determine the ground state dipole moment experimentally.

While the original Debye method [50] for the determination of dipole moments in solution is very time consuming due to temperature dependent measurements, the method according to Hedestrand, Guggenheim and Smith [41–45] works at a stable temperature and gives reliable results at low cost. The necessary experimental information here is the concentration dependent permittivity and refractive index of the sample molecule in a non-polar solvent and the density of the pure solvent. All measurements could be performed with the equipment already used for the determination of the solvent polarity parameters. The evaluation details and results was published in [23] right after the Method article.

Part III.

Complex Molecules

11. The next step

The basic method has been fully described. In the next step, more complex molecules with a higher number of atoms and also larger electronic π-systems are investigated and compared to already published data, reference methods and quantum chemical calculations. The investigated molecules here have been chosen because they are used in cooperation projects with the group led by Prof. Dr. Thomas J. J. Müller from the Heinrich-Heine-University [60] or because they are used in the (partially unpublished) investigation in other projects of our group [49]. Unfortunately, the results of 1-methylindole in the HRLIF-Stark spectroscopy were not available at the time when the manuscript was ready for publication. Due to the asymmetric structure of 1-methylindole, the evaluation of the rotational resolved spectra needs a special Hamiltonian, which was not available at this point. When the article about 1-methylindole in HRLIF-Stark spectroscopy is published, the results of the thermochromic method may be integrated into the discussion again to complete the comparison.

As the results in the following Chapters 12, 13 and 14 show, the thermochromic method in application brings reasonable results also for larger systems when compared to quantum chemical calculations. Additionally, the behaviour of molecules in solution and the difference to the isolated situation, or rather the diluted gas phase, can be discussed further. As the regular application of molecules with an enlarged electronic π-system, eventually as a part of proteinogenic amino acids, is in a liquid phase solution, this step to investigate excited state properties in solution in a reliable way, may be important for future applications in spectroscopy, microscopy and maybe even biochemical investigations.

12. Article - 1-Methylindole

Ground and Excited State Dipole Moments of 1-Methylindole from thermochromic shifts in absorption and emission spectra

Mirko Matthias Lindic and Michael Schmitt*

Heinrich-Heine-Universität, Institut für Physikalische Chemie I, D-40225 Düsseldorf, Germany, E-mail:mschmitt@hhu.de.

12.1. Abstract

The permanent dipole moments of 1-methylindole in its ground and lowest excited singlet $\pi\pi^*$-state have been determined using the method of thermochromic shifts of the absorption and fluorescence spectra and compared to *ab initio* calculated dipole moments. While *ab initio* theory predicts an excited state dipole moment, which nearly equals that of the ground state, the thermochromic shifts give an excited state dipole moment, which is about 2 Debye larger than that of the ground state. Perturbation of the excited state through the large electric field strength of the solvent cavity leads to strong mixing with the next excited singlet state, which has a considerably larger dipole moment. This perturbation is analyzed using the method described by Lombardi [John R. Lombardi *J. Phys. Chem.* A 1998, **102**, 2817-2823]. The perturbing state could be identified as ^1L_a-state, which is the second adiabatic state in the gas phase, but the lowest state in a polar surrounding.

12.2. Introduction

Knowledge of molecular dipole moments in electronically excited states is vital for the interpretation of the solvent dependence of electronic spectra. Furthermore, experimentally

determined dipole moments of electronically excited states can be used for evaluation of electronic wave function methods, since the permanent dipole moment depends only on the wave function of the excited state. The concept of molecular dipole moments as measure of charge distribution in molecules started with the works of Reinganum in 1903 and independently by Peter Debye 1929. They developed mathematical relations between dipole moments and other physical properties and introduced methods for determination of dipole moments in diluted gases and solutions. While their concept initially was tailored for the determination of charge distribution in molecules in their electronic ground state, extensions have been introduced in order to augment the method to electronically excited states.[50, 72, 110] One part to the success of the concept of permanent electrical dipole moments of molecules is the possibility to construct this moment from the atomic charges and their bond dipole moments along the chemical bonds [51, 111]. However, the concept of bond additivity rules fails completely, when it is applied to electronically excited states [80, 112, 113]. In addition, the concept of additive dipole moments reaches its limits already in the ground state, when looking at spatially extent molecules which consist of different chromophoric moieties.

For determination of permanent electrical dipole moments in the electronic ground state a vast number of well documented experimental techniques has been developed for the gas phase, liquid phase, and dilute solution. These range from microwave (far-infrared/infrared/ultraviolet) Stark spectroscopy [114–116] over coherent beat techniques with a Stark field[117–120] to measurements of the temperature dependence of the permittivity in dilute solutions [50] or of the concentration dependence of index of refraction and permittivity [42]. The proper determination of dipole moments in electronically excited singlet states is much more demanding. For molecules which can be transferred to the gas phase, rotationally resolved electronic Stark spectroscopy [71, 77, 79, 121] is the state-of-the art method for their experimental determination. The necessity of determining excited state dipole moments in solution is based on the experimental limitations of the gas phase method. With increasing size of the molecules, it gets harder to vaporize them without thermal decomposition and entrain the molecules into a molecular beam, which is mandatory for rotationally resolved electronic Stark spectroscopy. Additionally, the line density, even of the zero-field spectra of larger molecules, is too high to be fully resolved. A Stark effect extension to the method of rotational coherence spectroscopy (RCS)[122–125], which is especially suitable for large molecules would be highly desirable.

Probably the most popular approach for the determination of excited state dipole moments in solution is the evaluation of the changes of electronic absorption and emission spectra upon variation of the solvent. Lippert and Mataga investigated the effect of solvent permittivity and

index of refraction on the spectral (solvatochromic) shifts of absorption and emission spectra already in the 50's of the last century. [1, 2] In the solvatochromic method, the molecule of interest is dissolved in different solvents with different polarities and absorption and emission spectra are recorded. The basis is the Onsager reaction field theory [4] of a point dipole in a spherical cavity, surrounded by a dielectric continuum of permittivity ε. The point dipole induces a reaction dipole in the surrounding solvent molecules, causing an electric field which again reacts with the point dipole thus enabling a stabilization. Since this stabilization has to be different for different electronic states of the same molecule, its effect on the spectra can be used to calculate the dipole moment change after excitation.

Since variation of the solvent introduces more changes than solely the index of refraction and permittivity of the solvent, Kawski introduced the method of thermochromic shifts [6]. As both index of refraction and permittivity of the solvent are functions of the temperature, their variation can be achieved through a temperature change in spite of a solvent change.

A further improvement of the method was presented by Demissie *et al.* [7]. They replaced the concept of a solute dependent spherical cavity from the original Onsager model by a determination of the real cavity volume via concentration dependent density measurements. In a recent publication [8], we combined the methods of Kawski and Demissie by recording thermochromic spectra and using the experimentally determined cavity volume. Additionally, we included the temperature dependency of the cavity volume in the determination of the dipole moments.

The magnitude of molecular dipole moments in the equilibrium ground and excited Franck-Condon states and their relative orientations can be determined by electrooptic absorption (EOA) in solution, a method pioneered by Liptay [27, 82]. Recently, Nemkowich *et al.* have determined dipole moments of 4-substituted 3-hydroxyflavones and of unsubstituted diflavonol in the ground and lowest excited state, using EOA [126, 127]. This method has the advantage, that no Onsager radius or other cavity characteristics have to be determined, which, especially for non-spherical molecules, introduces quite some approximations.

In the present work, the dipole moments of ground and excited state of 1-methylindole are determined in solution and compared to the results of quantum chemical calculations. On the one hand, 1-methylindole is small enough to be investigated with different methods but nonetheless large enough to represent a group of biologically relevant molecules. The group of substituted indoles in general is of great interest for biological and chemical applications for being the chromophore of the proteinogenic amino acid tryptophan, and as part of complex chromophores [60].

12.3. Computational Methods

12.3.1. Quantum chemical calculations

Structure optimizations were performed employing Dunning's correlation consistent polarized valence triple zeta (cc-pVTZ) basis set from the TURBOMOLE library. [89, 90] The equilibrium geometries of the electronic ground and the lowest excited singlet states were optimized using the second order approximate coupled cluster model (CC2) employing the resolution-of-the-identity (RI) approximation. [91–93] For the structure optimizations spin-component scaling (SCS) modifications to CC2 were taken into account [128], since SCS-CC2 achieves a high accuracy for ground and excited state dipole moments[129]. The harmonic vibrational frequencies for both electronic states have been obtained from numerical second derivatives, using the NumForce script [130], which is implemented in the TURBOMOLE program suite [131]. Dipole moments are calculated as first derivatives of the respective energy with respect to an external field at the CC2 level of theory. The COnductor-like Screening MOdel (COSMO)[94], which is implemented in the ricc2 module of the TURBOMOLE package, was used for the calculation of ground and excited state dipole moments in solution.

12.3.2. Evaluation of ground state dipole moments from measurement of permittivity and index of refraction

Hedestrand, Guggenheim and Smith [42] presented a method for the evaluation of the permanent electric dipole moment of molecules in diluted solutions from mole fraction dependent permittivity ε_r^{mix} and refractive index n_r^{mix} data, which is shown in equation 12.1.

$$\mu_{sub} = \sqrt{\frac{27 \cdot M_m^{sub} \cdot \varepsilon_0 \cdot k_B \cdot T}{\rho^{sol} \cdot \left(\varepsilon_r^{sol} + 2\right)^2 \cdot N_A} \cdot (a - b)} \tag{12.1}$$

Here, μ is the permanent electric dipole moment, the superscripts sol and sub represent the solvent and the dissolved substance, k_B is the Boltzmann constant, T is the temperature, ε_0 is the permittivity of the vacuum, ρ is the density, ε_r is the relative permittivity, N_A is Avogadro's number and a and b result from the slopes of the graphs of the permittivity and refractive index versus the molar fraction x as shown in equations 12.2 and 12.3.

$$\varepsilon_r^{mix} = \varepsilon_r^{sol} + x^{sub} \cdot a \tag{12.2}$$

$$\left(n_r^{mix}\right)^2 = \left(n_r^{sol}\right)^2 + x^{sub} \cdot b \tag{12.3}$$

12.3.3. Evaluation of excited state dipole moments from thermochromic shifts

Temperature dependent permittivity and refractive index of ethyl acetate were used as formerly determined in Ref. [60]. Previous studies have shown, that for accurate description of the reaction field volume thermochromic measurements have several advantages compared to solvatochromic measurements [6, 35]. Additionally, the real cavity volume should be determined experimentally instead of using a constant Onsager radius [7, 8, 60]. The real cavity volume are determined by concentration and temperature dependent density measurements of 1-methylindole in ethyl acetate using Eq. 12.4.

$$\frac{1}{\rho} = \frac{1}{\rho^*} + \left(\frac{V_m}{M_m} - \frac{1}{\rho^*}\right) \cdot w \tag{12.4}$$

Here, ρ is the measured density of the solution, ρ^* is the measured density of the pure solvent, w is the mass fraction of the solute in the solution and M_m is the molar mass of the solute. The slope of the graph $\frac{1}{\rho}(w)$ gives the molar cavity volume V_m which can be divided by Avogadro's number to get the single cavity's volume. For the density data being collected at different temperatures, the cavity volume can be calculated at every temperature and the graph $V(T)$ can be fitted linearly to be used in further evaluation.

For evaluation and comparison two different methods of determining the (ground and) excited state dipole moment of 1-methylindole has been used, which are shown in Eq. 12.5 and 12.7.

$$\tilde{\nu}_A(T) + \tilde{\nu}_F(T) = -\frac{2(\mu_1^2 - \mu_0^2)}{3\varepsilon_0 hc} \cdot F_{BK}(T) + const. \tag{12.5}$$

$\nu_{A/F}$ are the maxima of the absorption and fluorescence spectra, ε_0 is the permittivity of the vacuum, h is Planck's constant and c is the speed of light. The evaluation according to Kawski[6] in Eq. 14.9 is suitable to determine only the excited state dipole moment μ_1 from

spectroscopic measurements. To perform the calculation, a value for the ground state dipole moment μ_0, obtained from other measurements or calculations, is mandatory. The solvent polarity function $F_{BK}(T)$ is shown in Eq. 12.6.

$$F_{BK}(T) = \frac{1}{V(T)} \left(\frac{2n(T)^2+1}{n(T)^2+2} \left(\frac{\varepsilon(T)-1}{\varepsilon(T)+1} - \frac{n(T)^2-1}{n(T)^2+2} \right) + \frac{3(n(T)^4-1)}{(n(T)^2+2)^2} \right), \quad (12.6)$$

where $V(T)$ is the temperature dependent cavity volume of the solute, $n(T)$ is the temperature dependent index of refraction of the solvent and $\varepsilon(T)$ is the temperature dependent permittivity of the solvent.

$$\tilde{\nu}_{A/E}(T) = \tilde{\nu}^0_{A/E}(T) - \frac{2\mu_{0/1}\left(\mu_1 - \mu_0\right)}{3\varepsilon_0 hc} \cdot F_{BK}(T) \quad (12.7)$$

The evaluation according to Demissie[7] in Eq. 12.7 allows to determine the ground and the excited state dipole moment simultaneously without utilization of literature values for the ground state dipole moment. This method allows to use different solvent polarity functions, but to keep the compared methods uniform only the solvent polarity function of Bilot and Kawski Eq. 12.6 has been used.

In order to calculate the dipole moments from Eq. 14.9 and 12.7, the slopes m, m_A and m_F from the graphs of the spectral maxima versus the solvent polarity function F_{BK} are used. Eq. 12.8, 12.9 and 12.10 show the final calculation for the resulting dipole moments, where Eq. 12.8 is used for the method according to Kawski and Eq. 12.9 and 12.10 are used for the method according to Demissie.

$$\mu_1 = \sqrt{\mu_0^2 + \frac{3\varepsilon_0 \cdot h \cdot c \cdot m}{2}} \quad (12.8)$$

$$\mu_0 = \sqrt{\frac{3\varepsilon_0 hcm_A^2}{2(m_F - m_A)}} \quad (12.9)$$

$$\mu_1 = \sqrt{\frac{3\varepsilon_0 hcm_F^2}{2(m_F - m_A)}} \quad (12.10)$$

12.4. Experimental Methods

1-Methylindole with 95% purity was purchased from fluorochem Ltd and used without further purification. Ethyl acetate with analytical reagent grade was purchased from fisher scientific and used without further purification. 1,4-Dimethylbenzene with 99% purity was purchased from Acros Organics and used without further purification.

12.4.1. Capacity measurements and refractive index

Five solutions of 1-methylindole in 1,4-dimethylbenzene with molar fractions of $x_{sub} = 0,\ 0.025,\ 0.05,\ 0.075$ and 0.1 have been prepared. The usage of a non polar solvent is mandatory for the correct determination of the ground state dipole moment to exclude dipole-dipole interactions. The refractive index of all solutions was determined using the Abbemat MW refractometer from Anton Paar. The density of the pure solvent was measured in a DMA4500M densitometer from Anton Paar. The permittivity of all solutions was calculated from capacitive measurements using the relation $\varepsilon_r = \frac{C}{C_0}$, where C is the capacity of a capacitor filled with the sample and C_0 is the capacity of the same capacitor filled with air. The capacity of all solutions was measured using a Keysight E4990A Impedance Analyzer in combination with the capacitor of a Keysight 16452A Test Fixture. All measurements of capacity and index of refraction have been performed at $20°C$

12.4.2. Thermochromic shifts

The densities ρ of eleven solutions with different mass fractions w, ranging from $w = 0$ up to $w = 0.00459$ in steps of 0.00046, of 1-methylindole in ethyl acetate were measured in a temperature range from $267.15\ K$ to $323.15\ K$ with an increment of $2\ K$ using an Anton Paar DMA 4500 M density meter. For all thermochromic measurements ethyl acetate is the solvent because it solves the solute even in higher concentrations, which are needed for the density measurements. Also ethyl acetate fits the temperature range which is applied in the spectroscopical measurements and it is perfectly suited as spectroscopic solvent.

Absorption and fluorescence emission spectra of 1-methylindole, dissolved in ethyl acetate with a weight fraction of $w = 2.3 \times 10^{-05}$ ($0.16\ mmol/l$), were recorded in a temperature range between $249.15\ K$ and $347.15\ K$ with an increment of $2\ K$. Temperature has been controlled by a custom built heatable and coolable cell holder which is powered by two stacked Peliter elements from Uwe Electronics GmbH, whose hot side is cooled with a liquid cooling cycle including a Julabo Corio 600F thermostatic circulator using Thermal

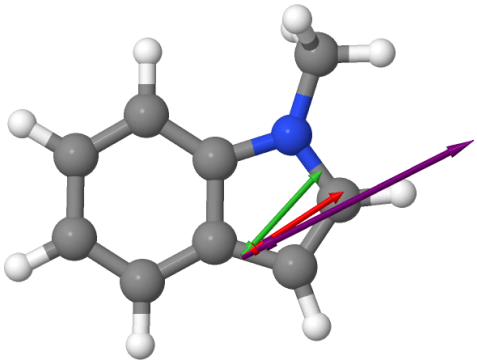

Figure 12.1.: CC2/cc-pVTZ optimized electronic ground state structure of 1-methylindole, dipole moments in the ground (green vector), first excited (red vector), and second excited (purple vector) singlet state, respectively. The angle between the dipole moments amounts to about $15°$ for ground and first excited state and about $21°$ for ground and second excited state.

G as cooling liquid. To inhibit the blinding of the cuvette's glass through condensation of humidity at low temperatures the cell holder is incorporated in a vacuum chamber, which allows spectroscopic measurements in the used spectrometers as well as permanent access to the cuvette through the lid [55] .The used spectrometers were a Varian Cary 50 Scan UV for absorption measurements and a Varian Cary Eclipse for fluorescence emission measurements.

12.5. Results

12.5.1. Computational Results

The structures of 1-methylindole in the electronic ground and excited states have been optimized at the CC2/cc-pVTZ level of theory, employing spin component scaling (SCS). The Cartesian coordinates of all optimized structures are given in Tables S7, S8 and S9 of the online supplementary material. In Table 12.1 all results on structures and dipole moments of 1-methylindole are collected along with the experimental results for comparison.

The first electronically excited singlet state (S_1) has an adiabatic excitation energy of 34937 cm^{-1}, the energetically following S_2-state is 1442 cm^{-1} higher in energy. The permanent dipole moments for the electronic ground and excited states of the isolated molecule were calculated to $2.48\ D$ (S_0), $2.54\ D$ (S_1), and $4.12\ D$ (S_2) while the simulation of a solvent continuum with implementation of the COSMO model gives $3.24\ D$ (S_0) and $3.54\ D$ (S_1), respectively. Fig. 12.1 shows the optimized ground state geometry of 1-methylindole containing the vectors of both the ground and the excited dipole moment.

The electron density difference, calculated between the S_0 and the S_1-state of 1-methylindole

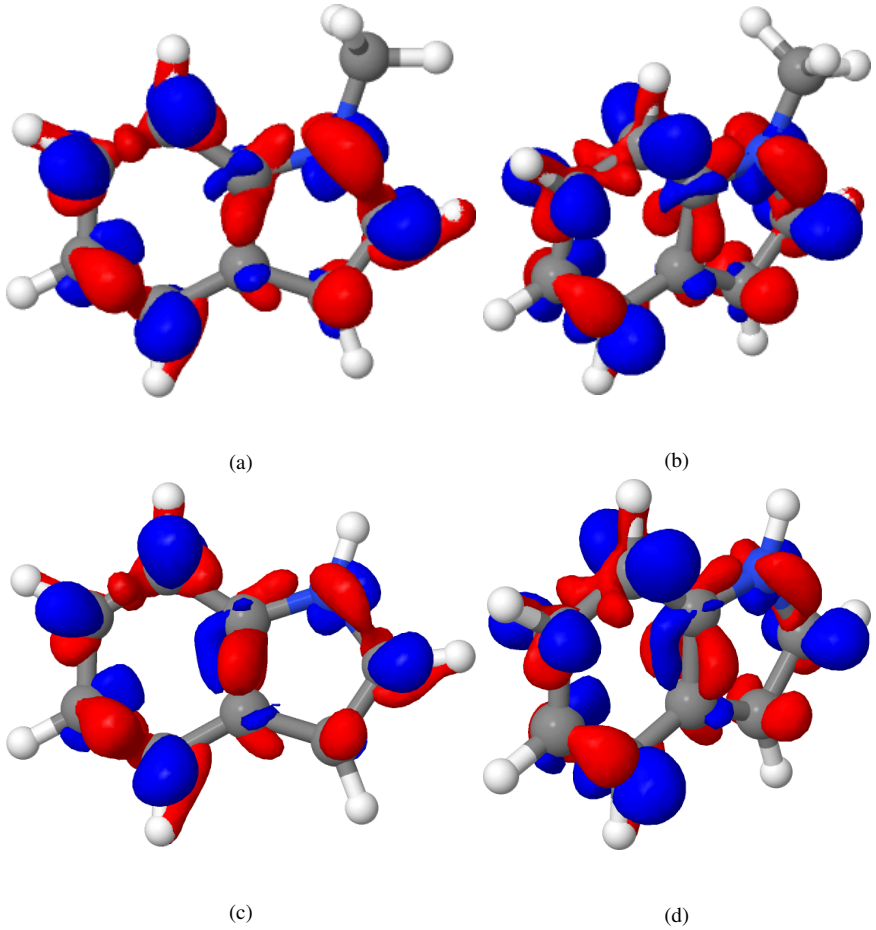

Figure 12.2.: Electron density difference plots, calculated between the S_0 and the S_1-states of 1-methylindole and indole from different perspectives. Blue areas indicate decrease of electron density and red areas represent increase of electron density upon excitation.
a) Electron density differences of 1-methylindole, frontal projection.
b) Electron density differences of 1-methylindole, twisted projection.
c) Electron density differences of indole, frontal projection.
d) Electron density differences of indole, twisted projection.

at the CC2/cc-pVTZ level of theory in Figure 12.2 shows a net decrease (blue area) of π electron density in the benzene moiety an an increase (red area) in the pyrrole ring. This shift of electron density is nearly balanced by an opposite shift of σ electron density, resulting in the small calculated dipole moment change upon excitation. For comparison, the electron density difference of indole is shown as well.

Figure 12.3 displays the frontier orbitals of 1-methylindole, including the excitations to the lowest two electronically excited singlet states. Here, the excitation to the lowest excited state S_1 is mainly characterized by a LUMO $\leftarrow$ HOMO-1 transition (coefficient 0.61) and a LUMO+2 $\leftarrow$ HOMO transition (coefficient 0.19). The LUMO+1 orbital is a Rydberg orbital with sigma character and is therefore not taken into account. The excitation to the S_2-state

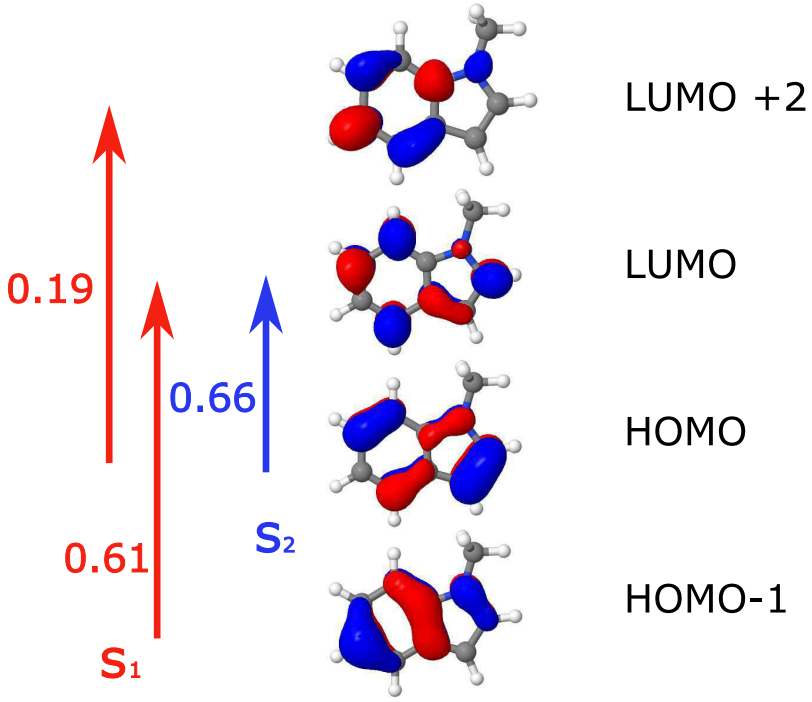

Figure 12.3.: Leading orbitals, which are involved in the transitions for the first two excited singlet states. In the nomenclature of Platt [132] for indoles, the S_1 is an ${}^1L_b$-state and the S_2 is an ${}^1L_a$-state.

is mainly characterized by a LUMO ← HOMO transition (coefficient 0.66). Thus, from the orbital contributions, the S_1-state can be classified as L_b and the S_2-state as L_a in the nomenclature of Platt [132]. This assignment is in agreement with the higher permanent dipole moment of the second excited singlet state, which is the normal case for L_a-states.

12.5.2. Experimental Results

Table 12.1.: Comparison of the experimental and calculated dipole moments and adiabatic excitation energies to the lowest two excited singlet states. μ_0 is the ground state dipole moment and μ_1 is the dipole moment of the first excited singlet state. μ_2 represents the dipole moment of the second excited singlet state, which was included for comparison.

	SCS-CC2/cc-pVTZ		Experiment		
	Isolated	COSMO	HGS-Method	Thermochromic shifts	
				Bilot-Kawski	Demissie (BK)
μ_0 / D	2.48	3.24	2.37(4)	-	0.346(12)
μ_1 / D	2.54	3.54	-	4.65(9)	4.02(11)
μ_2 / D	4.12	-	-	-	-
$\nu_{ad}^{S_1 \leftarrow S_0}$ / cm^{-1}	34937	-	-	-	-
$\nu_{ad}^{S_2 \leftarrow S_0}$ / cm^{-1}	36379	-	-	-	-

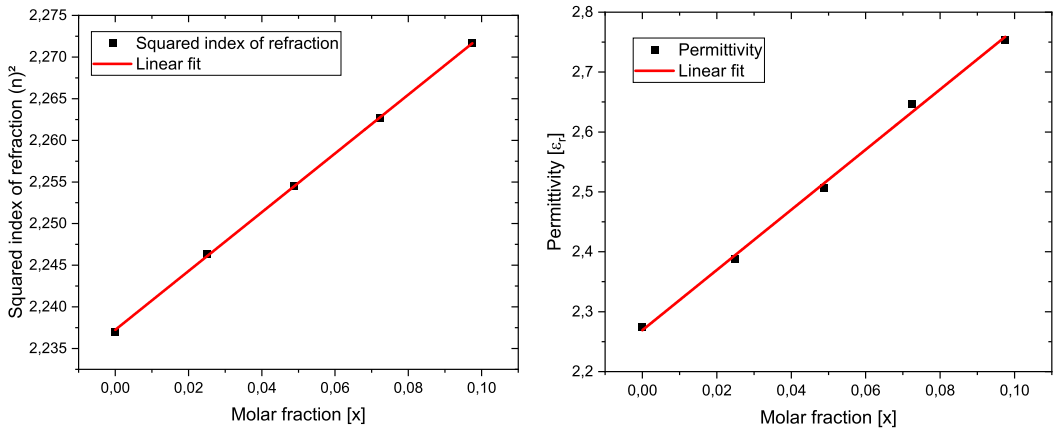

(a) (b)

Figure 12.4.: Plots of permittivity and the squared index of refractive as function of the molar fraction of the 1-methylindole solution, for the determination of the ground state dipole moment. The parameters a and b of equation 12.2 and 12.3 can be extracted as slopes of the linear fits. All error bars are too small to be visualized.
a) Refractive index of all measured solutions of 1-methylindole in 1,4-dimethylbenzene including linear fit of the data.
b) Permittivity of all measured solutions of 1-methylindole in 1,4-dimethylbenzene including linear fit of the data.

Ground state dipole moment of 1-methylindole from capacitive and refractive index measurements

Figure 12.4 shows the permittivity and the squared index of refractive as function of the molar fraction of the solution. According to equations 12.2 and 12.3, a and b are the slopes of these two graphs and determined to be $a = 5.0(2)$ and $b = 0.353(3)$, respectively. Using equation 12.1, the density of the solvent of $\rho^{sol} = 861.08$ kg/m^3, the permanent electric dipole moment of 1-methylindole in the electronic ground state is determined to be $\mu_0 = 2.37(4)$ D.

Ground and excited state dipole moments of 1-methylindole from thermochromic shifts

To determine the solvent polarity function, we calculated the cavity volume of 1-methylindole in ethyl acetate using equation 12.4. The slope of the graph of the inverse density of the solution $1/\rho$ versus the weight fraction w in Fig. 12.5 gives the molar cavity volume of 1-methylindole in ethyl acetate at $293.15\ K$. This measurement and calculation have been performed for all temperatures between $267.15\ K$ and $323.15\ K$. The graph of the cavity volume versus the temperature including the linear fit of the data is shown in Figure 12.6.

The absorption and fluorescence emission spectra of 1-methylindole in ethyl acetate, recorded

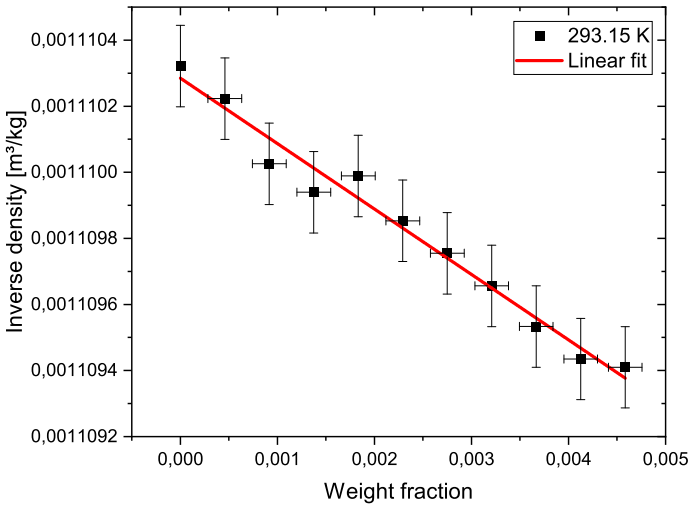

Figure 12.5.: Inverse densities of solutions of 1-methylindole in ethyl acetate plotted versus the weight fraction of the solutions measured at $293.15\ K$. The graph also includes the linear fit. From the slope of this graph the cavity volume at the given temperature can be calculated.

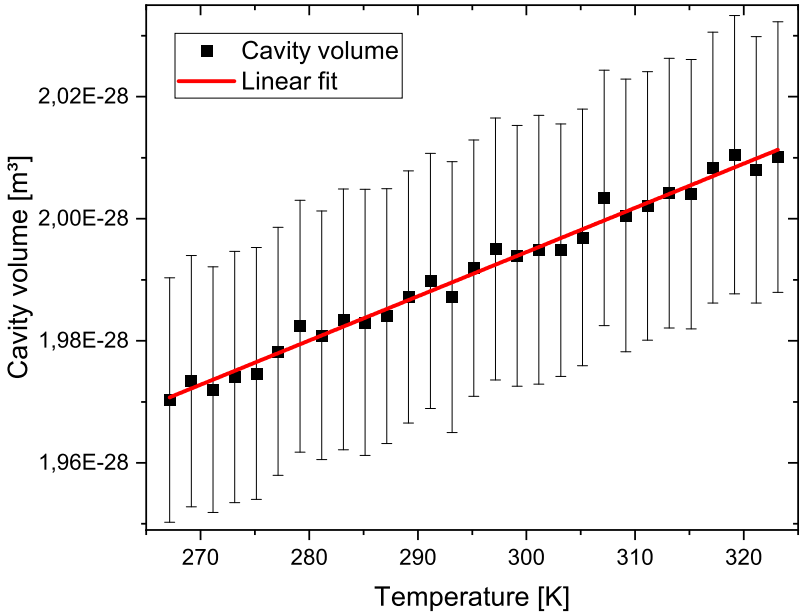

Figure 12.6.: Cavity volume of 1-methylindole in ethyl acetate plotted versus temperature. A linear fit to the data results in the following linear equation: $V(T) = 7.3(2) \times 10^{-32} \frac{m^3}{K} \cdot T + 1.777(6) \times 10^{-28} m^3$. The horizontal temperature error bars are too small to be visualized in this graph. The uncertainty of the temperature is about $\pm 0.02\ K$

.

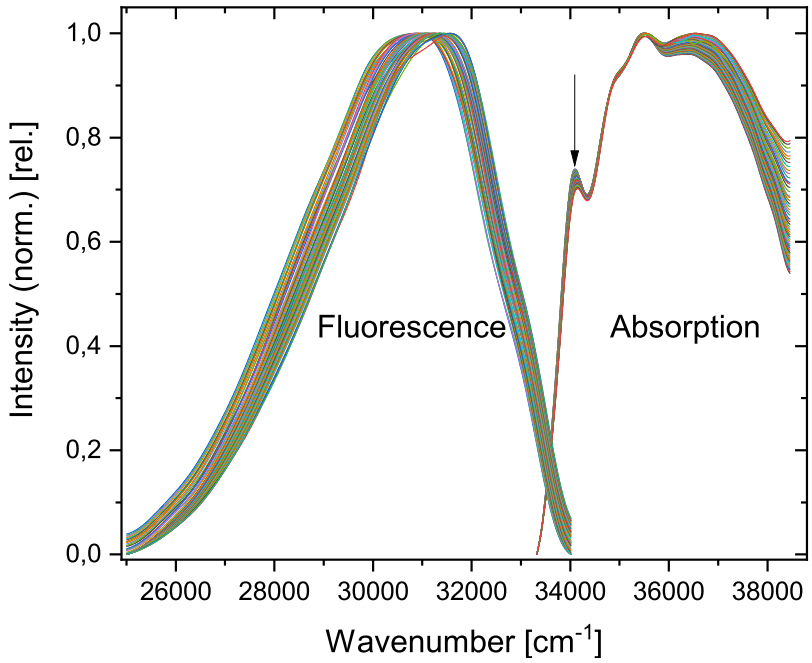

Figure 12.7.: Temperature dependent FFT-filtered absorption and fluorescence spectra of 1-methylindole. The relative intensities are normalized to 1 to allow uniform graphical presentation and comparability. The local absorption maximum, which is used for the evaluation, is marked with an arrow. The temperature increases from left (low wavenumber) to right (high wavenumber) for both absorption and fluorescence

between $249.15\ K$ and $347.15\ K$ are shown in Figure 12.7. For noise reduction and easier determination of the maximum wave number, the spectra were filtered with a FFT-Filter with a cutoff-frequency of $2.88 \times 10^{12} s^{-1}$ for the absorption spectra and $1.02 \times 10^{12} s^{-1}$ for the fluorescence spectra using a rectangular filter function. Figure 12.7 shows the filtered spectra. For the evaluation, the absorption maximum with the lowest energy and the overall maximum of the fluorescence emission spectrum have been used.

Although numerous methods were published to evaluate solvent polarity dependent spectral shifts, we restricted ourselves to the methods based on the publications of Bilot-Kawski [6] and Demissie [7], which already have been validated in our previous publications [8, 60].

According to equation 14.9, the sum of the absorption and emission maxima wavenumbers $\tilde{\nu}_A(T) + \tilde{\nu}_E(T)$ are plotted versus the solvent polarity function $F_{BK}(T)$, which is shown in Figure 12.8. The Bilot-Kawsky method allows only for the determination of the dipole moment change upon excitation. The resulting slope m in Figure 12.8 is used in equation 12.8, along with a value for the ground state dipole moment μ_0 of $2.37(4)\ D$, from the permittivity and refractive index measurements. We obtained a value of $4.65(9)\ D$ from the Bilot-Kawski method.

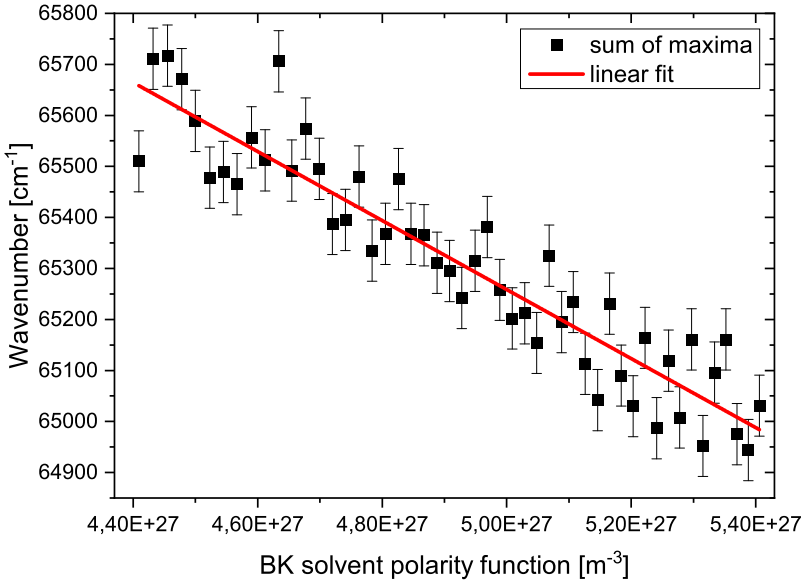

Figure 12.8.: Plot of the temperature dependent sum of spectral maxima versus temperature dependent Bilot-Kawski solvent polarity function, including linear fit of the data and error bars resulting from the accuracy of the spectral fit. The used maxima were taken from the FFT-filtered spectrum

The application of the method based on Demissie, using plots of both $\tilde{\nu}_A(T)$ and $\tilde{\nu}_E(T)$ versus $F_{BK}(T)$, allows for the determination of both ground and excited state dipole moment. Both graphs shown in Figure 12.9, and result in a ground state dipole moment of $0.346(12)\ D$ and an excited state dipole moment of $4.02(11)\ D$. All experimental results are summarized in Table 12.1.

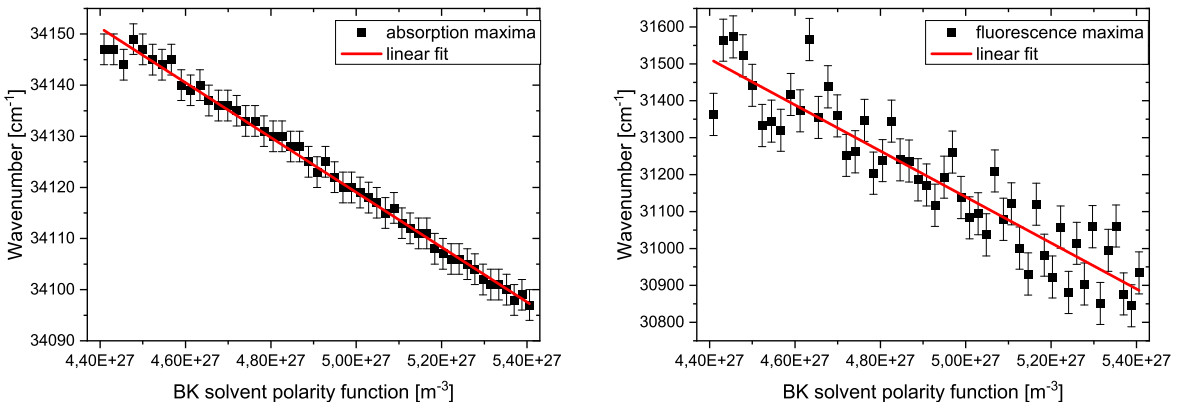

(a) (b)

Figure 12.9.: Plots according to the method of Demissie [7] using the maxima of the FFT-filtered spectra. Linear fits and error bars are included.
a) Temperature dependent absorption maxima of 1-methylindole in ethyl acetate plotted versus temperature dependent Bilot-Kawski solvent polarity function.
b) Temperature dependent fluorescence maxima of 1-methylindole in ethyl acetate plotted versus temperature dependent Bilot-Kawski solvent polarity function.

12.6. Discussion

The excited state dipole moment of 1-methylindole in its lowest excited singlet state has been determined from thermochromic shifts of UV/Vis-absorption and fluorescence spectra. The comparison with the experimentally determined ground state value μ_g of 2.37 D shows an increase $\Delta\mu$ of 2.28 D upon electronic excitation to the lowest excited singlet state. This result is in obvious disagreement with the the SCS-CC2/cc-pVTZ calculations, which predict nearly identical values for ground and excited state dipole moments of $\mu_g = 2.48$ D and $\mu_e = 2.54$ D, thus an increase of $\Delta\mu = 0.06$ D for 1-methylindole. Consequently, the method of thermochromic shifts overestimates the absolute excited state dipole moment μ_e of 1-methylindole by a factor of two and the change upon excitation $\Delta\mu$ even by a factor of 40. A similar behavior has been observed for aniline[133, 134] and indole [64], comparing the results from solvatochromic shifts and high resolution electronic Stark spectroscopy. These molecules have a close-lying second electronically excited state in common, which has a dipole moment that is considerably higher than that of the lower state. As far, as the electronic Stark experiments are concerned, we are dealing with the low-field approximation with field strengths much smaller than 1.000 V/cm. In this approximation, the originally excited rovibronic states are perturbed, if the product of transition moment between the excited states μ_{12} and the field strength $\mathbf{F}$ is larger than the zero-field energetic distance ΔE^0 of the perturbing states:

$$\mu_{12} \times \mathbf{F} > \Delta E^0 \tag{12.11}$$

For the determination of dipole moments from solvatochromic or thermochromic shifts, the situation is very different. The molecular dipole moment of the solute induces a dipole moment in the homogeneous solvent cavity. The so-called reaction dipole is the source of an electric field, which interacts with the molecular dipole, leading to a stabilization. In the case of 1-methylindole, the cavity volume is about 170 Å^3, equivalent to a cavity radius of 3.437 Å. With a reaction dipole of 3.5 Debye, a field strength in the cavity of $1.3 \cdot 10^8$ V/cm is reached, exceeding the field strength in the Stark experiment by a factor of 10.000. These large field strengths mix the electronically excited states E_1 and E_2, so that only an effective dipole moment μ_{eff} can be given. The excited-state eigenvalues $E_\pm$ of the perturbed Hamiltonian are then given by [64]:

$$\begin{aligned} E_\pm = &(1/2)\,(E_1 + E_2 - (\mu_1 + \mu_2)\cdot\mathbf{F}) \\ &\pm (1/2)\,\{(E_1 - E_2 - (\mu_1 - \mu_2)\cdot\mathbf{F})^2 + (4\mu_{12}\cdot\mathbf{F})^2\}^{1/2} \end{aligned} \tag{12.12}$$

which, in the high-field limit simplifies to:

$$E_\pm = (1/2)\,(E_1 + E_2) \pm \left(\mu^\pm_{eff}\cdot\mathbf{F}\right) \tag{12.13}$$

with

$$\mu^\pm_{eff} = (1/2)\,(\mu_1 + \mu_2) \pm (1/2)\,\{(\mu_1 - \mu_2)^2 + 4\mu_{12}^2\}^{1/2} \tag{12.14}$$

For aniline, the perturbing state has been postulated to be of $\pi\sigma$ (Rydberg)-character with a spacing of 10 cm^{-1} from the $\pi\pi^*$-state and a dipole moment of 6 D. For indole, the perturbing state is the second $\pi\pi^*$-state, which is the ^1L_a-state in the nomenclature of Platt [132]. It seems reasonable that the ^1L_a-state is also the perturbing state in 1-methylindole. Therefore, we also calculated the dipole moment of the second excited singlet state, which, according to Figure 12.3, is the ^1L_a-state and obtained a value of $\mu_2 = 4.12\ D$ at SCS-CC2/cc-pVTZ level of theory. From these calculations, the transition dipole moment (TDM) μ_{12} between the excited states has been determined to be 0.5 D. Using this TDM and the field strength of the reaction field in the cavity of $1.3 \cdot 10^8$ V/cm (see above), equation 12.11 predicts the perturbing state to be in the range of 0 - 1160 cm^{-1} above the first excited state, in fair agreement with the *ab initio* calculation which predicts the S_2 origin to be 1442 cm^{-1} above the S_1. From the orbital contributions this state has been identified as the L_a-state.

Figure 12.10 shows the avoided crossing of the perturbed energy levels $E_\pm$ according to equation 12.12 (straight lines), with a transition dipole moment of 0.5 D. The zero-field values are the unperturbed levels E_1 and E_2. If the two excited states are not coupled through a

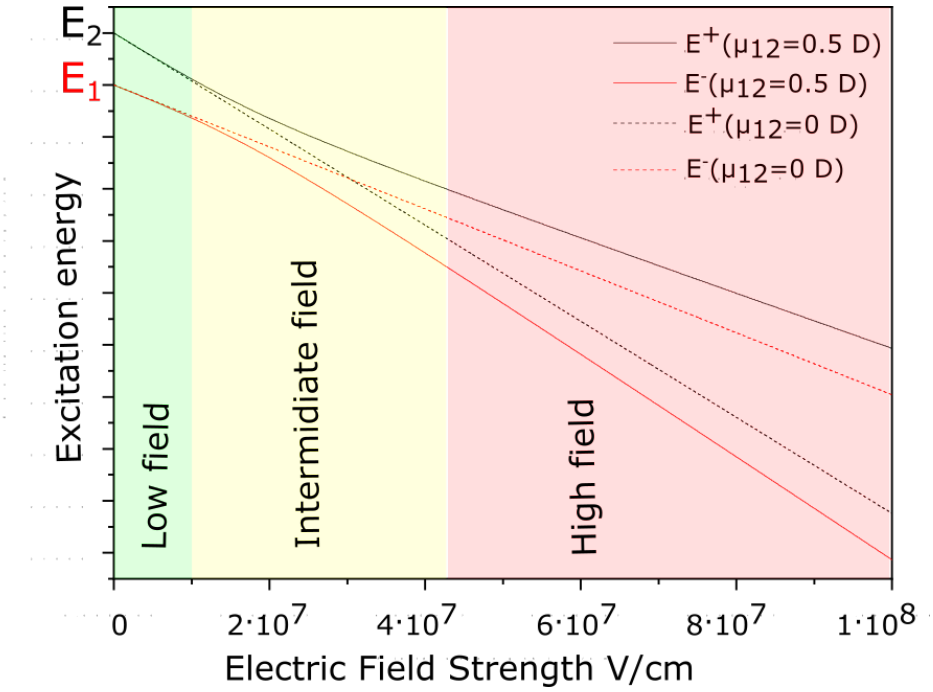

Figure 12.10.: Field induced perturbations of the energy levels of the electronically excited states.

non-zero transition dipole moment, the states cross (dotted lines). The dipole moment of the lower state, which is given by the slope of the $E(\mathbf{F})$ curve, is similar to that of the zero-field upper state and vice versa. The lower state gains the large dipole moment through the coupling to the higher perturbing state with large dipole moment, in the same way that a lower state gains intensity by Herzberg-Teller coupling to a higher state with large oscillator strength.

The plots of the absorption and fluorescence maxima vs. solvent polarity functions (Figures 12.8 and 12.9) show a strict linear behavior, proving that we are in the linear high-field regime, far away from the avoided crossing of the states. In this regime, equation 12.14 can be used to assess the dipole moment of the perturbed (lower) component μ^{+}_{eff} to 4.41 D, in good agreement with the value of 4.02 D from the Demissie evaluation and of 4.65 D from the Bilot-Kawski evaluation (cf. Table 14.1). The results of the Demissie evaluation show a similar behavior as reported in ref. [8]. The ground state dipole moment is close to zero, in obvious contradiction to the calculation, but the excited state dipole moment is in a comparable range to the result of the Bilot-Kawski evaluation. This observation further supports the statement, that the combination of absorption and fluorescence spectroscopy in solution can only give information about the differences of the dipole moments between the ground state and the fluorescing excited singlet state and no absolute information about the dipole moment of any of the states.

The SCS-CC2/cc-pVTZ COSMO calculations using a permittivity of 6.09 and refractive

index of 1.3725 gave a cavity volume of $1.7 \times 10^{-28}\ m^3$. On the other hand a cavity volume of $1.99(3) \times 10^{-28}\ m^3$ was calculated from weight fraction dependent solution density measurements. The deviation of 15% between this two methods is slightly less than has been reported before [8, 60] but lies in the same order of magnitude and shows the limitations of the COSMO method. The dipole moments, which has been calculated using the COSMO application, do not fit any of the other results in a reasonable way. In this case, the simulation of a solvent continuum seems not to describe the situation of 1-methylindole in ethyl acetate properly.

12.7. Conclusions

We used the methods of thermochromic shifts in absorption and fluorescence spectroscopy to determine the dipole moment in the first excited singlet state of 1-methylindole. From comparison to *ab initio* calculations on the SCS-CC2/cc-pVTZ level of theory we found that the first excited singlet state exhibits major L_a character when the molecule is solved in a polar solvent. This has most recently shown in an *ab initio* study by Brisker-Klaiman and Dreuw [135]. In the experiments described in the present work, the electric field of the solvent cavity is strong enough to mix the primarily excited L_b with the L_a-state. Thus, the high-field value of the permanent dipole moment of 1-methylindole is close to that of the L_a-state. The results of electronic Stark measurements, which still have to be performed, will be situated at the very left part of Figure 12.10 and will show the unperturbed value of the excited state dipole moment of the L_b-state.

12.8. Acknowledgements

Computational support and infrastructure was provided by the "Center for Information and Media Technology" (ZIM) at the Heinrich-Heine-University Düsseldorf.

12.9. Own share in the publication

The content of this chapter has already been published in the *Journal of Photochemistry and Photobiology A: Chemistry*, **406**, 112984, 2021 under the title *Ground and excited state dipole moments of 1-methylindole from thermochromic shifts in absorption and emission spectra* written by Mirko Matthias Lindic and Michael Schmitt.

My own share in the publication sums up to 70 % and consists of formal analysis, software, investigation, methodology, writing - original draft.

13. Article - 1-Benzofurane

The Excited State Effective Dipole Moment of 2,3-Benzofuran from Thermochromic Shifts in Absorption and Emission Spectra.

Mirko Matthias Lindic,[a] Tim Axel Oberkirch,[a] Jörg Tatchen,[b] and Michael Schmitt[a]*

[a]Heinrich-Heine-Universität, Institut für Physikalische Chemie I, D-40225 Düsseldorf, Germany, E-mail:mschmitt@hhu.de.

[b] Max Planck Institute for Solid State Research, Heisenbergstraße 1, 70569 Stuttgart, Germany, j.tatchen@fkf.mpg.de

13.1. Abstract

The excited state dipole moment of the lowest excited singlet state of 2,3-benzofuran in ethylacetate solution is determined using thermochromic spectroscopy and compared to the values which are obtained for the isolated molecule from electronic Stark spectroscopy (M.-L. Hebestreit, *et al.*, J. Mol. Struct., 2020, 1210, 127992) and to the results of *ab initio* calculations at coupled cluster level of theory. It is shown that the dipole moment from thermochromic shifts in solution deviates considerably from that of the isolated molecule. This finding can be traced back to a field induced mixing by the strong reaction field of the solvent, which exceeds the external Stark field applied in gas phase measurements by a factor of 10.000. Depending on the dipole moments of the perturbing state and its energy gap to the excited state, dipole moments from thermochromic shifts (and consequently also of solvatochromic shifts) might be considerably different to gas phase values. However, the alteration of the electronic configuration of the molecule via the reaction field of the solvent can be deperturbed in the high-field limit.

13.2. Introduction

The dipole moment as characterization of the inhomogeneous distribution of electron density in molecules was introduced by M. Reinganum and P. Debye at the beginning of the twentieth century [50, 72, 110]. Starting with the method of Debye [50], a multitude of different techniques for the experimental determination of molecular dipole moments in their electronic ground state have been developed. They comprise the measurement of permittivity and refractive indices of polar molecules diluted in a non-polar environment according to Hedestrand, Guggenheim and Smith [41–45], microwave spectroscopy using the Stark effect [46, 136, 137] and molecular beam electric resonance measurements [138].

Excited state molecular dipole moments gained interest when Lippert and Mataga in the mid 50's of the twentieth century developed a method to determine them experimentally from UV spectra in different solvents [1, 2]. The core idea is a result of the Onsager reaction field theory [4]. Through interactions of a point dipole in a cavity of polar solvent molecules a reaction dipole is induced, which creates an electric field inside of the cavity, leading to a stabilization of the initial point dipole. A large variety of similar methods, which are based on variation of the solvent, have been invented through the second half of the twentieth century. The three most popular ones of them may be those of Bakhshiev [139], McRae [101], and Bilot-Kawski [3] who all worked on the same solvatochromic idea and perturbation calculation basis but used different approximations resulting in individual equations and definitions of solvent polarity. Founding on this method, Kawski proposed to eliminate some sources of error by varying the solvent polarity function via the temperature of one solvent (thermochromism), instead of changing the solvent (solvatochromism) [5]. Another improvement was made by Demissie who eliminated the spherical approximation of the cavity [7] by replacement of the Onsager radius [4] with the experimentally determined cavity radius. In our group, the methods of Kawski and Demissie were combined to introduce the temperature dependent cavity volume into the thermochromic method [8].

Independent methods for the determination of dipole moments in electronically excited states are rotationally resolved electronic Stark spectroscopy of isolated molecules [71, 77, 79, 140] and Stark quantum beat spectroscopy [117–120]. Their drawback, however, is the need to vaporize the sample molecules without decomposition in order to be entrained into a supersonic beam which restricts the method to relatively small molecules. This can be circumvented by the use of electro-optical absorption measurements which have been pioneered by Liptay [27, 82].

The bicyclic heteroaromatic benzofuran (2,3-benzofuran, 1-benzofuran, coumarone, or

benzo[b]furan) is the oxygen analog of indole. While photophysics and photochemistry of indole, as chromophore of the natural amino acid tryptophane, has found widespread theoretical [135, 141–148] and experimental [18, 19, 149–167] interest, equivalent studies on benzofuran are sparse. Hollas has analyzed the vibronic spectrum of benzofuran [168]. The rotational contour of the electronic origin band of benzofuran was presented by Hartford *et al.* [169]. Fluorescence excitation, fluorescence emission and resonance enhanced two-photon ionization (R2PI) spectra of benzofuran, dibenzofuran and fluorene were reported by Yip *et al.* [170]. A vibrational assignment of the infrared and Raman spectra of benzofuran in the gas phase from a comparison to a normal mode analysis with the AM1 force field was given by Collier *et al.* [171] and later extended by Klots and Collier [172]. Smithson *et al.* deduced the coplanarity of the benzene and furan rings from far-infrared spectroscopy [173]. *Ab initio* quantum chemical calculations of the total energy, ionization potential and dipole moments of benzofuran were presented by Palmer and Kennedy [174]. Recently, the excited state dipole moments of benzofuran were determined in the gas-phase from rotationally resolved electronic Stark spectroscopy. The geometry changes upon excitation to the lowest excited singlet state were determined and point to ^1L_b character of the excited state [49]. Studies of indole and related compounds have shown that the lowest two electronically excited singlet states are energetically close, but the dipole moments of these states differ significantly. In general, the ^1L_a state shows a larger dipole moment, while the ^1L_b state has a small dipole moment which, in most cases, lies close to that of the electronic ground state [18, 19, 23].

A general criticism of solvatochromic studies for determination of excited state dipole moments has been given by Lombardi [70]: "*It is unfortunate so much energy has been expended in solvatochromic studies determining excited state dipole moments, many of which are highly suspect. It would be far preferable if we would treat the gas phase results for what they probably are, the most accurate current technique for determining molecular dipole moments of an isolated molecule, and to expend some energy instead utilizing the solvatochromic shifts as a good way to determine the effect of solvents on electronic reorganization upon excitation by judicious comparison with the gas phase results.*" This statement was guided by the observation that all excited state dipole moments which have been determined both in the gas phase with Stark techniques and in solution using solvatochromism are up to more than an order of magnitude different. A possible reason for this large discrepancy is the existence of a nearby state with high dipole moment, which borrows its dipole moment to the observed state, comparable to Herzberg-Teller intensity borrowing for vibronic intensities. Reliable results from solvatochromic or thermochromic studies can thus only be expected, when a larger number of systems is carefully studied using gas phase and solution conditions. With the present study of benzofuran we will show, that the reason for the observed discrepancies

can indeed be found in vibronic coupling of the lowest excited singlet states.

13.3. Computational Methods

13.3.1. Quantum chemical calculations

Structure optimizations were performed employing Dunning's correlation consistent polarized valence triple zeta (cc-pVTZ) basis set from the TURBOMOLE library. [89, 90] The equilibrium geometries of the electronic ground and the two lowest excited singlet states were optimized using the second order approximate coupled cluster model (CC2) employing the resolution-of-the-identity (RI) approximation. [91–93] For the structure optimizations spin-component scaling (SCS) modifications to CC2 were taken into account [128], since SCS-CC2 achieves a high accuracy for ground and excited state dipole moments[129]. The harmonic vibrational frequencies for all electronic states have been obtained from numerical second derivatives, using the NumForce script [130], which is implemented in the TURBOMOLE program suite [175]. Dipole moments are calculated as first derivatives of the respective energy with respect to an external field at the CC2 level of theory. Electron density difference maps (EDD) were calculated using the *-fanal* option in the ricc2 method with the density data of the according states.

Excitation energies and electric dipole (transition) moments were also studied along a linearly interpolated path (LIP) connecting the equilibrium geometries of the two lowest excited states S_1 and S_2. Molecular geometries for the points forming the LIP were generated by means of a home-made program called Distort. The latter performs a linear interpolation of Cartesian coordinates after rotating the geometry of second state into an Eckart frame with respect to the first one [176] (see [177] for the implementation of the transformation matrix). The quantum-chemical level of theory which was chosen for the LIP was the same as was employed within the geometry optimizations of the excited states.

In order to take into account solvent effects caused by electrostatic interactions with solvent dipoles, the LIP was afterwords recalculated employing an external electrostatic field within the SCF and CC2 calculations. Assuming a sphere-shaped solute cavity, the maximum field strength which may act on the molecule in solution can be obtained from the size (radius) of the cavity (300 pm) and the solvent point charges present at the surface of the sphere corresponding to a dipole of $8 \cdot 10^{-30}$ Cm. From these values, we estimate the field strength giving rise to polarization of the solute within the cavity to amount to in between 10^9 and 10^{10} V/m. In the calculations, the direction of this external field was chosen to coincide with

the electrostatic dipole moment which was calculated at the CC2 level for the ground state at its optimized geometry.

In the strict sense, an Eckart-type rotation of molecular Cartesian coordinate systems, this time between the ground and excited states, would again be necessary in order to determine the corresponding dipole moment vectors at the geometries of the excited states. However, inspection of the corresponding transformed Cartesian geometries revealed Eckart rotation effects to be rather minor in this case (changes occurring only on the order of 10^{-2} a.u. per atomic Cartesian coordinate). This behavior can be attributed to the relative stiffness of the benzofuran ring system and the absence of any large-amplitude geometry change within the excited states under consideration.

13.3.2. Evaluation of excited state dipole moments from thermochromic shifts

The temperature dependent permittivity and refractive index of ethyl acetate were used as previously determined in Ref. [60]. Previous studies have shown that thermochromic measurements have several advantages compared to solvatochromic measurements for determination of excited state dipole moments [6, 35]. Additionally, the real cavity volume should be determined experimentally, instead of using the constant Onsager radius [7, 8, 60]. This cavity volume is determined from concentration and temperature dependent density determinations of solutions of benzofuran in ethyl acetate using Eq. 13.1.

$$\frac{1}{\rho} = \frac{1}{\rho^*} + \left(\frac{V_m}{M_m} - \frac{1}{\rho^*} \right) \cdot w \tag{13.1}$$

Here, ρ is the measured density of the solution, ρ^* is the measured density of the pure solvent, w is the mass fraction of the solute in the solution and M_m is the molar mass of the solute. The slope of the graph $\frac{1}{\rho}(w)$ gives the molar cavity volume V_m which can be divided by Avogadro's number to get the single cavity's volume. From the density measurements, collected at different temperatures, the cavity volume can be calculated at each temperature and the graph $V(T)$ is fitted to a linear function which is used in the further evaluation.

Eq. 13.2 and 13.4 represent two different methods which have been used in this study to determine the ground and excited state dipole moment of 2,3-benzofuran.

$$\tilde{\nu}_A(T) + \tilde{\nu}_F(T) = -\frac{2(\mu_1^2 - \mu_0^2)}{3\varepsilon_0 hc} \cdot F_{BK}(T) + const. \tag{13.2}$$

ν_A and ν_F are the maxima of the absorption and fluorescence spectra, respectively. ε_0 is the permittivity of the vacuum, h is Planck's constant and c is the speed of light. The evaluation according to Kawski[6] in Eq. 13.2 is suitable to determine the change of the dipole moment upon electronic excitation from spectroscopic measurements. The evaluation of the excited state dipole moment μ_1 requires a value for the ground state dipole moment μ_0 obtained from other measurements or from *ab initio* calculations. The solvent polarity function $F_{BK}(T)$ is shown in Eq. 13.3.

$$F_{BK}(T) = \frac{1}{V(T)} \left(\frac{2n(T)^2 + 1}{n(T)^2 + 2} \left(\frac{\varepsilon(T) - 1}{\varepsilon(T) + 1} - \frac{n(T)^2 - 1}{n(T)^2 + 2} \right) + \frac{3(n(T)^4 - 1)}{(n(T)^2 + 2)^2} \right), \tag{13.3}$$

where $V(T)$ is the temperature dependent cavity volume of the solute, $n(T)$ is the temperature dependent index of refraction of the solvent and $\varepsilon(T)$ is the temperature dependent permittivity of the solvent.

$$\tilde{\nu}_{A/F}(T) = \tilde{\nu}^0_{A/F}(T) - \frac{2\mu_{0/1}(\mu_1 - \mu_0)}{3\varepsilon_0 hc} \cdot F_{BK}(T) \tag{13.4}$$

The evaluation according to Demissie[7] in Eq. 13.4 allows to determine the ground and the excited state dipole moment, simultaneously. This method allows to use different solvent polarity functions, but to keep the compared methods uniform only the solvent polarity function of Bilot and Kawski Eq. 13.3 has been used.

In order to calculate the dipole moments from Eq. 13.2 and 13.4, the slopes m, m_A and m_F from the graphs of the spectral maxima versus the solvent polarity function F_{BK} are used. Eq. 13.5, 13.6 and 13.7 show the final calculation for the resulting dipole moments, where Eq. 13.5 is used for the method according to Kawski and Eq. 13.6 and 13.7 are used for the method according to Demissie.

$$\mu_1 = \sqrt{\mu_0^2 + \frac{3\varepsilon_0 \cdot h \cdot c \cdot m}{2}} \tag{13.5}$$

$$\mu_0 = \sqrt{\frac{3\varepsilon_0 hcm_A^2}{2(m_F - m_A)}} \tag{13.6}$$

$$\mu_1 = \sqrt{\frac{3\varepsilon_0 hcm_F^2}{2(m_F - m_A)}} \tag{13.7}$$

13.4. Experimental Methods

Benzofuran (purity $\geq 99\%$) was purchased from Sigma Aldrich and used without further purification. Ethyl acetate with analytical reagent grade was purchased from Fisher Scientific and used without further purification.

13.4.1. Thermochromic shifts

The cavity volume was determined from density measurements of ten solutions of benzofuran in ethyl acetate with weight fractions between $w = 0.00044$ and $w = 0.00437$ at temperatures between $265.15\ K$ and $343.15\ K$ with an increment of $2\ K$ using an Anton Paar DMA 4500 M density meter.

Spectra of UV/Vis absorption and fluorescence emission of a solution of 2,3-benzofuran in ethyl acetate with a concentration of $w = 5.04 \times 10^{-5}$ ($3.86 \times 10^{-4} mol/L$) were recorded at temperatures between $231.15\ K$ and $347.15\ K$ with an increment of $2\ K$ using the Varian Cary 50 Scan UV for absorption spectra and a Varian Cary Eclipse for fluorescence spectra. The absorption and fluorescence spectra are recorded as a function of the wavelength and are subsequently converted to a function of the wavenumber for further evaluation. For the conversion of the fluorescence spectra to wavenumber units, the factor of λ^2 has been used in order to compensate for the error that the wavelength interval $\Delta\lambda$ is constant, while the wavenumber interval $1/\Delta\lambda$ is not. The temperature was controlled by a custom built heatable and coolable cell holder, which is powered by two stacked Peltier elements from Uwe Electronics GmbH. The hot side is cooled with a liquid cooling cycle including a Julabo Corio 600F thermostatic circulator using Thermal G as cooling liquid. To inhibit the blinding of the cuvette's glass by condensation of humidity at low temperatures the cell holder is incorporated in a vacuum chamber, which allows spectroscopic measurements in both used spectrometers as well as permanent access to the cuvette through the lid [55].

13.5. Results

13.5.1. Computational Results

The optimized geometries of the electronic ground and the lowest two excited singlet states (S_1 and S_2) of benzofuran from CC2/cc-pVTZ calculations, employing spin component scaling (SCS), were confirmed to be minima by a normal mode analysis. Their structures are given as Cartesian coordinates in Tables S1, S2 and S3 of the online supplementary material. Computed permanent dipole moments of all the states are shown in Table 13.1, along with adiabatic excitation energies.

Hellweg [129] gives methodological errors of dipole moments ($\mu - \mu_{ref}$) for a test set of 11 molecules with first row elements using the spin-component-scaled CC2 method with basis sets of triple-ζ quality of 0.07 D for the electronic ground state. The electronically excited state has mean errors of 0.17 D, but for a different test set. However, the errors for the excited state dipole moment of indole (0.07 D) and benzonitrile (0.04 D) are considerably smaller than the mean of the test set. We therefore assume the methodological error in the excited state of benzofuran, which is a comparable molecule to be the same as in the ground state. A benchmark study of Winter *et al.* [178] on the adiabatic excitation energies of a test set of 66 molecules yielded the smallest methodological errors for SCS-CC2 (mean absolute error 0.05 eV = 400 cm^{-1}).

The lowest two electronically excited singlet state minima are separated by 5 166 cm^{-1}, with an adiabatic excitation energy to the S_1 state of 37 883 cm^{-1}. The quantum chemical calculation of the dipole moments resulted in 0.717 D for the S_0 ground state, 0.856 D for the S_1 excited singlet state and 2.392 D for the S_2 excited singlet state. Angles and relative magnitudes of the three dipole moments are shown in Fig. 13.1 at the example of the S_0 geometry.

To give a better interpretation on the formation of the permanent dipole moments, the electron density difference (EDD) maps for both transitions are given in Fig. 13.2. The EDD map of the excitation to the S_1 state just shows a similar electron density change in both the benzene and the furane moieties. The EDD map of the excitation to the S_2 state shows a high increase of electron density in the furane ring after excitation while the benzene ring show light decrease.

Figure 13.3 gives an overview to the excitations into the two lowest excited singlet states and the involved frontier orbitals of benzofuran. In this case, the S_1 state transition is mainly characterized by the LUMO $\leftarrow$ HOMO-1 (coefficient 0.44) transition with a minor proportion

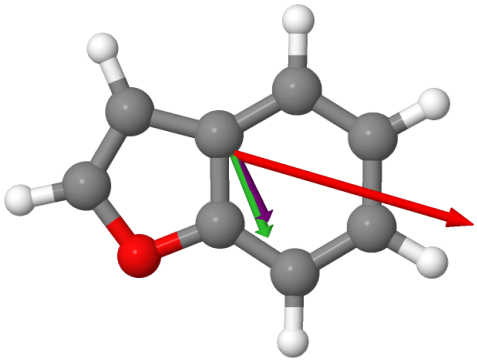

Figure 13.1.: CC2/cc-pVTZ optimized electronic ground state structure of benzofuran, dipole moments in the ground (purple vector), first excited (green vector), and second excited (red vector) singlet state, respectively. The angle between the dipole moments amounts to about $4.5°$ for ground and first excited state and about $47.5°$ for ground and second excited state.

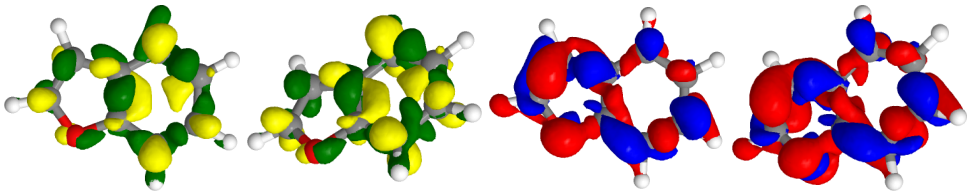

(a) (b) (c) (d)

Figure 13.2.: Electron density difference plots of benzofuran for the first two electronically excited singlet states shown in different perspectives. Blue (yellow) areas indicate a decrease of electron density and red (green) areas represent an increase of electron density upon excitation. The difference in color is solely for an easier differentiation and has no scientific meaning (a) Electron density difference of benzofuran calculated between the S_0 and S_1-states, frontal projection. (b) Electron density difference of benzofuran calculated between the S_0 and S_1-states, twisted projection. (c) Electron density difference of benzofuran calculated between the S_0 and S_2-states, frontal projection. (d) Electron density difference of benzofuran calculated between the S_0 and S_2-states, twisted projection.

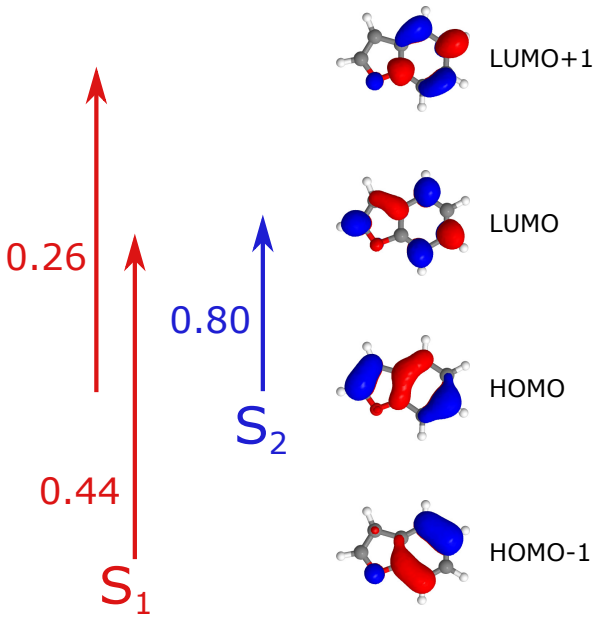

Figure 13.3.: Frontier orbitals and dominating excitations for the lowest excited singlet states of benzofuran along with the coefficients (Qualitative scheme not considering the actual values of HF orbital energy differences which are basically insufficient for reliably predicting excitation energies and energetic orderings of state). The numbers in the figure give the squared coefficients x 100 at the respective optimized geometry.

of the LUMO+1 $\leftarrow$ (coefficient 0.26) HOMO transition, while the S_2 state transition is essentially a LUMO $\leftarrow$ HOMO (coefficient 0.8) transition. According to this, the S_1 state can be named a ^1L_b state while the S_2 state represents the ^1L_a state in the nomenclature of Platt [132]. Another indicator for this assignment are the different dipole strengths, because ^1L_a states are known to have a significantly higher dipole moment than the related ^1L_b states [19, 23, 135, 144, 147].

13.5.2. Experimental Results

Table 13.1.: Comparison of the experimental and calculated dipole moments and adiabatic excitation energies to the lowest two excited singlet states. μ_0 is the ground state dipole moment and μ_1 is the dipole moment of the first excited singlet state. μ_2 represents the dipole moment of the second excited singlet state, which was included for comparison.

	SCS-CC2/cc-pVTZ	Experiment		
	Isolated	Gas Phase	Thermochromic shifts	
		HRLIF[49]	Bilot-Kawski	Demissie (BK)
μ_0 / D	0.717	0.77(1)	-	0.21(2)
μ_1 / D	0.856	0.91(1)	2.07(3)	1.95(3)
μ_2 / D	2.392	-	-	-
$\nu_{ad}^{S_1 \leftarrow S_0}$ / cm^{-1}	37883	35950.01	-	-
$\nu_{ad}^{S_2 \leftarrow S_0}$ / cm^{-1}	43049	-	-	-

Ground and excited state dipole moments of 2,3-benzofuran from thermochromic shifts

Temperature dependent permittivity and index of refraction values of ethyl acetate have previously been published [60]. The cavity volume is determined from the slope of the graph of $\frac{1}{\rho}$ versus w, according to Eq. 13.1, shown exemplarily in Fig. 13.4 for a temperature of 293.15 K. A linear regression is performed for the resulting cavity values versus their respective temperatures which gives the necessary function shown in Fig. 13.5.

Figure 13.6 displays the recorded absorption and fluorescence emission spectra of benzofuran in ethyl acetate. To ensure an accurate determination of the exact maxima positions, all graphs have been fitted with a low band pass FFT-Filter with average cutt-off frequencies of $1.07 \times 10^{13}\ s^{-1}$ for the absorption spectra and $1.02 \times 10^{13}\ s^{-1}$ for the fluorescence emission spectra, using a rectangular filter function. The maxima for the evaluations were taken from the lowest-energy absorption band and the overall highest emission band. An intensity gap in the fluorescence emission spectra arises between 299.15 K and 305.15 K, which can not be explained, no detail of the regular measurement process was changed during the time this data were recorded. All data above 300 K will be dismissed from the evaluation of the dipole moments.

In previous works we found, that even though there are known numerous different methods to evaluate spectral shifts caused by solvent polarity, the methods according to Kawski and Demissie give results which have close agreement with calculated values or those from reference methods [6–8, 23, 60].

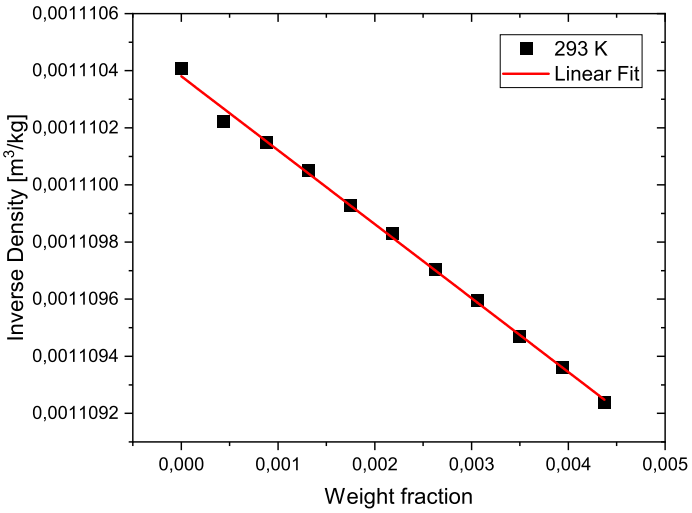

Figure 13.4.: Plot of the inverse densities of 2,3-benzofuran in ethyl acetate versus the weight fraction of the solutions at 293.15 K. The slope of the included linear fit is used to calculate the cavity volume of the solute at the given temperature.

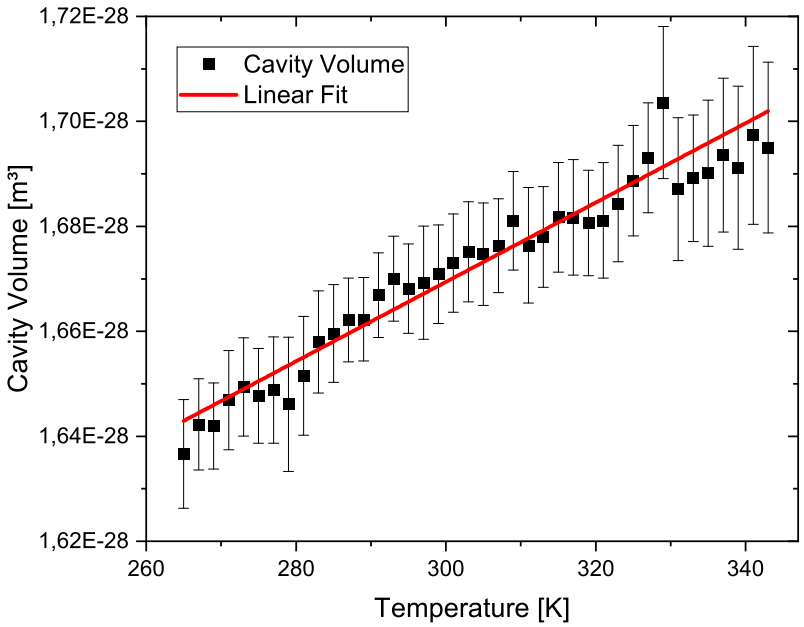

Figure 13.5.: Plot of the cavity volumes of benzofuran in ethyl acetate versus the respective temperatures. The linear regression of the data results in the function V(T)=7.4×10^{-32} $m^3K^{-1}\cdot$ T + 1.448×10^{-28} m^3. The horizontal temperature error bars are too small to be visualized here. The temperatures uncertainty of the density meter is about $\pm$ 0.02 K.

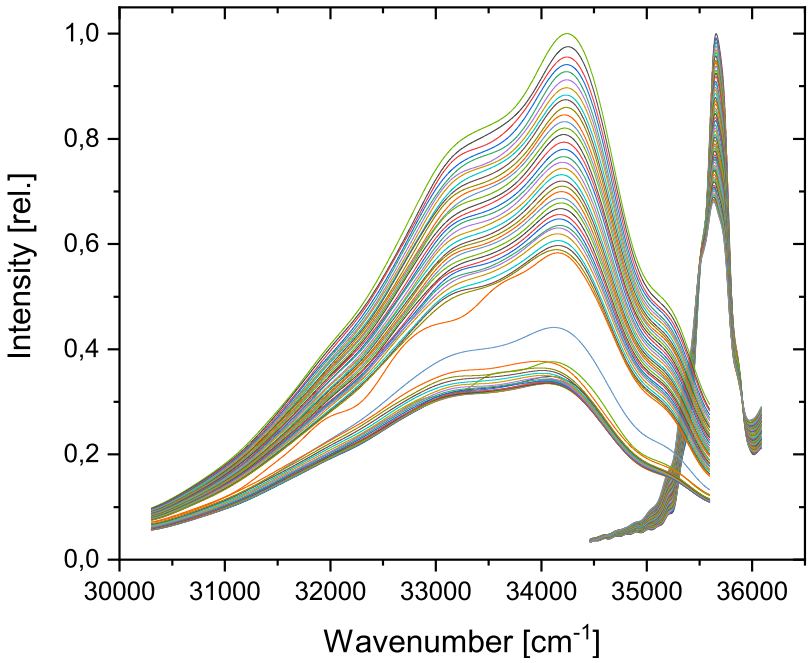

Figure 13.6.: Absorption and fluorescence emission spectra of benzofuran in ethyl acetate recorded at temperatures between 231.15 K and 347.15 K. The graphs are FFT-filtered for better determination of maxima positions. With rising temperature the intensity of both absorption and emission spectra decreases.

To obtain excited state dipole moments according to Kawski[6], the wavenumber at the respective maxima positions of absorption and fluorescence spectra at the same temperature are summed up and plotted versus the temperature dependent solvent polarity function, like defined in Eq. 13.2. The slope of the linear fit of the graph in Fig. 13.7 is used to calculate the excited state dipole moment according to Eq. 13.5. Using a ground state dipole moment of 0.717 D from the SCS-CC2/cc-pVTZ calculations, the excited state dipole moment is determined to be μ_1=2.07(3) D.

For the determination of the ground and excited state dipole moment simultaneously according to the method of Demissie [7], the wavenumber of the maxima positions in absorption and fluorescence spectra are plotted separately versus the solvent polarity function like defined in Eq. 13.4. Both slopes are calculated from the linear fit in Fig. 13.8 and used in Eqs. 13.7 and 13.6 for determination of the dipole moments. According to this method, we obtain a ground state dipole moment of μ_0=0.21(2) D and an excited state dipole moment of μ_1=1.95(3) D. The dipole moments based on experimental data are listed in Tab. 13.1 along with the *ab initio* calculated values.

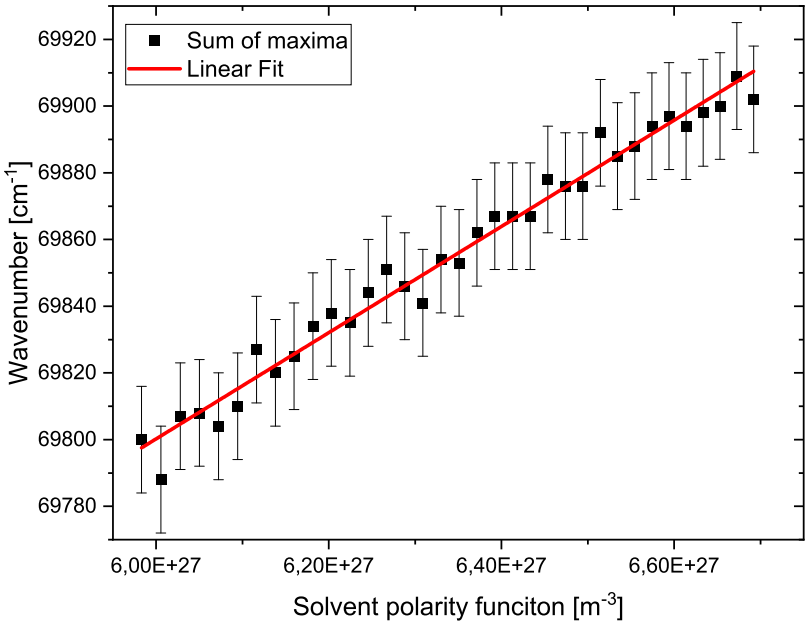

Figure 13.7.: Sum of the maximum positions wavenumber of absorption and fluorescence emission spectra of benzofuran in ethyl acetate plotted versus the temperature dependent solvent polarity function. The maxima positions were taken from the FFT-filtered spectra.

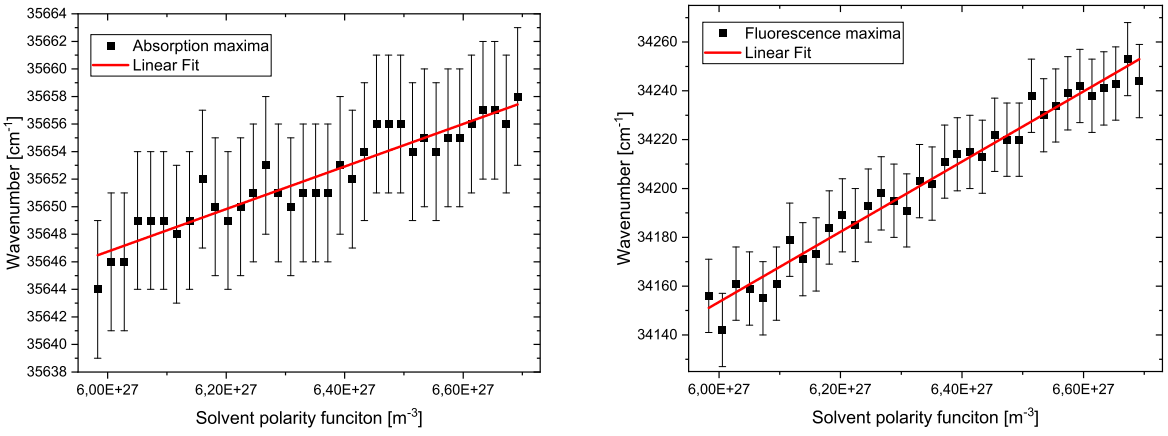

(a) (b)

Figure 13.8.: Plots according to the method of Demissie [7]. The maxima of the FFT-filtered spectra were used and error bars are included as well as linear fits, whose slopes are used in the further evaluation to calculate the ground and excited stated dipole moments. (a) Temperature dependent absorption maxima of benzofuran in ethyl acetate plotted versus temperature dependent Bilot-Kawski solvent polarity function. (b) Temperature dependent fluorescence maxima of benzofuran in ethyl acetate plotted versus temperature dependent Bilot-Kawski solvent polarity function.

13.6. Discussion

Upon comparison of the experimentally determined dipole moments in Table 13.1 with those from the SCS-CC2/cc-pVZZ calculations one finds excellent agreement with the gas-phase values from Ref. [49] for both ground and lowest excited singlet state. This excited state is clearly the ^1L_b-state, as can be inferred rom the mixed LUMO $\leftarrow$ HOMO - 1 / LUMO +1 $\leftarrow$ HOMO excitations, shown in Figure 13.3, while the second excited singlet state is the ^1L_a-state (LUMO $\leftarrow$ HOMO). This assignment is also supported by the similarity of the S_1-state dipole with that of the ground state S_0. ln most bicyclic heteroaromatics, the ^1L_b dipole is close to that of the ground state, while the ^1L_a has a considerably larger dipole moment.

However, the dipole moments of benzofuran in solution, determined from thermochromic shifts, show a quite different result. Both evaluations following Bilot-Kawski (2.07 D) and Demissie (1.95 D), result in excited state dipole moment which is more than two times larger than that from Stark measurements (0.91 D) and from the *ab initio* predictions (0.86 D). Interestingly, the solution value is quite close to what is calculated for the second excited singlet state ^1L_a (2.39 D).

Lombardi[63] was the first to point out that nearby electronic states with different dipole moments can perturb each other in the presence of very strong fields. The fields which are used in gas-phase Stark spectroscopy ($\approx 10^5$ V/m) of isolated systems are orders of magnitude smaller than the reaction fields in solvent cavities of molecular dimensions ($\approx 10^{10}$ V/m). We calculated a linearly interpolated path between the ^1L_a and ^1L_b minima on the potential energy surface of benzofuran i) under zero-field conditions, ii) with a small field of 10^5 V/m and iii) with a large electric field of 10^{10} V/m using SCS-CC2/cc-pVTZ. The electric field is oriented in the direction of the excited state dipole moment. Figure 13.9 shows the results of these calculations. Under zero-field conditions, the minima of the ^1L_a and ^1L_b state are well separated (^1L_b at 0 and ^1L_b at 1 in Figure 13.9). Unlike the case of indole, where the ^1L_a state at its minimum is the first electronically excited state (S_1) (cf. Figure 3 in Ref. [19]), there is no sign of such a mixing without field effects in benzofuran.

The low field virtually does not change the energies of the respective excited states and is not shown in the Figure. However, an avoided crossing appears at field strengths of 10^{10} V/m, due a considerable amount of mixing between the two excited singlet states. This shows the need to consider perturbation effects in the excited state dipole moments.

Lombardi gave the excited-state eigenvalues of the electric field perturbed Hamiltonian in the basis of zero-field wave functions as [63]:

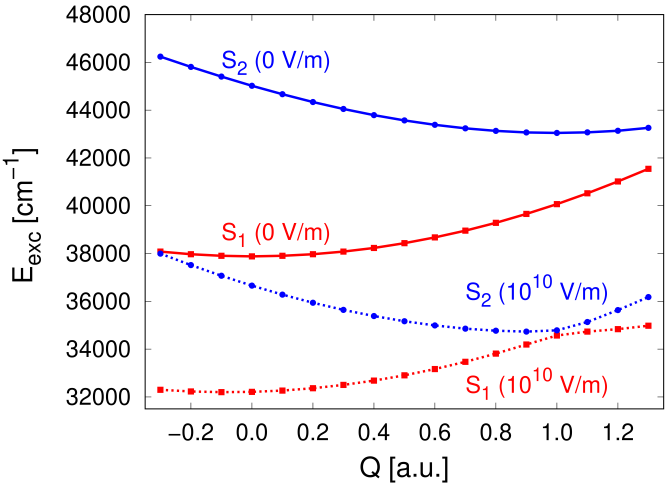

Figure 13.9.: CC2/cc-pVTZ calculated path, linearly connecting the ^1L_a and ^1L_b minima on the potential energy surface of benzofuran

$$E_{\pm} = (1/2)\,(E_1 + E_2 - (\mu_1 + \mu_2)\cdot\mathbf{F}) \\ \pm \left[(1/2)\,(E_1 - E_2 - (\mu_1 - \mu_2)\cdot\mathbf{F})^2 + 4\,(\mu_{12}\cdot\mathbf{F})^4\right]^{(1/2)} \tag{13.8}$$

This function of the applied field $\mathbf{F}$ of the lowest two excited states is shown in Figure 13.10 for dipole moments of the S_1-state of 0.9 D, of the S_2-state of 2.0 D, and for a transition dipole μ_{12} = 0.1 D and μ_{12} = 0.5 D.

The energies of the perturbed states in the high-field limit are:

$$E_{\pm} = (1/2)\,(E_1 + E_2) \pm \mu_{eff}\cdot\mathbf{F} \tag{13.9}$$

with the effective dipole moment μ_{eff} of an electronic state (1) (with a zero-field dipole moment μ_1), with a nearby perturbing state (2) (with a zero-field dipole moment μ_2) in the high-field limit :

$$\mu^{\pm}_{eff} = (1/2)\,(\mu_1 + \mu_2) \pm (1/2)\left[(\mu_1 - \mu_2)^2 + 4\mu_{12}^2\right]^{1/2} \tag{13.10}$$

where μ_{12} is the transition dipole moment between the two interacting states, resulting in a perturbation of the zero-order Hamiltonian without field.

In the high-field limit the effective dipole moment of the lower perturbed state is close to that of the upper zero field state (2), while that of the upper perturbed state is closer to that

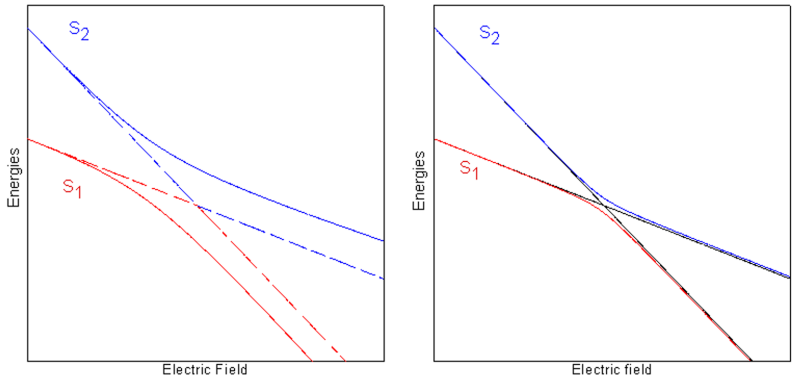

Figure 13.10.: Excited-state eigenvalues of the perturbed Hamiltonian for μ_1 = 0.9 D, μ_2 = 2.0 D and μ_{12} = 0.1 D (left) and μ_{12} = 0.5 D (right).

of the lower zero-field state (1). The smaller the transition dipole moment between the two interacting states is, the more similar gets the perturbed dipole moment of state (1) to that of the unperturbed state (2).

In the high field limit we can estimate the effective dipole moment of the lower excited state μ_{eff}^{+} to be 2.58 D and that of the higher excited state μ_{eff}^{-} to be 0.70 D, from the unperturbed values of μ_1, μ_2, and μ_{12} given in Table 13.2 using equation 13.10. The value of μ_{eff}^{+} = 2.58 D is in quite good agreement with that of the thermochromic shift method, showing that indeed mixing of S_1 and S_2 is responsible for the unexpectedly high dipole moment compared to the gas phase Stark measurements.

The SCS-CC2/cc-pVTZ dipole moments calculated at zero-field and with a field of 10^{10} V/m in direction of the S_1 dipole are given in Table 13.2 along with the transition dipole moment between the excited states μ_{12}. The entries given in bold numbers represent the dipole moment at the respective optimized geometry. Under field-free conditions, the S_2 dipole is 2.8 times larger than the S_1 dipole moment. Switching on the electric field, both dipole moments increase but notably the dipole moments of the S_1 state is now much closer to that of the S_2 state giving further evidence for the discussed state mixing.

Additionally to the altered effective dipole moments from perturbation of the lower state, Lombardi discussed the occurrence of field induced intensity borrowing, equivalent to Herzberg-Teller coupling. Field induced state mixing leads to intensity borrowing of modes for which the product of vibrational and electronic symmetry is the same as for the perturbing state. While for (ro)vibronically resolved spectroscopy this effect can be studied on a line-to-line basis, the broadening present in solution measurements leads to complete overlap of the vibronic bands, resulting in an apparent shift of maxima which are due to changing intensities

Table 13.2.: SCS-CC2/cc-pVTZ calculated dipole moments (in Debye) of the ground at lowest two excited singlet states, without electric field and with field of 10^{10} V/m at the three optimized geometries S_0, S_1 and S_2.

	@ opt. S_0	@ opt. S_1	@ opt. S_2
μ_1 0 V/m	0.877	**0.856**	0.683
μ_2 0 V/m	2.320	2.130	**2.392**
μ_1 10^{10} V/m	5.941	**5.992**	6.831
μ_2 10^{10} V/m	9.297	9.184	**8.069**
$\lvert\mu_{12}\rvert$ 0 V/m		**0.57**	

within the homogeneously broadened spectral envelope.

13.7. Conclusions

While the determination of excited state dipole moments from solvatochromic shifts has found widespread use, early criticism on the accuracy and applicability of the method [63, 70] has largely been ignored. While the most obvious shortcomings of dipole moment determination from solvatochromic shifts, like the differing interaction of the target molecule with different solvents can be avoided using thermochromic shifts [6, 8, 35, 60], the problem of state mixing from the large reaction fields in solution remain. We have shown, that the excited state dipole moment of 2,3-benzofuran, determined from thermochromic shifts is more than twice as large as the gas-phase value from electronic Stark spectroscopy. SCS-CC2 energy calculations performed at a path, which connects linearly the L_b- and L_a-minima of benzodioxan show an avoided crossing, which explains the "dipole stealing" of the lower singlet state (L_b) from the higher singlet state (L_a). Larger systems tend to have higher state densities with states that have potentially higher dipole moments than the addressed state. This analysis shows that the electronic configuration of a molecule in solution is different from that in the gas phase. Permanent dipole moments, determined with both methods are therefore not comparable and should be viewed as what they are: A measure of the electronic molecular configuration in the respective medium.

Acknowledgements

Computational support and infrastructure was provided by the "Center for Information and Media Technology" (ZIM) at the Heinrich-Heine-University Düsseldorf. Financial support of the German Research Foundation (DFG, Deutsche Forschungsgemeinschaft) via grant

SCHM1043/16-1 is gratefully acknowledged. We thank one of the reviewers for pointing out the benefits of the current analysis.

13.8. Own share in the publication

The content of this chapter has already been published in the *Journal of Photochemistry and Photobiology A: Chemistry*, **419**, 113476, 2021 under the title *Excited State Effective Dipole Moment of 2,3-Benzofuran from Thermochromic Shifts in Absorption and Emission Spectra.* written by Mirko Matthias Lindic, Tim Axel Oberkirch, Jörg Tatchen and Michael Schmitt.

My own share in the publication sums up to $60\,\%$ and consists of formal analysis, software, investigation, methodology, writing - original draft.

14. Article - Substituted Quinoxaline

The Excited State Dipole Moment of 2-[(4-Methoxyphenyl)ethynyl]-3-(1-methyl-1*H*-indol-3-yl)-quinoxaline from Thermochromic Shifts.

Mirko Matthias Lindic[a], Matthias Zajonz[a], Charlotte Gers-Panther[b], Thomas J. J. Müller[b], and Michael Schmitt[a 1]

[a] Heinrich-Heine-Universität, Institut für Physikalische Chemie I, D-40225 Düsseldorf, Germany, E-mail:mschmitt@hhu.de.
[b] Heinrich-Heine-Universität, Institut für Organische Chemie und Makromolekulare Chemie, D-40225 Düsseldorf, Germany

14.1. Abstract

The excited state dipole moment of 2-[(4-methoxyphenyl)ethynyl]-3-(1-methyl-1*H*-indol-3-yl)-quinoxaline has been determined in ethyl acetate solution using the method of thermochromic shifts. Three different models have been tested and are compared to each other and to the results of *ab initio* calculations at the coupled cluster CC2/cc-pVTZ and SCS-CC2/cc-pVTZ level of theory. Good agreement is obtained for solvent polarity functions as defined by Bilot and Kawski (L. Bilot and A. Kawski, *Z. Naturforsch.*, 1962, **17A**, 621−627), while the original Lippert-Mataga type polarity functions fail to describe the excited state dipole moment correctly. We report an excited state dipole moment of the title compound of 8.5 D and a change upon excitation of 5.5 D.

[1] mschmitt@hhu.de

14.2. Introduction

The concept of electric dipole moment, as a measure of charge distribution in molecules, was used very successfully, since it was originally introduced by Max Reinganum in 1903 and later, independently by Peter Debye in 1905 [50, 72, 110]. One of the reasons for the success of this model among chemists, is the concept of bond dipoles [51, 111, 179], which can be added up in a vectorial manner in order to result in a microscopically interpretable picture of the origin of dipole moments. Although, it had been shown that it is wrong to assume that any bond moment would point along the line joining the atoms which are connected by the chemical bond, as has been shown by Bader[180], the concept is still sufficiently accurate for non-vibrating molecules in their electronic ground states. For electronically excited states of even relatively small molecules, however, neither magnitude nor direction of the dipole moment can be deduced with sufficient accuracy from simple sum rules[80, 112, 113]. While the reason for this discrepancy is still not clear, Pratt and coworkers have shown that if the geometry of the substructures, which are used to calculate the bond dipole moments, remain unchanged, dipole moments might be added also for the electronically excited state [181]. However, to our knowledge, this has only been shown for a single example. For large dipole moment changes in multichromophores, which take place more or less localized in one of the chromophores, the additional problem of induction of dipoles in the other chromophores has to be considered.

Since the electron distribution changes considerably upon electronic excitation, molecular dipole moments change both their magnitude and orientation upon electronic excitation [48]. There are several experimental approaches to the values of the excited state dipole moments in the gas phase. Probably the most accurate method is rotationally resolved electronic Stark spectroscopy of cold isolated molecules [71, 77–81, 112]. The dependence of the absorption coefficient of an applied electric ac field for the determination of excited state dipole moments (electrochromic absorption) has been pioneered by Buckingham, Ramsey, Bridge and Liptay in the late 60s of the last century[27, 82].

Stark spectroscopy, however, despite its accuracy has several drawbacks, which prevent the broad application of this method. The most severe obstacle is that many molecules are thermally labile, and cannot transferred into the gas phase without heavy decomposition. Until now this problem remains unresolved, since the inherently large spectral resolution, which is needed to resolve the different M components in the electric field, requires non-Fourier-limited continuous laser beams, and thus prohibits the use of (pulsed) laser desorption techniques due to the too small duty cycle. Apart from this restriction, the resolution, which is needed to resolve even the zero-field spectra of large molecules, comes to a limit for molecules

with rotational constants of the order of a few hundred MHz [48].

Electrochromic absorption of molecules in non-polar solvents has been shown for a variety of molecules to yield reliable excited state dipole moments [27, 39, 82, 182].

A conceptionally simpler approach uses the solvatochromic shifts of the molecule under investigation in solvents of different dielectric constants and index of refraction [1, 2, 61, 69]. It can be traced back to Onsager's reaction field theory, which assumes a point dipole in a spherical cavity of radius a in a homogeneous and isotropic solvent with the permittivity ϵ [4]. The molecular dipole moment of the solute in the cavity induces a dipole moment in the solvent, which counterpropagates the inducing dipole moment. This so called reaction dipole generates an electric field, which stabilizes the molecular dipoles in both states, enabling a determination of the dipole change upon excitation from the spectral shifts in different solvents.

Although, the original Lippert-Mataga based approaches only allow for the determination of the absolute value of the dipole changes, Abe presented a method for the estimation of the angle θ between the ground and excited state dipole moments[85].

The method of thermochromic shifts was introduced by Kaswski [6], although already Suppan pointed out the temperature dependence of the solvatochromic shifts [31]. Later, Lindic *et al.* combined the method of thermochromic shifts with the replacement of the Onsager radius by the real cavity volume [8]. This procedure resulted in a good agreement of the excited state dipole moment of anisole for gas phase (from Stark spectroscopy) and condensed phase (from thermochromic shifts) values.

The synthesis of 2-[(4-methoxyphenyl)ethynyl]-3-(1-methyl-1*H*-indol-3-yl)-quinoxaline (**1a**) through a glyoxylation-Stephens-Castro coupling-cyclocondensation protocol is described in Ref. [183]. There, an analysis of the cavity radius has been performed using solvatochromic shifts and the calculated excited state dipole moment.

14.3. Theoretical and Experimental Methods

14.3.1. Quantum Chemical Calculations

Structure optimizations were performed employing Dunning's correlation consistent polarized valence triple zeta (cc-pVTZ) basis set from the TURBOMOLE library [89, 90]. The equilibrium geometries of the electronic ground and the lowest excited singlet states were optimized

using the second order approximate coupled cluster model (CC2) employing the resolution-of-the-identity (RI) approximation and the algebraic diagrammatic construction through second order model ADC(2) [91–93]. For the structure optimizations spin-component scaling (SCS) modifications to CC2 were taken into account [128], since SCS-CC2 achieves a high accuracy for ground and excited state dipole moments[129]. The harmonic vibrational frequencies for both electronic states have been obtained from numerical second derivatives, using the NumForce script [130], which is implemented in the TURBOMOLE program suite [184]. Dipole moments are calculated as first derivatives of the respective energy with respect to an external field at the CC2 level of theory.

The COnductor-like Screening MOdel (COSMO)[94], which is implemented in the ADC(2) module of the TURBOMOLE package, was used for the optimization of ground and excited state structures in bulk solution of ethyl acetate (permittivity ε = 6.09, index of refraction n = 1.376) using the cc2cosmo script of TURBOMOLE.

14.3.2. Experimental Methods

Ethyl acetate (EA) p.a. was purchased from Fisher scientific, and used without further purification. **1a** has been synthesized in a consecutive four-component synthesis, starting from 1-methylindole, oxalyl chloride, 1-ethynyl-4-methoxybenzene, and 1,2-diaminobenzene as described in Ref. [183].

Determination of the temperature dependent permittivity and index of refraction

The permittivity of the solvent ethyl acetate has been determined by measuring the capacity in the well defined capacitor of the Keysight 16452A Test Fixture combined with the Keysight E4990A Impedance Analyzer. The permittivity of ethyl acetate was measured in a temperature range from $277.15\ K$ to $327.15\ K$ with an AC frequency of 1 MHz. The temperature of the capacitor was controlled using an ethylene glycol bath, whose temperature was regulated by a LKB 2219 Multitemp II thermostatic circulator.

The refractive index of ethyl acetate was measured using an Anton Paar Abbemat MW refractometer in a temperature range from 283.15 K to 343.15 K at a wavelength of 598.6 nm.

Density measurements

The density ρ of eleven solutions with different mass fractions w of **1a** in ethyl acetate has been measured at temperatures between 263.15 K and 343.15 K with an increment of 2 K using the Anton Paar DMA 4500M density meter.

UV/Vis absorption and emission spectroscopy

Absorption and fluorescence spectra of **1a**, dissolved in ethyl acetate, were measured at temperatures between 245.15 K and 349.15 K with an increment of 2 K. For temperature control, a special heatable and cooled cell holder has been constructed, including two Peltier elements from Uwe Electronics GmbH, whose hot side is cooled using a Julabo Corio 600F liquid cooling device with Thermal G as cooling liquid. To prevent condensation of humidity on the cuvette's glass at low temperatures, the cell is mounted into a vacuum chamber, which was customized to fit in the absorption and fluorescence emission spectrometers. Absorption spectra were recorded, using a Varian Cary 50 Scan UV spectrometer. Fluorescence emission spectra were recorded on a Varian Cary Eclipse spectrometer.

14.4. Results

14.4.1. Computational Results

The structures of 2-((4-methoxyphenyl)ethynyl)-3-(1-methyl-1H-indol-3-yl)quinoxaline in the electronic ground and excited states were optimized at the CC2 and ADC(2)/cc-pVTZ level of theory, and additionally reoptimized using the COnductor Like Screening MOdel (COSMO), in order to simulate the solvent represented as dielectric continuum. The minimum of the potential energy surface has been proven by a normal mode analysis for each electronic state. All Cartesian coordinates of the optimized structures are given in the online supporting material. The atom numbers used are shown in Figure 14.1a.

We will start the discussion of the structural changes upon excitation with the two dihedral angles (for definitions of dihedral angles, cf. Figure 14.1a) that define the relative orientation of the anisole, the quinoxaline, and the N-methylindole moieties. In the electronic ground state the dihedral angle (24,23,2,1) is found to be 8°, i.e. anisole and quinoxaline are nearly co-planar. On the other hand, an angle of 57° is found for the dihedral angle (2,3,13,12) for the relative orientation of the quinoxaline and N-methylindole moieties. In the lowest electronically excited singlet state the dihedral angle between anisole and quinoxaline slightly

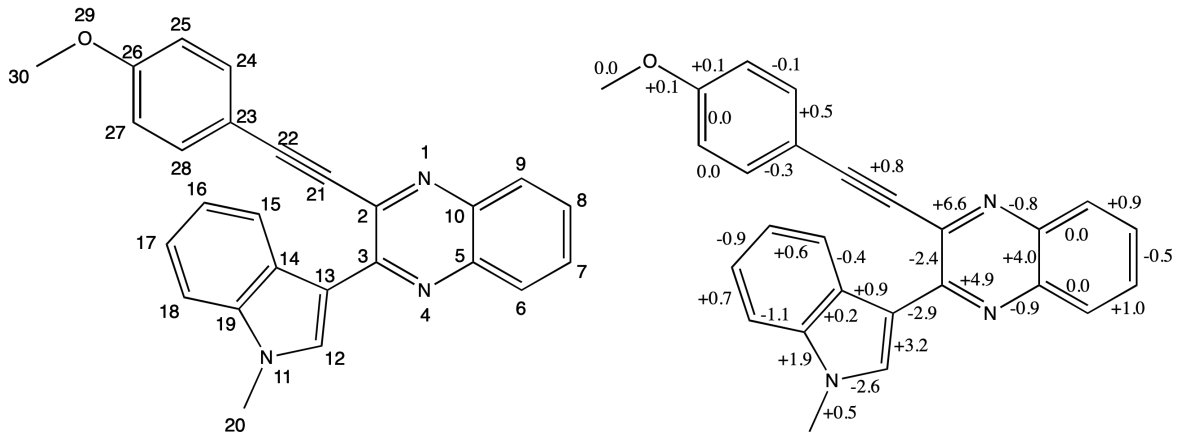

Figure 14.1.: a) Atomic numbering of **1a**.
b) Bond lengths changes (in pm) upon electronic excitation to the lowest excited singlet state, from the CC2/cc-pVTZ optimized structures.

decreases to 0.5°, while the angle between quinoxaline and N-methylindole strongly decreases to 23°. Hence, in the lowest excited singlet state quinoxaline and anisole are virtually coplanar, the N-methylindole and quinoxaline planes are tilted by 23°. This planarization points to a delocalized excitation, which involves all three chromophores. The bond length changes upon electronic excitation to the lowest excited singlet state are shown in Figure 14.1b. Strong variations of the bond lengths are found in the quinoxaline ring, mainly localized in the pyrazine moiety of quinoxaline. The intermediate bond length changes in the N-methylindole are alternating, an indication of an L_a like excitation[2] in the indole chromophore[18, 19, 186–188], while the bond lengths in the anisole moiety remain surprisingly small.

The permanent dipole moment of isolated **1a** in the ground state was calculated at MP2/cc-pVTZ level of theory to be 3.27 D. For the first excited singlet state, the calculated dipole moment is 10.33 D using ADC(2)/cc-pVTZ. In solution, with EA as solvent, employing COSMO, the calculated dipole moments increases to 4.07 D in the electronic ground state and to 14.98 D in the first excited singlet state. From the SCS-CC2/cc-pVTZ calculations, a ground state dipole moment of 3.35 D is obtained, which increases to 8.00 D upon electronic excitation to the first excited singlet state. All calculated dipole moments are compiled in Table 14.1. The molecular structure of the ground state and the dipole moments in both electronic states at the SCS-CC2 level of theory are shown in Figure 14.2. The ground state dipole moment is shown as green vector, and the excited state dipole moment as orange vector, both pointing in the direction from positive to negative center of charge. The angle between

[2]The L_a and L_b notation has been introduced by Platt for cata-condensed aromatic hydrocarbons[132]. This labeling scheme has later been extended to indoles by Weber[185]. One has to keep in mind however, that for molecules without two-fold rotation axis along the long inertial axis of the molecule, the meaningfulness of this nomenclature is doubtful.

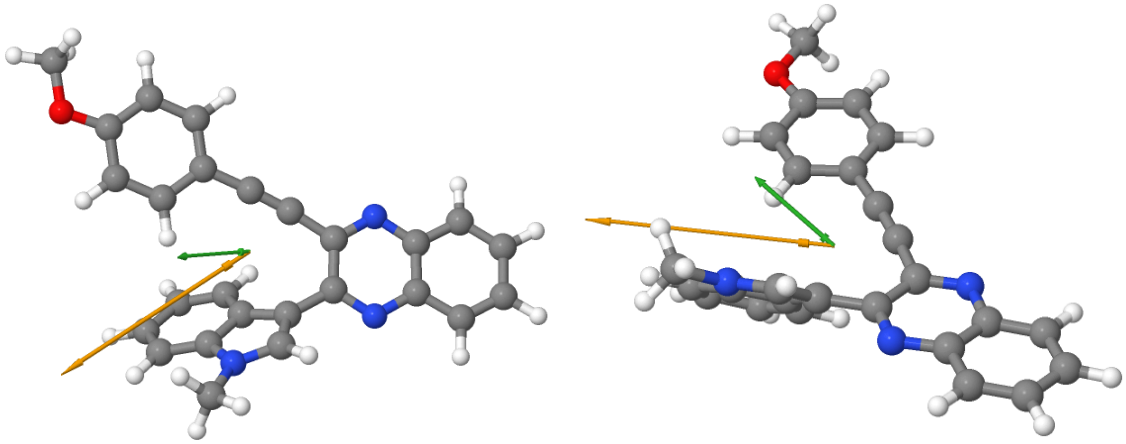

Figure 14.2.: CC2/cc-pVTZ optimized ground state structure and dipole moments of **1a** in the ground (green vector) and lowest electronically excited singlet state (orange vector), respectively. The angle between the dipole moment vectors of ground and excited state amounts to 36°. The two subfigures show different projections of the same molecular structure for sake of clearness.

the dipole moment vectors of ground and excited state amounts to 36°. For direct comparison, the excited state dipole vector is given in the geometry of the ground state. However, it has to be kept in mind that the excited state structure is different from the ground state.

With the results of the COSMO calculation at the ground state geometry of **1a**, which was optimized at the MP2 level of theory, the volume of the EA cavity has been determined to be $4.74 \cdot 10^{-28}$ m^3. This value slightly decreases to $4.73 \cdot 10^{-28}$ m^3 at the ADC(2) optimized structure of the excited state.

Figure 14.3 shows the frontier orbitals of the isolated molecule and the excitations to the lowest two electronically excited states. The excitation to the S_1 state is characterized by a nearly pure LUMO ← HOMO transition (coefficient 0.92), while excitation to the S_2 state is comprised of similar contributions of LUMO + 1 ← HOMO (0.70) and LUMO ← HOMO - 1 (-0.59).

From the CC2 wave functions, the density differences have been calculated and displayed in Figure 14.4. The blue shaded areas show decreased electron density upon excitation, while the red shaded areas represent increased electron density.

Inspection of Figure 14.4 shows that the π-electron density decreases at the methoxy moiety and increases at the N-methylindole moiety. A vector through the density changes has the general direction of the difference vector of S_0 and S_1 dipole moments in Figure 14.2.

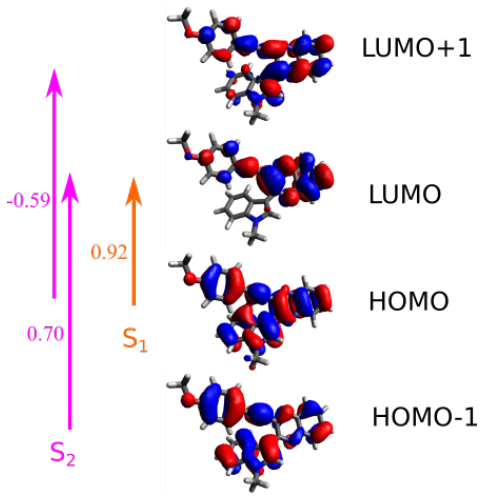

Figure 14.3.: Frontier orbitals of the isolated molecule and the excitations to the lowest two electronically excited states. The numbers at the arrows give the contributions to the excitation to the S_1 and S_2 states, respectively.

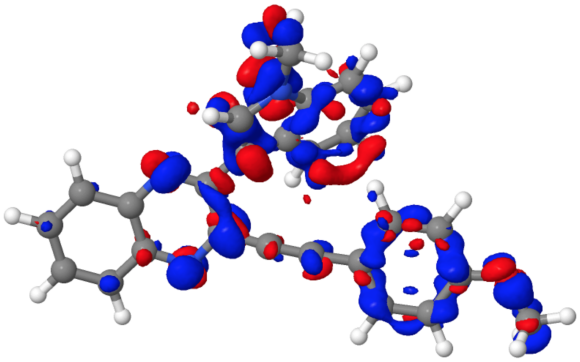

Figure 14.4.: Electron density difference plot of **1a** using the CC2 wavefunctions.

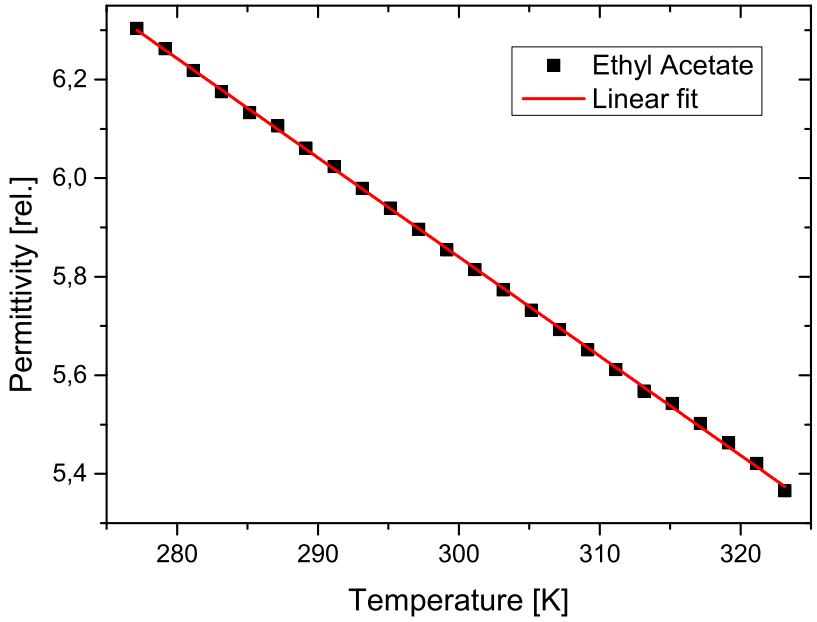

Figure 14.5.: Temperature dependent permittivity of ethyl acetate and applied linear fit in the range of 277.15 K to 327.15 K.

14.4.2. Experimental Results

Temperature Dependent permittivity and index of refraction

The permittivity was calculated by dividing the capacity of the capacitor filled with ethyl acetate through the capacity of the capacitor filled with air $\varepsilon_r = \frac{Cp}{Cp^0}$. The resulting temperature dependent permittivities are shown in Fig. 14.5. For further evaluation purposes the graph was fitted with a linear function, $\varepsilon_r(T) = 11.88 - 0.02013K^{-1}T$, which gave an R^2 value of $0,99966$.

The temperature dependent index of refraction (measured at 589.3 nm) was fitted to a third order polynomial function, $n(T) = 1.43766 + 2.2616 \times 10^{-4}K^{-1}T - 2.07045 \times 10^{-6}K^{-2}T^2 + 1.83987 \times 10^{-9}K^{-3}T^3$, for usage in further evaluation. The measured indices of refraction and the fit function are shown in Fig. 14.6.

Temperature Dependent Cavity Volume

A central point in the determination of dipole moment changes upon excitation from solvent shifts of absorption/emission spectra is the so called Onsager radius of the solvent cavity [4]. Since this radius enters the Lippert-Mataga [1, 2] and the Bilot-Kawski [3, 6] equations for the calculation of dipole moments in cubic power, small errors in Onsager radius cause large deviations in the experimentally determined dipole moments. Instead of using the Onsager

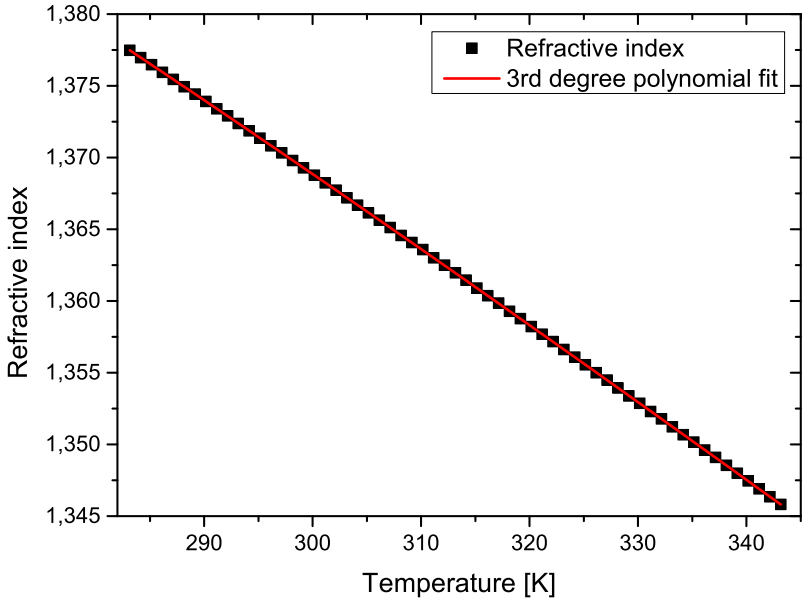

Figure 14.6.: Temperature dependent index of refraction of ethyl acetate and applied cubic polynomial fit in the range of 283.15 K to 343.15 K.

radius, which is not unequivocally defined, the real cavity volume can be used, as has been shown by Demissie *et al.* [7]. This quantity is accessible experimentally from simple density measurements of the solutions. The relation between the weight fraction w and molar cavity volume V_m is given by equation (14.1), where ρ is the density of the solution, ρ^* is the density of the solvent, w is the weight fraction of solvent and solute, V_m is the molar cavity volume and M is the molar mass of the solute.

$$\frac{1}{\rho} = \frac{1}{\rho^*} + \left(\frac{V_m}{M} - \frac{1}{\rho^*}\right) \cdot w \tag{14.1}$$

Using the slope m_d of the plot of inverse density of the solution versus the weight fraction, the molar cavity volume can be calculated according to equation (14.2).

$$V_m = M \cdot \left(m_d + \frac{1}{\rho^*}\right) \tag{14.2}$$

According to equations (14.1) and (14.2) the molar cavity volume can directly be calculated from the slope of a linear fit of the plot of the inverse density $\frac{1}{\rho}$ versus the weight fraction w. In this way, the single cavity volume at $293.15\ K$ has been evaluated to $6.04(4) \times 10^{-28}\ m^3$. This procedure was repeated for all temperatures, which are used in the thermochromic shifts. The graph $V_m(T)$, including the result of a linear fit, is shown in Fig. 14.7. The dependence of

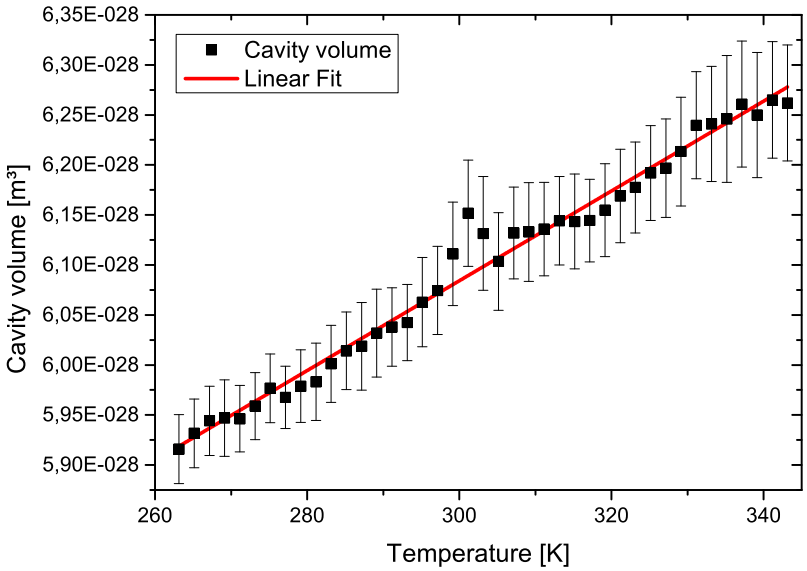

Figure 14.7.: Temperature dependent cavity volume of **1a** in ethyl acetate, along with a linear fit of the data.

the molar cavity volume from the temperature is described by the following linear equation:

$$V_m(T) = 4.5(1) \times 10^{-30}\ m^3 K^{-1} \cdot T + 4.74(4) \times 10^{-28}\ m^3. \tag{14.3}$$

Evaluation of Excited State Dipole Moments from Thermochromic Shifts

Even though the determination of excited state dipole moments using absorption and fluorescence emission spectroscopy in solution has already been invented in the mid 50s of the last century by Lippert [1] and Mataga [2], many improvements of their original method have been given in the meantime. While the original Lippert-Mataga theory exploited solvatochromic shifts in different solvents, Kawski proposed to use the temperature dependence of the permittivity ε and index of refraction n of the solvent to induce the spectral shifts of the solutions. In the present work, the methods of Lippert-Mataga[1, 2], Bilot-Kawski[3, 6], and Demissie[7] will be used and compared.

The original equation for solvatochromic shifts according to Lippert and Mataga can be used for thermochromic shifts as well, when the temperature dependence of ϵ and n is known:

$$\tilde{\nu}_A - \tilde{\nu}_F = -\frac{2(\mu_e - \mu_g)^2}{4\pi\varepsilon_0 hca^3} \cdot F_{LM} + const. \tag{14.4}$$

where ε_0 is the vacuum permittivity, h the Planck constant, c the speed of light, a the Onsager

cavity radius, and F_{LM} the solvent polarity function according to Lippert and Mataga[1, 2]:

$$F_{LM} = \frac{\varepsilon - 1}{2\varepsilon + 1} - \frac{n^2 - 1}{2n^2 + 1} \tag{14.5}$$

Equations (14.6) and (14.7) show the relation between spectral shifts and the solvent polarity function, where $\tilde{\nu}_A$ and $\tilde{\nu}_F$ are the wavenumbers of the maxima in absorption and fluorescence spectra, μ_g and μ_e are the ground and excited state dipole moment, respectively, ε_0 is the dielectric constant of the vacuum, $V(T)$ is the temperature dependent cavity volume, $\varepsilon(T)$ is the temperature dependent permittivity of the solvent and $n(T)$ is the temperature dependent refractive index of the solvent. Due to its temperature dependence, the cavity volume, which replaces the Onsager radius a in the original Lippert-Mataga theory, is included in the solvent polarity function. This replacement of the Onsager radius has first been suggested by Demissie *et al.*[7].

$$\tilde{\nu}_A(T) - \tilde{\nu}_F(T) = -\frac{2\left(\mu_e - \mu_g\right)^2}{3\varepsilon_0 hc} \cdot F_{LM}(T) + const. \tag{14.6}$$

$$F_{LM}(T) = \frac{1}{V(T)} \cdot \left[\frac{\varepsilon(T) - 1}{2\varepsilon(T) + 1} - \frac{n(T)^2 - 1}{2n(T)^2 + 1}\right] \tag{14.7}$$

The plot of $\tilde{\nu}_A(T) - \tilde{\nu}_F(T)$ (equation 14.6) versus F_{LM} (14.7) yields the change of the dipole moment upon electronic excitation from the slope m_{LM} of the respective graph:

$$\Delta\mu_g = \sqrt{\frac{3m_{LM}\varepsilon_0 hc}{2}} \tag{14.8}$$

Equations 14.9 and 14.10 describe the method of Bilot and Kawski and the corresponding solvent polarity function [3]. Also here, the temperature dependent cavity volume has been included in the solvent polarity function $F_{BK}(T)$, replacing the Onsager radius in the Bilot-Kawski expression in equation (14.9).

$$\tilde{\nu}_A(T) + \tilde{\nu}_F(T) = -\frac{2\left(\mu_e^2 - \mu_g^2\right)}{3\varepsilon_0 hc} \cdot F_{BK}(T) + const. \tag{14.9}$$

$$F_{BK}(T) = \frac{1}{V(T)} \cdot \left[\frac{2n(T)^2 + 1}{n(T)^2 + 2} \cdot \left(\frac{\varepsilon(T) - 1}{\varepsilon(T) + 1} - \frac{n(T)^2 - 1}{n(T)^2 + 2}\right) + \frac{3\left(n(T)^4 - 1\right)}{\left(n(T)^2 + 2\right)^2}\right] \tag{14.10}$$

From the slope m of the plot of $(\tilde{\nu}_A + \tilde{\nu}_F)$ versus $F_{BK}(T)$ (eq. 14.9), the excited state dipole moment can be evaluated, given that the ground state dipole moment μ_g is known:

$$\mu_e = \sqrt{\mu_g^2 + \frac{3\varepsilon_0 \cdot h \cdot c \cdot m}{2}} \tag{14.11}$$

Another equation for describing solvatochromic shifts was given and discussed by Demissie *et al.*[7]. We have modified this equation, in order to facilitate its use for thermochromic shifts as well:

$$\tilde{\nu}_{A/E}(T) = \tilde{\nu}^0_{A/E}(T) - \frac{2\mu_{g/e}\,(\mu_e - \mu_g)}{3\varepsilon_0 hc} \cdot F_{BK}(T) \tag{14.12}$$

Using equation (14.12), the slopes m_A and m_F of the respective plots of $\tilde{\nu}_A(T)$ and $\tilde{\nu}_E(T)$ versus the solvent polarity functions $F_{BK}(T)$ are used to calculate the dipole moments of ground and excited state independently:

$$\mu_g = \sqrt{\frac{3\varepsilon_0 hc m_A^2}{2(m_F - m_A)}} \tag{14.13}$$

$$\mu_e = \sqrt{\frac{3\varepsilon_0 hc m_F^2}{2(m_F - m_A)}} \tag{14.14}$$

While, in the original paper of Demissie *et al.*, both Lippert-Mataga and Bilot-Kawski solvent polarity functions have been used, we restrict ourselves to the case of the Bilot-Kawski (BK) solvent polarity function.

Fig. 14.8 shows the absorption and fluorescence emission spectra of **1a**, dissolved in ethyl acetate, at temperatures between $245.15\ K$ and $349.15\ K$. For exact determination of the maxima all spectra were filtered with a low band pass fast Fourier transform filter. For the evaluation we used the maximum of the lowest energy band of the absorption spectra as $\tilde{\nu}_A$ and the overall maximum of the fluorescence emission spectra as $\tilde{\nu}_F$.

In order to compare the different approaches of theory, described above, the data have been evaluated using three different methods. According to Kawski, the plot of the sum of wavenumber of the maxima $\tilde{\nu}_A + \tilde{\nu}_F$ versus the solvent polarity function of Bilot and Kawski $F_{BKD}(T)$ is shown in Fig. 14.9. From the slope of the linear fit function, the permanent dipole moment of the first excited singlet state can be determined to $8.62(3)\ D$, using the value of 3.35 from the CC2/cc-pVTZ calculation as ground state dipole moment. Alternatively,

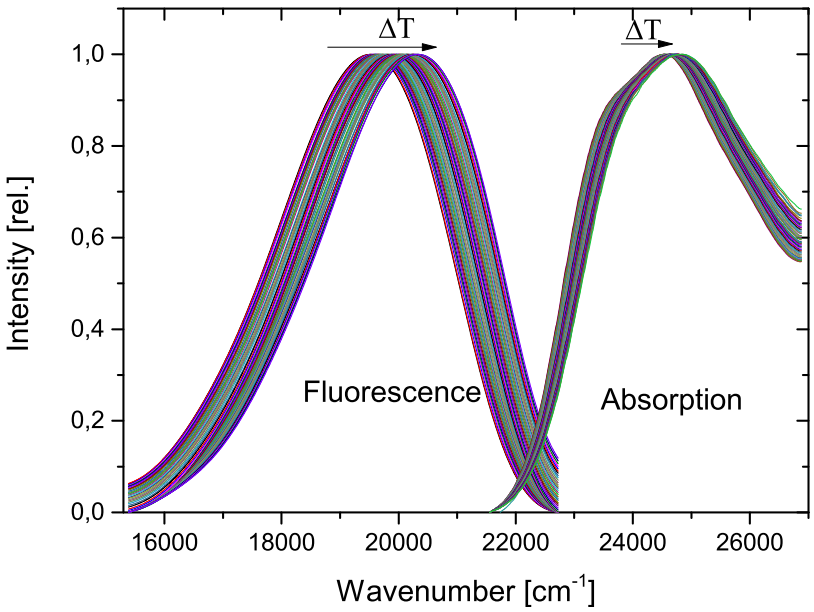

Figure 14.8.: Absorption and fluorescence emission spectra at temperatures between 245.15 K and 349.15 K.

the excited state dipole moment has been evaluated, using the method of Demissie with the solvent polarity function of Bilot and Kawski (BK). From the slope of $\tilde{\nu}_A$ or $\tilde{\nu}_F$ versus F_{BK} the dipole moments of ground and excited state can be obtained independently. For Demissie with the BK solvent polarity functions, a ground state dipole moment of 3.0 D and an excited state dipole moment of 8.49 D is obtained. As reference, we also used the original method of Lippert-Mataga, which was developed for solvatochromic shifts. With this method, a change of the dipole moment $\Delta\mu$ of 14.7 D was calculated. The plots for the evaluation of the data, following Lippert-Mataga and Demissie (BK), are given in the online supporting material. As in the case of the Bilot-Kawski evaluation (Figure 14.9), all plots show good linear dependence of the shifts from the different solvent polarity functions. All results are compiled in Table 14.1.

14.5. Discussion

The SCS-CC2/cc-pVTZ and CC2/cc-pVTZ optimized structures of **1a** have been proven to be minima, both in the ground state and in the electronically excited states, from normal mode analyses, using numerical second derivatives of the potential energy implemented in the NumForce script in TURBOMOLE [130]. Using the equilibrium structures and the numerical Hessian of ground and excited states, the 3 x 3 Hougen-Watson (HW) rotational matrix[189], which determines the rotation of the inertial axis system upon electronic excitation, has been evaluated. From the HW matrix Euler angles of θ = -1.0°, ϕ = 1.1°, and χ = -5.9° were

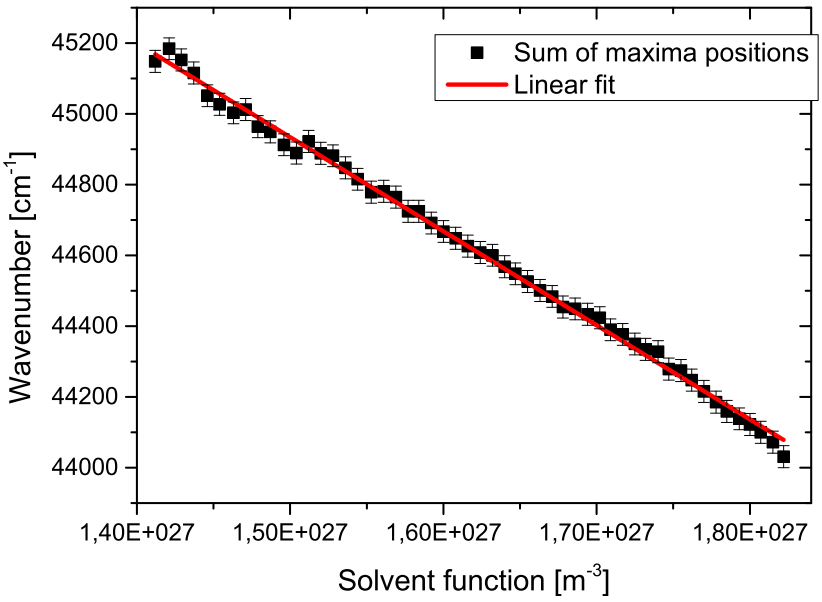

Figure 14.9.: Sum of the wavenumbers of spectral maxima versus solvent polarity function according to Kawski[3, 6], along with a linear fit of the data

Table 14.1.: Resulting dipole moments from different computational methods and thermochromic measurements with different evaluations. For each method the number of equation for determination of the slope and the solvent polarity function F are given. All values which are not directly calculated with the mentioned method are gray colored. Ground state dipole moment value is taken from SCS-CC2/cc-pVTZ calculations, since it was shown by Hellweg[129] that spin-component scaled CC2 yields a high accuracy of dipole moments in ground and electronically excited states, and a very good correlation of the computed dipole moments with data from high-resolution spectroscopy.
[a] Using the SCS-CC2/cc-pVTZ value for the ground state dipole moment.

Method	slope	F	μ_g [D]	μ_e [D]	$\Delta\mu$ [D]
MP2/ADC(2)/cc-pVTZ	-	-	3.27	10.33	7.06
COSMO MP2/ADC(2)/cc-pVTZ	-	-	4.07	14.98	10.91
CC2/cc-pVTZ	-	-	3.70	10.18	6.48
COSMO CC2/cc-pVTZ	-	-	4.71	12.66	7.95
SCS-CC2/cc-pVTZ	-	-	3.35	8.00	4.65
COSMO SCS-CC2/cc-pVTZ	-	-	3.75	9.93	6.18
Lippert-Mataga[a]	(14.4)	(14.7)	3.35	17.55(20)	14.7(2)
Bilot-Kawski[a]	(14.9)	(14.10)	3.35	8.62(3)	5.27(3)
Demissie(BK)	(14.12)	(14.10)	3.0(1)	8.49(6)	5.49(11)

obtained. Thus, it is roughly justified, to depict the dipole moment orientations for the ground and excited singlets states in Figure 14.2 in a common coordinate system.

From weight fraction dependent solution density measurements a cavity volume of $6.05 \cdot 10^{-28}$ m^3 for **1a** dissolved in EA has been determined at 293.15 K. Assuming a spherical cavity, this volume is equivalent to a cavity radius a of 524.7 pm. The *ab initio* calculated value from COSMO SCS-CC2/cc-pVTZ, using a solvent permittivity ϵ of 6.09, is $4.74 \cdot 10^{-28}$ m^3, which is equivalent to a spherical cavity with a radius of 483.7 pm. An underestimation of the cavity size of 20 % from COSMO SCS-CC2/cc-pVTZ calculations has been found on the much smaller anisole system[8], and seems to be the limit of the method. Gers *et al.* estimated the cavity radius of **1a** to be between 440 and 540 pm, with an average of 490 pm from solvatochromic shifts[183].

Hellweg[129] showed that highly accurate dipole moments in ground and electronically excited states, and a very good correlation of the computed dipole moments with data from high-resolution spectroscopy can be achieved using spin-component scaled CC2. Thus, we took the SCS-CC2 computed ground state dipole moment as basis for the methods, which result only in dipole moment changes upon electronic excitation in order to assess the dipole moments in the excited state. Demissie's method results in ground and excited state dipole moments, independently. Using the solvent polarity function of Bilot and Kawski, a ground state dipole moment of 3.0(1) D is obtained, which is close to the value of 3.35 D from the SCS-CC2/cc-pVTZ calculations.

The excited state dipole moments obtained from the methods of Kawski and of Demissie, with the BK solvent polarity function, show good agreement with the *ab initio* SCS-CC2/cc-pVTZ calculated values, cf. Table 14.1. Genuine CC2 and ADC(2) calculations, both with the cc-pVTZ basis set yield values, which are about 2 Debye higher than that of the spin-component scaled CC2 variant.

The main reason for the deviation of experimental and computed excited state dipole moments from shifts of absorption and/or emission spectra, apart from the known deficiencies of the method[63, 64] [3] , is the fact that the direction of the dipole moment changes upon excitation, cf. Figure 14.1. An additional source of error is the temperature dependence of the maximum of the contour of the absorption spectra due to emerging hot bands. Thus, there is a subtle

[3]The main deficiencies are (i) The Onsager radius is hard to determine, especially for molecules with a non-spherical shape, but enters the equations in cubic power. (ii) The inherently low resolution of the spectra in solution makes the determination of spectral shifts cumbersome. (iii) The large field strengths of the reaction field in solution lead to perturbative state mixing with nearby electronic states of different dipole moment.

balance between small temperature ranges for thermochromic shifts, which will decrease the accuracy and large ranges, which increase the possible errors due to hot bands. The system chosen here is in that respect very favorable, since the dipole moment change is large and hence the spectral shifts can be measured accurately already for small temperature changes.

14.6. Conclusions

The method of thermochromic shifts has been utilized to determine the dipole moment of 2-[(4-Methoxyphenyl)ethynyl]-3-(1-methyl-1*H*-indol-3-yl)-quinoxaline in the lowest electronically excited singlet state and compared to the results of *ab initio* calculations at the spin-component scaled coupled cluster CC2 level of theory.

We found that the replacement of the Onsager radius a by the real molar cavity volume $V_m = 4/3\pi a^3$ and inclusion of V_m into the solvent polarity function, improves the accuracy of the experimentally determined excited state dipole moments considerably. Since the cavity volume is a function of density, temperature, and molecular parameters[190], it has to be evaluated at the respective temperatures of the thermochromic shift measurements, i.e. the quantity $V_m(T)$ has to be determined experimentally. No deviations from linearity of the thermochromic shifts have been observed in the temperature range studied here. Thus, we conclude that the influence of hot bands on the determination of excited state dipole moments is negligible. This, however, has to be confirmed for other systems with smaller dipole moment changes and hence smaller spectral shifts in a given temperature interval.

14.7. Acknowledgements

Computational support and infrastructure was provided by the "Center for Information and Media Technology" (ZIM) at the Heinrich-Heine-University Düsseldorf.

14.8. Own share in the publication

The content of this chapter has already been published in the journal *Spectrochimica Acta Part A: Molecular and Biomolecular Spectroscopy*, **228**, 117574, 2020 under the title *The excited state dipole moment of 2-[(4-methoxyphenyl)ethynyl]-3-(1-methyl-1H-indol-3-yl)-quinoxaline from thermochromic shifts* written by Mirko Matthias Lindic, Matthias Zajonz, Charlotte Gers-Panther, Thomas J. J. Müller and Michael Schmitt.

My own share in the publication sums up to $50\,\%$ and consists of formal analysis, software, investigation, methodology, writing - original draft.

Part IV.

Summary, Outlook, Lists and more

15. Summary

The main focus of this thesis lies in the development and testing of a reliable thermochromic method to determine dipole moments of fluorescing molecules in solution. For testing and comparison of the obtained results the methods of High Resolution Laser Induced Fluorescence Stark spectroscopy (HRLIF-Stark) for smaller molecules and *ab initio* calculations on the CC2/cc-pVTZ level of theory for larger molecules are used.

Chapter 4, 6 and 10 contain the condensed information about the developed method. The full experimental setup as well as the procedures of density measurement, recording of spectra and data procession, including the fitting of UV/Vis absorption and fluorescence spectra, are described there in detail. Also, the determination of the parameters for the solvent polarity function is presented as well as the determination of ground state dipole moments. Finally, differences occurring in the evaluation of different molecules and the reliability of several presented methods are discussed. In Section 10.1, the spectroscopy chamber, which was specially constructed for this experiment to fulfil all requirements for reliable temperature control and the alterations of both used spectrometers, is shown in details including the process of construction and, up to now, unpublished design details.

In Chapter 7, the ideas of Kawski [6] and Demissie [7] were combined. The idea behind this was to include the advantage of accuracy and precision that Demissie could observe with the experimental determination of the cavity volume into Kawskis thermochromic method, which itself tends to give more reasonable results than any solvatochromic method before. Additionally the experimentally determined cavity volume was determined depending on the temperature of the solution to enhance the accuracy even further.

As sample molecule for this first step, anisole (methoxybenzene) [8] was chosen. This choice has been made, because anisole was already measured in the HRLIF-Stark spectroscopy and therefore a comparison to a reference experiment was possible in addition, whith regards to quantum chemical calculations. Also, a derivative form of anisole is a substituent in the molecule shown in Chapter 14 and the results could possibly be used for later reconstruction calculations. On the example of anisole, a variety of evaluation methods has been tested all

using the identical measurement data of thermochromic absorption and emission spectroscopy. Namely, the modified methods of Kawski, Lippert-Mataga and Demissie, using both the Bilot-Kawski [3, 28] and Lippert-Mataga [1, 2] solvent polarity function, employing the experimentally determined temperature dependent cavity volume, has been evaluated and compared to HRLIF-Stark values and *ab initio* calculations. The results here showed clearly, that only the models which use the solvent polarity function of Bilot-Kawski, respecting the polarizability of the solvent, give results which can reasonably be compared to gas phase experiments and calculations of isolated molecules. Also, the determination of the ground state dipole moment using solvent spectra which was published by Demissie [7] did not yield correct results compared to HRLIF-Stark and *ab initio* calculations. This fact supports the theory, that the evaluation of solution spectra only ever give information about the difference between the two involved electronic states and no absolute information about one of the states. To enable the scientific community to check and reproduce our results or use it for further evaluations, the complete data from the anisole measurements have been published in the journal "Data in Brief" (cf. Chapter 9 together with some graphs which was not shown in [8].

After the basic method and a simple molecule have been covered in the first chapters, the following Chapters 12, 13 and 14, focus on larger molecular systems with more complex behaviour. First, Chapter 12 looks at the molecule 1-methylindole, which is electronically nearly identical to indole, the chromophore of the amino acid tryptophan, and therefore is of interest for biochemical applications. The results of the thermochromic measurements and evaluation here show a clear discrepancy compared with *ab initio* calculations, HRLIF-Stark results are unfortunately not available at this point. An analysis using the perturbation theory of Lombardi [64] resulted in the idea of state mixing under high-field interactions which could be verified through further evaluations and comparison with quantum chemical calculations of the second excited singlet state. The conclusion here clearly shows, that like primary shown by Brisker et al. [135], the first excited singlet state of 1-methylindole gains major ^1L_a character from high-field state mixing with the second excited singlet state when dissolved in a polar solvent. It can be expected, that the HRLIF-Stark results, when they are available, will verify the *ab initio* results showing the first excited singlet state with major ^1L_b character in the isolated molecule.

The results of studies on 2,3-benzofuran in Chapter 13 have shown a great similarity to what have been concluded for 1-methylindole. In this case, comparable results from HRLIF spectroscopy were present and behaved exactly as proposed above. For 2,3-benzofuran also, the studies on the mixing of states in the high electric field have been intensified. A linear interpolated path has been calculated between the S_1 and S_2 states at different field strengths

to find the avoided crossing, where state mixing appears. At an electric field strength of $10^{10}\ \mathrm{V\,cm^{-1}}$, the avoided crossing could be found which verifies the previous assumption. The effective dipole moment of the lower excited state could be found in good agreement with the experimental results from the thermochromic method. Concluding from both Chapters 12 and 13 it can be stated, that no result from a solvatochromic or thermochromic method can be valid without comparisons to gas phase methods or quantum chemical calculations including information about the mixing of near excited states. The results of solvatochromic or thermochromic methods on their own solely can be seen as rough estimate giving an idea about the upper boundary of the excited state dipole moment.

In Chapter 14, the step to molecules which are too large to be vaporized into a molecular beam in HRLIF-Stark spectroscopy is made. The molecule of interest in this article is a push-pull system chromophore including the three systems quinoxaline, anisole (bridged with ethinyl) and 1-methylindole. Interesting points for molecules of this size regarding special solution methods are the changing of the dipole angle upon excitation and the (de)localization of the excitation through all the aromatic rings. Changes of the dipole angle are larger for this molecule than with any other in this work. This observation is interesting regarding the results of the thermochromic method, because the angular change is in no way respected in the basic theory. Through comparison of the dihedral angles it could be determined that the excitation is delocalized over all three chromophore parts. Contrary to this, the bond length changes upon excitation, which seems to predict a localization mainly on the pyrazine moiety of the quinoxaline chromophore and the 1-methylindole chromophore. Additionally, the alternating intermediate bond length changes in the 1-methylindole chromophore thus indicating what was finally confirmed in Chapter 12: The excitation into the first electronically excited singlet state leads to a major ^1L_a character for the 1-methylindole chromophore. The experimental results verify some of the observations which have been made in other articles, too: the results from the Kawski evaluation fit very well with the results of SCS-CC2/cc-pVTZ calculations and the results of all evaluations with the Lippert-Mataga solvent polarity function completely exaggerate the values from any of the experimental and computational methods in comparison. Most of the *ab initio* methods show dipole moments slightly above the results of the SCS-CC2/cc-pVTZ method but none of them can get near the Lippert-Mataga values. One observation absolutely does not fit the results of other experiments and publications: the ground state dipole moment from the Demissie evaluation using the Bilot-Kawski solvent polarity function fits nearly perfect with the ground state dipole moment from the SCS-CC2/cc-pVTZ calculations. Both former and later experiments support the theory that it shall only be possible to get information about the difference between two states and no absolute values for both involved states, but here with the large push-pull molecule the

results seem to fit perfectly.

What can be assumed from all of the experiments is, that the developed method as a blend of the Kawski [6] equations using the idea of a experimentally determined cavity volume introduced by Demissie [7] and then determining the volume of a single molecular cavity depending on the temperature, works successfully on various different systems. Also, comparisons with quantum chemical calculations introducing the **CO**nductor-like **S**creening **MO**del (COSMO) it can be assumed that in all cases the COSMO calculation underestimates the cavity radius by about $15 - 20\%$, resulting in a underestimation of the excited state dipole moment if used for the shown evaluations.

16. Outlook

On the foundation of the studies which are discussed in this thesis, a project for the investigation of certain molecules with the ability to perform ICT and TADF has been started and is founded by the German Research Foundation (DFG, Deutsche Forschungsgemeinschaft). Beginning with substructures as triphenylamine and the dicyanobenzenes (cf. Fig. 16.1b and 16.1a), the aim is to study the excited state dipole moment and behaviour of excited states in solution of 4'-(diphenylamino)-[1,1'-biphenyl]-2,5-dicarbonitrile (cf. Fig. 16.2). Additionally, the molecules 4,4'-(quinoxaline-5,8-diyl)bis(N,N-diphenylaniline) and 2,8-di(10H-phenothiazin-10-yl)dibenzo[b,d]thiophene 5,5-dioxide (cf. Fig. 16.3 and 16.4) are meant to be investigated with thermochromic UV/Vis absorption and fluorescence emission spectroscopy. From the results of these studies an increased understanding of large chromophores in solution can be gained. Additionally, the combination of knowledge about the large chromophores and their smaller building blocks should give a deeper insight into the spectroscopic behaviour of electronic states in general which will help to design high performance dyes in the future.

Basically, the thermochromic method can be applied everywhere as a substitute in studies where solvatochromic methods are used today. The applications, mentioned in Chapter 1, can all profit from innovations and development in the field of dipole moment determination in solution, especially when the evaluation in comparison with ab initio methods can give advanced insight into the general behaviour of excited states depending on the molecular surrounding.

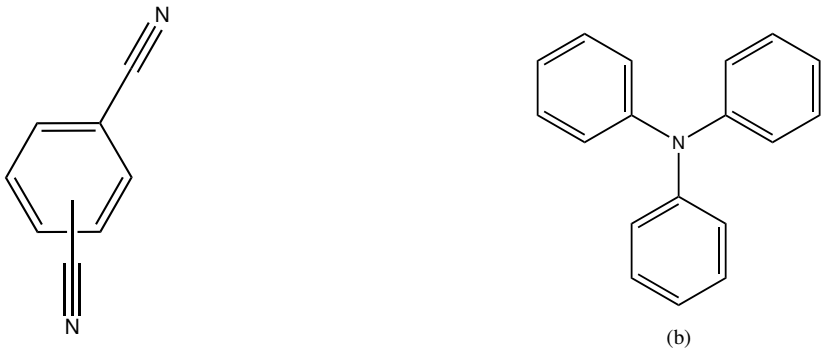

Figure 16.1.: Schematic structures of the dicyanobenzenes (a). The second cyano group can be located in any free position. Structure of triphenylamine (b). It has to be kept in mind, that the nitrogen has an electron lone pair.

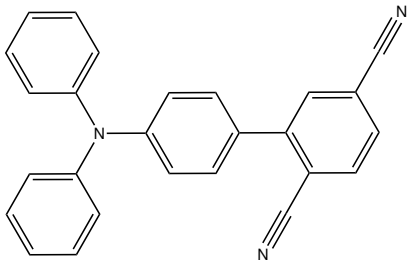

Figure 16.2.: Structure of 4'-(diphenylamino)-[1,1'-biphenyl]-2,5-dicarbonitrile.

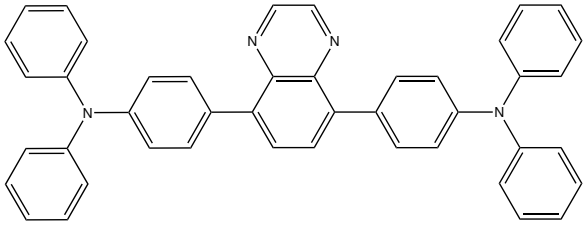

Figure 16.3.: Structure of 4,4'-(quinoxaline-5,8-diyl)bis(N,N-diphenylaniline).

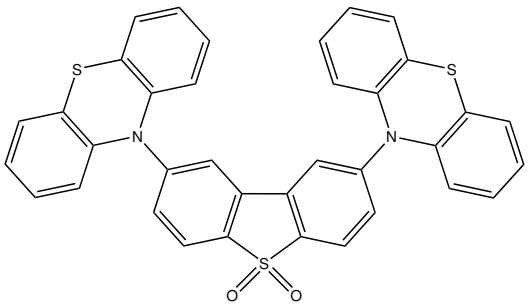

Figure 16.4.: Structure of 2,8-di(10H-phenothiazin-10-yl)dibenzo[b,d]thiophene 5,5-dioxide.

Complete list of publications and conference contributions

Publications

- Michael Schneider, Marie-Luise Hebestreit, **Mirko Matthias Lindic**, Hilda Parsian, América Yareth Torres-Boy, Leonardo Álvarez-Valtierra, W. Leo Meerts, Ralf Kühnemuth and Michael Schmitt: Rotationally resolved electronic spectroscopy of 3-cyanoindole and the 3-cyanoindole–water complex. *PCCP*, **20**, 23441-23452, 2018

- **Mirko Matthias Lindic**, Matthias Zajonz, Marie-Luise Hebestreit, Michael Schneider, W. Leo Meerts, Michael Schmitt: Excited state dipole moments of anisole in gas phase and solution. *JPPA*, **365**, 213-219, 2018

- **Mirko Matthias Lindic**, Matthias Zajonz, Marie-Luise Hebestreit, Michael Schneider, W. Leo Meerts, Michael Schmitt: Additional data for evaluation of the excited state dipole moments of anisole. *Data in Brief*, **21**, 313-315, 2018

- Marie-Luise Hebestreit, Michael Schneider, Hilda Lartian, Vivienne Betz, Michael Heinrich, **Mirko Lindic**, Myong Yong Choi and Michael Schmitt: Structures, dipole moments and excited state lifetime of isolated 4-cyanoindole in its ground and lowest electronically excited singlet states. *PCCP*, **21**, 14766-14774, 2019

- **Mirko Matthias Lindic**, Matthias Zajonz, Charlotte Gers-Panther, Thomas J. J. Müller, Michael Schmitt: The excited state dipole moment of 2-[(4-methoxyphenyl)ethynyl]-3-(1-methyl-1H-indol-3-yl)-quinoxaline from thermochromic shifts. *SAA*, **228**, 117574, 2020

- **Mirko Matthias Lindic**, Matthias Zajonz, Marie-Luise Hebestreit, Michael Schneider, W. Leo Meerts, Michael Schmitt: Determination of excited state dipole moments in solution via thermochromic methods. *MethodsX*, **7**, 101101, 2020

- **Mirko Matthias Lindic**, Michael Schmitt: Ground and excited state dipole moments

of 1-methylindole from thermochromic shifts in absorption and emission spectra. *JPPA*, **406**, 112984, 2021

- **Mirko Matthias Lindic**, Tim Axel Oberkirch, Jörg Tatchen, Michael Schmitt: The Excited State Effective Dipole Moment of 2,3-Benzofuran from Thermochromic Shifts in Absorption and Emission Spectra. *JPPA*, 2021, accepted for publication, Reference: JPC_113476,

Active Conference Contributions

- Oral presentation: **Mirko Lindic**, Michael Schneider, Marie-Luise Hebestreit, and Michael Schmitt. Dipole Moments of Anisole in Ground and Excited State via Condensed Phase Thermochromic Spectroscopy and Gas Phase HRLIF Spectroscopy. 82nd Annual Conference of the DPG and DPG Spring Meeting 03/2018.
- Oral presentation: **Mirko Lindic**, Michael Schneider, Marie-Luise Hebestreit and Michael Schmitt. Dipole Moments of Anisole in Ground and Excited State via Condensed Phase Thermochromic Spectroscopy and Gas Phase HRLIF Spectroscopy. XXXIV European Congress on Molecular Spectroscopy - EUCMOS 2018 08/2018
- Oral presentation: **Mirko Lindic**, Matthias Zajonz, Tim Oberkirch, and Michael Schmitt. Excited state dipole moment of 2-((4-methoxyphenyl)ethynyl)-3-(1-methyl-1H-indol-3-yl)quinoxaline via condensed phase thermochromic spectroscopy. 83rd Annual Conference of the DPG and DPG Spring Meeting 03/2019.

Bibliography

[1] Lippert, E. Dipolmoment und Elektronenstruktur von angeregten Molekülen. *Z. Naturforsch.* **1955**, *10A*, 541.

[2] Mataga, N.; Kaifu, Y.; Koizumi, M. Solvent Effects upon Fluorescence Spectra and the Dipolemoments of Excited Molecules. *Bull. Chem. Soc. Jpn* **1956**, *29*, 465.

[3] Bilot, L.; Kawski, A. Zur Theorie des Einflusses von Lösungsmitteln auf die Elektronenspektren der Moleküle. *Z. Naturforsch.* **1962**, *17A*, 621–627.

[4] Onsager, L. Electric Moments of Molecules in Liquids. *J. Am. Chem. Soc.* **1936**, *58*, 1486–1493.

[5] Gryczynski, I.; Kawski, A. Temperaturabhängigkeit der statischen Dielektrizitätskonstante und des optischen Brechungsindexes von Flüssigkeiten. *Z. Naturforsch.* **1975**, *30A*, 287–291.

[6] Kawski, A.; Kuklinski, B.; Bojarski, P. Dipole moment of aniline in the excited S_1 state from thermochromic effect on electronic spectra. *Chem. Phys. Letters* **2005**, *415*, 251–255.

[7] Demissie, E. G.; Mengesha, E. T.; Woyessa, G. W. Modified Solvatochromic equations for better estimation of ground and excited state dipole moments of p-aminobenzoicacid (PABA): Accounting for real shape over hypothetical spherical solvent shell. *J. Photochem. and Photobiol. A* **2016**, *337*, 184–191.

[8] Lindic, M. M.; Zajonz, M.; Hebestreit, M.-L.; Schneider, M.; Meerts, W. L.; Schmitt, M. Excited state dipole moments of anisole in gas phase and solution. *Journal of Photochemistry and Photobiology A: Chemistry* **2018**, *365*, 213 – 219.

[9] Lakowicz, J. *Principles of Fluorescence Spectroscopy*, 2nd ed.; Plenum: New York, USA, 1999.

[10] Abeywickrama, C.; Premaratne, M.; Gunapala, S. D.; Andrews, D. L. Impact of a

charged neighboring particle on Förster resonance energy transfer (FRET). *Journal of Physics: Condensed Matter* **2019**, *32*, 095305.

[11] Jana, D.; Jana, S. Donor–Pyrene–Acceptor Distance-Dependent Intramolecular Charge-Transfer Process: A State-Specific Solvation Preferred to the Linear-Response Approach. *ACS Omega* **2020**, *5*, 9944–9956.

[12] Ye, J.-T.; Wang, H.-Q.; Zhang, Y.; Qiu, Y.-Q. Regulation of the Molecular Architectures on Second-Order Nonlinear Optical Response and Thermally Activated Delayed Fluorescence Property: Homoconjugation and Twisted Donor–Acceptor. *The Journal of Physical Chemistry C* **2020**, *124*, 921–931.

[13] Ramprasad Misra, S. B. *Intramolecular Charge Transfer*; John Wiley and Sons, Ltd, 2018; Chapter 1, pp 1–27.

[14] Shirakawa, H.; Louis, E. J.; MacDiarmid, A. G.; Chiang, C. K.; Heeger, A. J. Synthesis of electrically conducting organic polymers: halogen derivatives of polyacetylene, (CH). *J. Chem. Soc., Chem. Commun.* **1977**, 578–580.

[15] Howard, W. E. Better displays with organic films. *Scientific American* **2004**, *290*, 76–81.

[16] Endo, A.; Sato, K.; Yoshimura, K.; Kai, T.; Kawada, A.; Miyazaki, H.; Adachi, C. Efficient up-conversion of triplet excitons into a singlet state and its application for organic light emitting diodes. *Applied Physics Letters* **2011**, *98*, 083302.

[17] Penfold, T. J.; Dias, F. B.; Monkman, A. P. The theory of thermally activated delayed fluorescence for organic light emitting diodes. *Chem. Commun.* **2018**, *54*, 3926–3935.

[18] Küpper, J.; Pratt, D. W.; Leo Meerts, W.; Brand, C.; Tatchen, J.; Schmitt, M. Vibronic coupling in indole: II. Investigation of the 1La–1Lb interaction using rotationally resolved electronic spectroscopy. *Phys. Chem. Chem. Phys.* **2010**, *12*, 4980–4988.

[19] Brand, C.; Küpper, J.; Pratt, D. W.; Meerts, W. L.; Krügler, D.; Tatchen, J.; Schmitt, M. Vibronic coupling in indole: I. theoretical description of ^1L_a and ^1L_b interactions and the absorption spectrum. *Phys. Chem. Chem. Phys.* **2010**, *12*, 4968–4997.

[20] Brand, C. Shaping and Modeling Electronically Excited States of Indole. Ph.D. thesis, Heinrich-Heine-Universität Düsseldorf, 2013.

[21] Capar, O. Forschungspraktikum, Arbeitsgruppe für Hochauflösende UV-Laserspektroskopie, Heinrich-Heine-Universität Düsseldorf. 2015.

[22] Wilke, M. Einfluss unterschiedlicher Substituenten auf den Charakter elektronisch angeregter Zustände. Inaugural-Dissertation, Heinrich-Heine-Universität Düsseldorf, 2017.

[23] Lindic, M. M.; Schmitt, M. Ground and excited state dipole moments of 1-methylindole from thermochromic shifts in absorption and emission spectra. *Journal of Photochemistry and Photobiology A: Chemistry* **2021**, *406*, 112984.

[24] Stark, J. Beobachtungen über den Effekt des elektrischen Feldes auf Spektrallinien I. Quereffekt. *Annalen der Physik* **1914**, *43*, 965–983.

[25] Surdo, A. L. Sul fenomeno analogo a quello di zeeman nel campo elettrico. *Rendiconti della Reale Accademia dei Lincei* **1913**, *22*, 664–666.

[26] Ooshika, Y. Absorption Spectra of Dyes in Solution. *Journal of the Physical Society of Japan* **1954**, *9*, 594–602.

[27] Liptay, W. Electrochromism and Solvatochromism. *Angew. Chem. internat. Edit.* **1969**, *8*, 177–188.

[28] Bilot, L.; Kawski, A. Der Einfluß des Lösungsmittels auf die Elektronenspektren lumineszierender Moleküle. *Zeitschrift für Naturforschung A* **1963**, *18*, 10 – 15.

[29] Bilot, L.; Kawski, A. Notizen: Dipolmomente einiger Phthalimid-Derivate im ersten angeregten Singulettzustand. *Zeitschrift für Naturforschung A* **1963**, *18*, 256 – 256.

[30] Czekalla, J. Zwei Elektro-Optische Methoden Zur Bestimmung Von Dipolmomenten Angeregter Molekule. *Chimia* **1961**, *15*, 26–+.

[31] Suppan, P.; Tsiamis, C. Temperature effects in solvatochromic shifts. *J. Chem. Soc., Faraday Trans. 2* **1981**, *77*, 1553–1562.

[32] Kawski, A.; Kukliński, B.; Bojarski, P. Thermochromic Shifts of Absorption and Fluorescence Spectra and Excited State Dipole Moment of PRODAN. *Z. Naturforsch.* **2000**, 550–554.

[33] Kawski, A.; Kukliński, B.; Bojarski, P. Thermochromic Absorption, Fluorescence Band Shifts and Dipole Moments of BADAN and ACRYLODAN. *Z. Naturforsch.* **2002**, 716–722.

[34] Kawski, A.; Kuliński, B.; Bojarski, P. Thermochromic Excited-State Dipole Moment

Measurements of p-Cyano-N,N-diethylaniline in Ethyl Acetate. *Z. Naturforsch.* **2003**, 118–120.

[35] Kawski, A.; Kukliński, B.; Bojarski, P. Dipole moment of benzonitrile in its excited S_1 state from thermochromic shifts of fluorescence spectra. *Chemical Physics Letters* **2006**, 306–312.

[36] Kawski, A.; Kukliński, B.; Bojarski, P. Excited state dipole moments of N,N-dimethylanilinefrom thermochromic effect on electronic absorptionand fluorescence spectra. *Chemical Physics Letters* **2006**, 118–192.

[37] Kawski, A.; Kukliński, B.; Bojarski, P. Temperature influence on dual fluorescence of4-(dimethylamino)benzaldehyde in 1,2-dichloroethane and ethyl acetate. *Chemical Physica Letters* **2008**, 52–54.

[38] Kawski, A.; Kukliński, B.; Bojarski, P. Photophysical properties and thermochromic shifts of electronic spectra of NileRed in selected solvents. Excited states dipole moments. *Chemical Physics* **2009**, 58–64.

[39] Liptay, W. Optical Absorption of Molecules in Liquid Solutions in an Applied External Electric Field (Electrochromism). *Berichte der Bunsen-Gesellschaft* **1976**, *80*, 207–217.

[40] Nemkovich, N. A.; Detert, H.; Pivovarenko, V. G.; Sobchuk, A. N.; Tomin, V. I.; Wroblewski, T. Specific orientation of dipole moments in azocrown cetocyanine dyes determined byelectrooptical absorption measurements (EOAM). *Journal of Luminescence* **2019**, *208*, 218–224.

[41] Guggenheim, E. A. A proposed simplification in the procedure for computing electric dipole moments. *Trans. Faraday Soc.* **1949**, *45*, 714–720.

[42] Guggenheim, E. A. The computation of electric dipole moments. *Trans. Faraday Soc.* **1951**, *47*, 573–576.

[43] Hedestrand, G. Die Berechnung der Molekularpolarisation gelöster Stoffe bei unendlicher Verdünnung. *Zeitschrift für physikalische Chemie* **1929**, *2*, 428–444.

[44] Smith, J. W. Some developments of Guggenheim's simplified procedure for computing electric dipole moments. *Trans. Faraday Soc.* **1950**, *46*, 394–399.

[45] Czekalla, J. Zur Berechnung von Dipolmomenten aus Messungen an verdünnten Lösungen. *Zeitschrift für Elektrochemie, Berichte der Bunsengesellschaft für physikalische Chemie* **1956**, *60*, 145–147.

[46] Desyatnyk, O.; Pszczolkowski, L.; Thorwirth, S.; Krygowski, T. M.; Kisiel, Z. The rotational spectra electric dipole moments and molecular structures of anisole and benzaldehyde. *Phys. Chem. Chem. Phys.* **2005**, *7*, 1708–1715.

[47] Loomis, F. W.; Wood, R. W. The Rotational Structure of the Blue-Green Bands of Na_2. *Phys. Rev* **1928**, *32*, 223–236.

[48] Schmitt, M.; Meerts, W. L. In *Frontiers and Advances in Molecular Spectroscopy*; Laane, J., Ed.; Elsevier, 2017; Chapter Structures and Dipole Moments of Molecules in Their Electronically Excited States, pp 143 – 194.

[49] Hebestreit, M.-L.; Lartian, H.; Schneider, M.; Kühnemuth, R.; Torres-Boy, A. Y.; Romero-Servin, S.; Ruiz-Santoyo, J. A.; Alvarez-Valtierra, L.; Meerts, W. L.; Schmitt, M. Structure and excited state dipole moments of oxygen containing heteroaromatics: 2,3-benzofuran. *Journal of Molecular Structure* **2020**, *1210*, 127992.

[50] Debye, P. *Polar molecules*; S. Hirzel: Leipzig, 1929.

[51] Williams, D. E. Representation of the Molecular Electrostatic Potential by Atomic Multipole and Bond Dipole Models. *J. Comp. Chem.* **1988**, *9*, 745–763.

[52] Lindic, M. M. Evaluation of Ground- and Excited State Dipole Moments via Thermochromic Fluorescence Spectroscopy - Studies with Improved Solvent Effect Approximation. mathesis, Heinrich-Heine-University Düsseldorf, 2018.

[53] Horng, M. L.; Gardecki, J. A.; Papazyan, A.; Maroncelli, M. Subpicosecond Measurements of Polar Solvation Dynamics: Coumarin 153 Revisited. *The Journal of Physical Chemistry* **1995**, *99*, 17311–17337.

[54] Kawski, A. On the Estimation of Excited-State Dipole Moments from Solvatochromic Shifts of Absorption and Fluorescence Spectra. *Z. Naturforsch.* **2002**, *57a*, 255–262.

[55] Lindic, M. M.; Zajonz, M.; Hebestreit, M.-L.; Schneider, M.; Meerts, W. L.; Schmitt, M. Determination of excited state dipole moments in solution via thermochromic methods. *MethodsX* **2020**, *7*, 101101.

[56] Kasha, M. Characterization of electronic transitions in complex molecules. *Discuss. Faraday Soc.* **1950**, *9*, 14–19.

[57] Lindic, M. M.; Zajonz, M.; Hebestreit, M.-L.; Schneider, M.; Meerts, W. L.; Schmitt, M. Additional data for evaluation of the excited state dipole moments of anisole. *Data in Brief* **2018**, *21*, 313 – 315.

[58] da Luz de Sousa, I.; Ximenes, V. F.; de Souza, A. R.; Morgon, N. H. Solvent-induced Stokes' shift in DCJTB: Experimental and theoretical results. *Journal of Molecular Structure* **2019**, *1192*, 186 – 191.

[59] Budzák, i.; Laurent, A. D.; Laurence, C.; Medved', M.; Jacquemin, D. Solvatochromic Shifts in UV–Vis Absorption Spectra: The Challenging Case of 4-Nitropyridine N-Oxide. *Journal of Chemical Theory and Computation* **2016**, *12*, 1919–1929, PMID: 26967198.

[60] Lindic, M. M.; Zajonz, M.; Gers-Panther, C.; Müller, T. J.; Schmitt, M. The excited state dipole moment of 2-[(4-methoxyphenyl)ethynyl]-3-(1-methyl-1H-indol-3-yl)-quinoxaline from thermochromic shifts. *Spectrochimica Acta Part A: Molecular and Biomolecular Spectroscopy* **2019**, 117574.

[61] Suppan, P. Invited review solvatochromic shifts: The influence of the medium on the energy of electronic states. *J. Photochem. Photobiol. A* **1990**, *50*, 293.

[62] Marini, A.; Muñoz-Losa, A.; Biancardi, A.; Mennucci, B. What is Solvatochromism? *The Journal of Physical Chemistry B* **2010**, *114*, 17128–17135, PMID: 21128657.

[63] Lombardi, J. R. Solvatochromic Shifts: A Reconsideration. *J. Phys. Chem. A* **1998**, *102*, 2817–2823.

[64] Lombardi, J. R. Solvatochromic Shifts Reconsidered: Field-Induced Mixing in the Nonlinear Region and Application to Indole. *J. Phys. Chem. A* **1999**, *103*, 6335–6338.

[65] Kawski, A.; Bojarski, P. Comments on the determination of excited state dipole moment of molecules using the method of solvatochromism. *Spectrochim. Acta A* **2011**, *82*, 527–528.

[66] Loukova, G. V.; Milov, A. A.; Vasiliev, V. P.; Minkin, V. I. Dipole moments and solvatochromism of metal complexes: principle photophysical and theoretical approach. *Phys. Chem. Chem. Phys.* **2016**, *18*, 17822–17826.

[67] Meng S., G. C. e. a., Caprasecca S. Negative solvatochromism of push-pull biphenyl compounds: a theoretical study. *Theor Chem Acc* **2015**, *134*, 150.

[68] Patrizi, B.; Iagatti, A.; Abbondanza, L.; Bussotti, L.; Zanardi, S.; Salvalaggio, M.; Fusco, R.; Foggi, P. Ultrafast Intramolecular and Solvation Dynamics in 4,7-Bis (4,5-dibutylbenzo[1,2-b:4,3-b']bisthiophene[1,2-b:4,3-b']bisthiophen-2-yl)-2,1,3-benzothiadiazole. *The Journal of Physical Chemistry C* **2019**, *123*, 5840–5852.

[69] Abe, T.; Iweibo, I. Comparison of the Excited-state Dipole Moments and Polarizabilities Estimated from Solvent Spectral Shifts with Those from Electrooptical Measurements. *Bull. Chem. Soc. Jpn.* **1984**, *58*, 3415–3422.

[70] Lombardi, J. R. On the comparison of solvatochromic shifts with gas phase Stark effect measurements. *Spectrochim. Acta* **1987**, *43A*, 1223–1324.

[71] Wilke, J.; Wilke, M.; Meerts, W. L.; Schmitt, M. Determination of ground and excited state dipole moments via electronic Stark spectroscopy: 5-methoxyindole. *J. Chem. Phys.* **2016**, *144*, 044201–1–044201–10.

[72] Debye, P. Some Results of a Kinetic Theory of Insulators. *Phys. Z.* **1912**, *13*, 97.

[73] Baron, Vapor-Phase Dipole Moment Values from Solution Measurements. *J. Phys. Chem.* **1985**, *89*, 4873–4875.

[74] Suppan, P.; Ghoneim, N. *Solvatochromism*; Royal Society of Chemistry: Cambridge, 1997.

[75] Förster, T. Zwischenmolekulare Energiewanderung und Fluoreszenz. *Ann. Phys.* **1948**, *437*, 55–75.

[76] van Amerongen, H.; Valkunas, L.; van Grondelle, R. *Photosynthetic Excitons*; World Scientific Publishing: Singapore, 2000.

[77] Freeman, D. E.; Klemperer, W. Electric Dipole Moment of the $^1A_2$ Electronic State of Formaldehyde. *J. Chem. Phys.* **1966**, *45*, 52–57.

[78] Lombardi, J. R.; Campbell, D.; Klemperer, W. Electric Dipole Moment of the $n - \pi^*$ Singlet State of HCOF. *J. Chem. Phys.* **1967**, *46*, 3482–3486.

[79] Korter, T. M.; Borst, D. R.; Butler, C. J.; Pratt, D. W. Stark Effects in Gas-Phase Electronic Spectra. Dipole Moment of Aniline in Its Excited S1 State. *J. Am. Chem. Soc.* **2001**, *123*, 96–99.

[80] Reese, J. A.; Nguyen, T. V.; Korter, T. M.; Pratt, D. W. Charge Redistribution on Electronic Excitation. Dipole Moments of cis- and trans-3-Aminophenol in Their S_0 and S_1 Electronic States. *J. Am. Chem. Soc.* **2004**, *126*, 11387–11392.

[81] Nguyen, T.; Pratt, D. Permanent electric dipole moments of four tryptamine conformers in the gas phase: A new diagnostic of structure and dynamics. *J. Chem. Phys.* **2006**, *124*, 054317(1–6).

[82] Liptay, W. In *Excited States*; Lim, E., Ed.; Academic Press: New York, 1974; Vol. I; Chapter 4, pp 129–229.

[83] Fowler, F. W.; Katritzky, A. R.; Rutherford, R. J. D. The correlation of solvent effects on physical and chemical properties. *J. Chem. Soc. B* **1971**, 460–469.

[84] Taft, R. W.; Abboud, J.-L. M.; Kamlet, M. J.; Abraham, M. H. Linear solvation energy relations. *J. Sol. Chem.* **1985**, *14*, 153–186.

[85] Abe, T. Estimation of Angles Between Ground- and Excited-State Dipole Moments From Solvent Spectral Frequency Shifts. *Bull Chem. Soc. Jpn.* **1991**, *64*, 3224–3228.

[86] Eisenhardt, C.; Pietraperzia, G.; Becucci, M. The high resolution spectrum of the $S_0 \leftarrow S_1$ transition of anisole. *Phys. Chem. Chem. Phys.* **2001**, *3*, 1407.

[87] Ribblett, J. W.; Sinclair, W. E.; Borst, D. R.; Yi, J. T.; Pratt, D. W. High Resolution Electronic Spectra of Anisole and Anisole-Water in the Gas Phase: Hydrogen Bond Switching in the S1 State. *J. Phys. Chem. A* **2006**, *110*, 1478–1483.

[88] Pasquini, M.; Schiccheri, N.; Becucci, M.; Pietraperzia, G. High resolution electronic spectroscopy on deuterated anisole. *J. Mol. Struct.* **2009**, *924*, 457–460.

[89] Ahlrichs, R.; Bär, M.; Häser, M.; Horn, H.; Kölmel, C. Electronic Structure Calculations on Workstation Computers: The Program System TURBOMOLE. *Chem. Phys. Letters* **1989**, *162*, 165–169.

[90] T. H. Dunning, J. Gaussian basis sets for use in correlated molecular calculations. I. The atoms boron through neon and hydrogen. *J. Chem. Phys.* **1989**, *90*, 1007–1023.

[91] Hättig, C.; Weigend, F. CC2 excitation energy calculations on large molecules using the resolution of the identity approximation. *J. Chem. Phys.* **2000**, *113*, 5154–5161.

[92] Hättig, C.; Köhn, A. Transition moments and excited-state first-order properties in the coupled cluster model CC2 using the resolution-of-the-identity approximation. *J. Chem. Phys.* **2002**, *117*, 6939–6951.

[93] Hättig, C. Geometry optimizations with the coupled-cluster model CC2 using the resolution-of-the-identity approximation. *J. Chem. Phys.* **2002**, *118*, 7751–7761.

[94] Klamt, A.; Schürmann, G. COSMO: A new approach to dielectric screening in solvents with explicit expressions for the screening energy and its gradient. *J. Chem. Soc. Perkin Trans.* **1993**, *2*, 799–805.

[95] Meerts, W. L.; Schmitt, M.; Groenenboom, G. New applications of the Genetic Algorithm for the interpretation of High Resolution Spectra. *Can. J. Chem.* **2004**, *82*, 804–819.

[96] Meerts, W. L.; Schmitt, M. A new automated assign and analyzing method for high resolution rotational resolved spectra using Genetic Algorithms. *Phys. Scripta* **2005**, *73*, C47–C52.

[97] Meerts, W. L.; Schmitt, M. Application of genetic algorithms in automated assignments of high-resolution spectra. *Int. Rev. Phys. Chem.* **2006**, *25*, 353–406.

[98] Schmitt, M.; Meerts, W. L. In *Handbook of High Resolution Spectroscopy*; Quack, M., Merkt, F., Eds.; John Wiley and Sons, 2011; ISBN: 978-0-470-06653-9.

[99] Ostermeier, A.; Gawelcyk, A.; Hansen, N. In *Parallel Problem Solving from Nature, PPSN III*; Davidor, Y., Schwefel, H.-P., Männer, R., Eds.; Springer: Berlin/Heidelberg, 1994.

[100] Hansen, N.; Ostermeier, A. Completely derandomized self-adaptation in evolution strategies. *Evolutionary Computation* **2001**, *9*, 159–195.

[101] Rae, E. M. Theory of solvent effects on molecular electronic Spectra. Frequency shifts. *J. Phys. Chem.* **1957**, *61*, 562–572.

[102] Gerstenkorn, S.; Luc, P. *Atlas du spectre d'absorption de la molécule d'iode 14800–20000 cm*$^{-1}$; CNRS: Paris, 1986.

[103] Schmitt, M. Spektroskopische Untersuchungen an Wasserstoffbrückenbindungen. Habilitation, Heinrich-Heine-Universität, Math. Nat. Fakultät, Düsseldorf, 2000.

[104] Schmitt, M.; Küpper, J.; Spangenberg, D.; Westphal, A. Determination of the structures and barriers to hindered internal rotation of the phenol-methanol cluster in the S_0 and S_1 state. *Chem. Phys.* **2000**, *254*, 349–361.

[105] Farmer, D. B.; Holt, A.; Walker, S. Dielectric Studies. IX. Relaxation Processes of Anisole- and Fluorine-Substituted Anisoles. *J. Chem. Phys.* **1966**, *44*, 4116–4120.

[106] Muenter, J. S.; Laurie, V. W. Deuterium Isotope Effects on Molecular Dipole Moments by Microwave Spectroscopy. *J. Chem. Phys.* **1966**, *35*, 855–858.

[107] Omidyan, R.; Rezaei, H. Excited state deactivation pathways of neutral/protonated

anisole and p-fluoroanisole: a theoretical study. *Phys. Chem. Chem. Phys.* **2014**, *16*, 11679–11689.

[108] Murthy, S. S. N.; Gangasharan,; Nayak, S. K. Novel differential scanning calorimetric studies of supercooled organic liquids. *J. Chem. Soc., Faraday Trans.* **1993**, *89*, 509–514.

[109] Frenzel, F.; Borchert, P.; Anton, A. M.; Strehmel, V.; Kremer, F. Charge transport and glassy dynamics in polymeric ionic liquids as reflected by their inter- and intramolecular interactions. *Soft Matter* **2019**, *15*, 1605–1618.

[110] Reinganum, M. Uber Molekularkräfte und elektrische Ladungen der Moleküle. *Annalen der Physik* **1903**, *315*, 334–353.

[111] Tripathy, T.; De, B. R. Making sense about dipole moments. *Journal of Physical Sciences* **2008**, *12*, 155–172.

[112] Wilke, J.; Wilke, M.; Brand, C.; Meerts, W. L.; Schmitt, M. On the Additivity of Molecular Fragment Dipole Moments of 5-Substituted Indole Derivatives. *ChemPhysChem* **2016**, *17*, 2736–2743.

[113] Schneider, M.; Wilke, M.; Hebestreit, M.-L.; Henrichs, C.; Meerts, W.; Schmitt, M. Excited-State Dipole Moments and Transition Dipole Orientations of Rotamers of 1,2-, 1,3-, and 1,4-Dimethoxybenzene. *ChemPhysChem* **2018**, *19*, 307–318, cited By 4.

[114] Gordy, W.; Cook, R. L. *Microwave Molecular Spectra*, 3rd ed.; Wiley: New York, 1984.

[115] Henningesen, J. O. Stark effect in the CO2 laser-pumped CH3OH far-infrared laser as a technique for high-resolution infrared spectroscopy. *J. Mol. Spec.* **1980**, *83*, 70–93.

[116] Chattopadhyay, A.; Boxer, S. G. Vibrational Stark Effect Spectroscopy. *J. Am. Chem. Soc.* **1995**, *114*, 1449–1450.

[117] Brieger, M.; A. Hese, A. R.; Sodeik, A. The Dipole moment of ^{7}LiH in the electronically excited $A^{1}\Sigma^{+}$ state. *Chem. Phys. Letters* **1980**, *76*, 465–468.

[118] Brucat, P. J.; Zare, R. N. Determination of the effective electric dipole moments of selected NO_2 $^{2}B_2$ fine structure levels. *Mol. Phys.* **1985**, *55*, 277–285.

[119] Schmidt, P.; Bitto, H.; Huber, J. R. Excited state dipole moments in a polyatomic

molecule determined by Stark quantum beat spectroscopy. *J. Chem. Phys.* **1988**, *88*, 696–704.

[120] Ohta, N.; Tanaka, T. Stark quantum beats and electric dipole moment in the S_1 state of pyrimidine vapor. *J. Chem. Phys.* **1993**, *99*, 3312 – 3319.

[121] Okruss, M.; Müller, R.; Hese, A. High-resolution ultraviolet laser spectroscopy on jet-cooled benzene molecules: Ground and excited electronic state polarizabilities determined from static Stark effect measurements. *J. Chem. Phys.* **1999**, *110*, 10393–10402.

[122] Felker, P. M. Rotational coherence spectroscopy: studies of the geometries of large gas-phase species by picosecond time-domain methods. *J. Phys. Chem.* **1992**, *96*, 7844–7857.

[123] Riehn, C. High-resolution pump-probe rotational coherence spectroscopy - rotational constants and structure of ground and electronically excited states of large molecular systems. *Chem. Phys.* **2002**, *297*, 283.

[124] Frey, H.-M.; Kummli, D.; Lobsiger, S.; Leutwyler, S. *Handbook of High-resolution Spectroscopy*; John Wiley & Sons, Ltd, 2011.

[125] Kummli, D. S.; Lobsiger, S.; Frey, H.-M.; Leutwyler, S.; Stanton, J. F. Accurate Determination of the Structure of Cyclooctatetraene by Femtosecond Rotational Coherence Spectroscopy and ab Initio Calculations. *The Journal of Physical Chemistry A* **2008**, *112*, 9134–9143.

[126] Nemkovich, N. A.; Baumann, W.; Pivovarenko, V. G.; Rubinov, A. N. Determination of the dipole moments of the molecules of 4-substituted 3-Hydroxyflavones using the electrooptic absorption method. *J. Appl. Spect.* **2003**, *70*, 230–237.

[127] Nemkovich, N. A.; Baumann, W.; Kruchenok, Y. V.; Kurilo, G. I.; Pivovarenko, V. G.; Rubinov, A. N. Spectroscopy of Molecular Stark Effect of Diflavonol and Inhomogeneous Broadening of Its Electronic Spectra in Erythrocyte Membranes. *Opt. Spect.* **2011**, *110*, 541–549.

[128] Hellweg, A.; Grün, S.; Hättig, C. Benchmarking the performance of spin-component scaled cc2 in ground and electronically excited states. *Phys. Chem. Chem. Phys.* **2008**, *10*, 1159–1169.

[129] Hellweg, A. The accuracy of dipole moments from spin-component scaled CC2 in

ground and electronically excited states. *The Journal of Chemical Physics* **2011**, *134*, 064103.

[130] Deglmann, P.; Furche, F.; Ahlrichs, R. An efficient implementation of second analytical derivatives for density functional methods. *Chem. Phys. Letters* **2002**, *362*, 511–518.

[131] TURBOMOLE V7.2 2017, a development of University of Karlsruhe and Forschungszentrum Karlsruhe GmbH, 1989-2007, TURBOMOLE GmbH, since 2007; available from
http://www.turbomole.com.

[132] Platt, J. R. Classification of Spectra of Cata-Condensed Hydrocarbons. *J. Chem. Phys.* **1949**, *17*, 484–495.

[133] Lombardi, J. R. Electric Field Induced Perturbations in the Ultraviolett Spectrum of of Aniline. Vibronic Origin of the Perturbing State. *J. Chem. Phys.* **1972**, *56*, 2278–2281.

[134] Lombardi, J. R. Electric Field Induced Perturbations in the $^1B_2$ $^1 \leftarrow A_1$ Transition of Aniline. *Chem. Phys.* **1978**, *28*, 41–45.

[135] Brisker-Klaiman, D.; Dreuw, A. Explaining Level Inversion of the Laand LbStates of Indole and Indole Derivatives in Polar Solvents. *ChemPhysChem* **2015**, *16*, 1695–1702.

[136] Townes, C. H.; Schawlow, A. L. *Microwave Spectroscopy*; Dover Publications: New York, 1975.

[137] Dijkerman, H.; Ruitenberg, G. Determination of the dipole moment of OCS with a microwave absorption cavity. *Chem. Phys. Letters* **1969**, *3*, 172–174.

[138] Shulman, R. G.; Townes, C. H. Molecular Dipole Moments and Stark Effects. II. Stark Effects in OCS. *Phys. Rev.* **1950**, *77*, 500–506.

[139] Bakhshiev, N. Universal intermolecular interactions and their effect on the position of the electronic spectra of molecules in two component solutions. *Opt. Spectrosk.* **1962**, *13*, 24–29.

[140] Lombardi, J. R. Stark Effect in Electronic Spectra: The Asymmetric Rotor. *The Journal of Chemical Physics* **1968**, *48*, 348–353.

[141] Callis, P. R. *J. Chem. Phys.* **1991**, *95*, 4230.

[142] Slater, L. S.; Callis, P. R. *J. Phys. Chem.* **1995**, *99*, 8572.

[143] Callis, P. R.; Vivian, J. T.; Slater, L. S. *Chem. Phys. Letters* **1995**, *244*, 53.

[144] Serrano-Andrés, L.; Roos, B. O. Theoretical Study of the Absorption and Emission Spectra of Indole in the Gas Phase and in a Solvent. *J. Am. Chem. Soc.* **1996**, *118*, 185–195.

[145] Borin, A. C.; Serrano-Andrés, L. A theoretical study of the absorption spectra of indole and its analogs: indene, benzimidazole, and 7-azaindole. *Chem. Phys.* **2000**, *262*, 253–265.

[146] Serrano-Andrés, L.; Borin, A. C. A theoretical study of the emission spectra of indole and its analogs: indene, benzimidazole, and 7-azaindole. *Chem. Phys.* **2000**, *262*, 267–283.

[147] Sobolewski, A. L.; Domcke, W. Ab initio investigations on the photophysics of indole. *Chem. Phys. Letters* **1999**, *315*, 293–298.

[148] Nenov, A.; Rivalta, I.; Mukamel, S.; Garavelli, M. Bidimensional electronic spectroscopy on indole in gas phase and in water from first principles. *Computational and Theoretical Chemistry* **2014**, *1040-1041*, 295–303, Excited states: From isolated molecules to complex environments.

[149] Zuclich, J.; von Schütz, J. U.; Maki, A. H. PHOSPHORESCENT STATE OF INDOLE - OBSERVATIONS USING OPTICALLY DETECTED MAGNETIC-RESONANCE. *J. Am. Chem. Soc.* **1974**, *96*, 710–714.

[150] Hager, J. W.; Wallace, S. C. *J. Phys. Chem.* **1983**, *87*, 2121.

[151] Hager, J. W.; Wallace, S. C. *J. Phys. Chem.* **1984**, *88*, 5513.

[152] Philips, L. A.; Levy, D. H. The rotationally resolved electronic spectrum of indole in the gas phase. *J. Chem. Phys.* **1986**, *85*, 1327–1332.

[153] Suenram, R. D.; Lovas, F. J.; Fraser, G. T. Microwave Spectrum and ^{14}N Quadrupole Coupling Constants of Indole. *J. Mol. Spec.* **1988**, *127*, 472–480, Note that the reported C constant in this paper is misprinted. The correct value is 1150.9 MHz (private communication with G. T. Fraser).

[154] Bickel, G. A.; Demmer, D. R.; Outhouse, E. A.; Wallace, S. C. *J. Chem. Phys.* **1989**, *91*, 6013.

[155] Caminati, W.; di Bernardo, S. Microwave Spectrum and Amino Hydrogen Location in Indole. *J. Mol. Struct.* **1990**, *240*, 253–262.

[156] Sammeth, D. M.; Yan, S.; Spangler, L. H.; Callis, P. R. Two-photon fluorescence excitation spectra of indole in vapor and jet: 1La states. *J. Phys. Chem.* **1990**, *94*, 7340.

[157] Tubergen, M. J.; Levy, D. H. Spectroscopy of Indole van der Waals Complexes: Evidence for a Conformation-Dependent Excited State. *J. Phys. Chem.* **1991**, *95*, 2175.

[158] Albinsson, B.; Nordén, B. Excited-State Properties of the Indole Chromophore – Electronic-Transition Moment Directions from Linear Dichroism Measurements – Effect of Methyl and Methoxy Substituents. *J. Phys. Chem.* **1992**, *96*, 6204.

[159] Barstis, T. L. O.; Grace, L. I.; Dunn, T. M.; Lubman, D. L. *J. Phys. Chem.* **1993**, *97*, 5820.

[160] Berden, G.; Meerts, W. L.; Jalviste, E. Rotationally Resolved Ultraviolet Spectroscopy of Indole, Indazole and Benzimidazole: Inertial Axis Reorientation in the $S_1(^1L_b) \leftarrow S_0$ Transition. *J. Chem. Phys.* **1995**, *103*, 9596–9606.

[161] Helm, R. M.; Clara, M.; Grebner, T. L.; Neusser, H. J. Hydrogen bonding in the indole-water complex: A high resolution UV study of the hydrogen donor conformer. *J. Phys. Chem. A* **1998**, *102*, 3268–3272.

[162] Carney, J. R.; Hagemeister, F. C.; Zwier, T. S. The hydrogen-bonding of indole-$(water)_n$ clusters from resonant ion-dip infrared spectroscopy. *J. Chem. Phys.* **1998**, *108*, 3379–3382.

[163] Short, K. W.; Callis, P. R. Evidence of pure L-1(b) fluorescence from redshifted indolepolar solvent complexes in a supersonic jet. *J. Chem. Phys.* **1998**, *108*, 10189–10196.

[164] Fender, B. J.; Short, K. W.; Hahn, D. K.; Callis, P. R. Vibrational assignments for indole with the aid of ultrasharp phosphorescence spectra. *Int. J. Quantum Chem.* **1999**, *72*, 347–356.

[165] Jalviste, E.; Ohtab, N. Stark absorption spectroscopy of indole and 3-methylindole. *J. Chem. Phys.* **2004**, *121*, 4730–4739.

[166] Kang, C.; Korter, T. M.; Pratt, D. W. Experimental measurement of the induced dipole moment of an isolated molecule in its ground and electronically excited states: Indole and indole-H_2O. *J. Chem. Phys.* **2005**, *122*, 174301.

[167] Godfrey, T. J.; Yu, H.; Biddle, M. S.; Ullrich, S. A wavelength dependent investigation of the indole photophysics via ionization and fragmentation pump–probe spectroscopies. *Phys. Chem. Chem. Phys.* **2015**, *17*, 25197–25209.

[168] Hollas, J. M. Vapour-phase ultra-violet absorption spectra of indene, indole, coumarone and thionaphthene. *Spectrochimica Acta* **1963**, *19*, 753–767.

[169] Hartford, A.; Muirhead, A. R.; Lombardi, J. R. Hybrid Character and Rotational Structure of the Transitions of Thionaphthene and Benzofuran. *J. Mol. Spec.* **1970**, *35*, 199.

[170] Yip, W. T.; Levy, D. H. Excimer Exciplex Formation in van der Waals Dimers of Aromatic Molecules. *J. Phys. Chem.* **1996**, *100*, 11539–11545.

[171] Collier, W. B. Vibrational frequencies for polyatomic molecules I. Indole and 2,3-benzofuran spectra and analysis. *J. Chem. Phys.* **1988**, *88*, 7295–7306.

[172] Klots, T. D.; Collier, W. B. Heteroatom derivatives of indene Part 3. Vibrational spectra of benzoxazole, benzofuran, and indole. *Spectrochim Acta A* **1995**, *51*, 1291–1316.

[173] Smithson, T. L.; Shaw, R. A.; Wieser, H. The vapor phase far-infrared spectra of 1 H-indene, benzo[b]furan, 1, 3, 2- benzodioxaborole, and indole: Evidence for planar skeletons and kinetic anharmonicity in the out-of-plane ring deformations. *J. Chem. Phys.* **1984**, *81*, 4281–4287.

[174] Palmer, M. H.; Kennedy, S. M. F. The Electronic Structure of Aromatic Molecules. Non-empirical Calculations on Indole, Benzofuran, Benzothiophen, and Related Hydrocarbons. *J. Chem. Soc. Perkin. Trans.* **1974**, *2*, 1893–1903.

[175] TURBOMOLE V7.3 2019, a development of University of Karlsruhe and Forschungszentrum Karlsruhe GmbH, 1989-2007, TURBOMOLE GmbH, since 2007; available from
`http://www.turbomole.com`.

[176] Eckart, C. *Phys. Rev.* **1935**, *47*, 552.

[177] Strauss, H. L.; Pickett, H. M. Conformational structure, energy, and inversion rates of cyclohexane and some related oxanes. *Journal of the American Chemical Society* **1970**, *92*, 7281–7290.

[178] Winter, N. O. C.; Graf, N. K.; Leutwyler, S.; Hättig, C. Benchmarks for 0–0 transitions of aromatic organic molecules: DFT/B3LYP, ADC(2), CC2, SOS-CC2 and SCS-

CC2 compared to high-resolution gas-phase data. *Phys. Chem. Chem. Phys.* **2013**, *15*, 6623–6630.

[179] Exner, O. *Dipole Moments in Organic Chemistry*; Georg Thieme Publishers: Stuttgart, 1975.

[180] Bader, R. F. Atoms in molecules. *Acc. Chem. Res.* **1985**, *18*, 9–15.

[181] Borst, D. R.; Korter, T. M.; Pratt, D. W. On the additivity of bond dipole moments. Stark effect studies of the rotationally resolved electronic spectra of aniline, benzonitrile and aminibenzonitrile. *Chem. Phys. Letters* **2001**, *350*, 485–490.

[182] Lee, H.; Choi, J.-H.; Cho, M. Vibrational solvatochromism and electrochromism of cyanide, thiocyanate, and azide anions in water. *Phys. Chem. Chem. Phys.* **2010**, *12*, 12658–12669.

[183] Gers, C. F.; Nordmann, J.; Kumru, C.; Frank, W.; Müller, T. J. J. Solvatochromic Fluorescent 2-Substituted 3-Ethynyl Quinoxalines: Four-Component Synthesis, Photophysical Properties, and Electronic Structure. *J. Org. Chem.* **2014**, *79*, 3296–3310.

[184] TURBOMOLE V6.3 2012, a development of University of Karlsruhe and Forschungszentrum Karlsruhe GmbH, 1989-2007, TURBOMOLE GmbH, since 2007; available from
http://www.turbomole.com.

[185] Weber, G. Fluorescence-Polarization Spectrum and Electronic-Energy Transfer in Tyrosine, Tryptophan and Related Compounds. *Biochem. J.* **1960**, *75*, 335–345.

[186] Oeltermann, O.; Brand, C.; Wilke, M.; Schmitt, M. Ground and Electronically Excited Singlet State Structures of the syn and anti Rotamers of 5-Hydroxyindole. *J. Phys. Chem. A* **2012**, *116*, 7873–7879.

[187] Brand, C.; Oeltermann, O.; Wilke, M.; Tatchen, J.; Schmitt, M. Ground and electronically excited singlet state structures of 5-fluoroindole, deduced from rotationally resolved electronic spectroscopy and *ab initio* theory. *ChemPhysChem* **2012**, *13*, 3134–3138.

[188] Brand, C.; Oeltermann, O.; Wilke, M.; Schmitt, M. Position Matters: High Resolution Spectroscopy on 6-Methoxyindole. *J. Chem. Phys.* **2013**, *138*, 024321.

[189] Hougen, J. T.; Watson, J. K. G. Anomalous Rotational Line Intensities in Electronic

Transitions of Polyatomic Molecules: Axis-Switching. *Can. J. Phys.* **1965**, *43*, 298–320.

[190] Linder, B.; Hoernschemeyer, D. Cavity Concept in Dielectric Theory. *J. Chem. Phys.* **1967**, *46*, 784–790.

List of Figures

List of Tables

Supplementary material

This chapter contains material, which was published as online supporting information with the articles.

1. Supporting information for chapter 9

Supplementary data associated with this article can be found
in the online version at https://doi.org/10.1016/j.dib.2018.09.110.

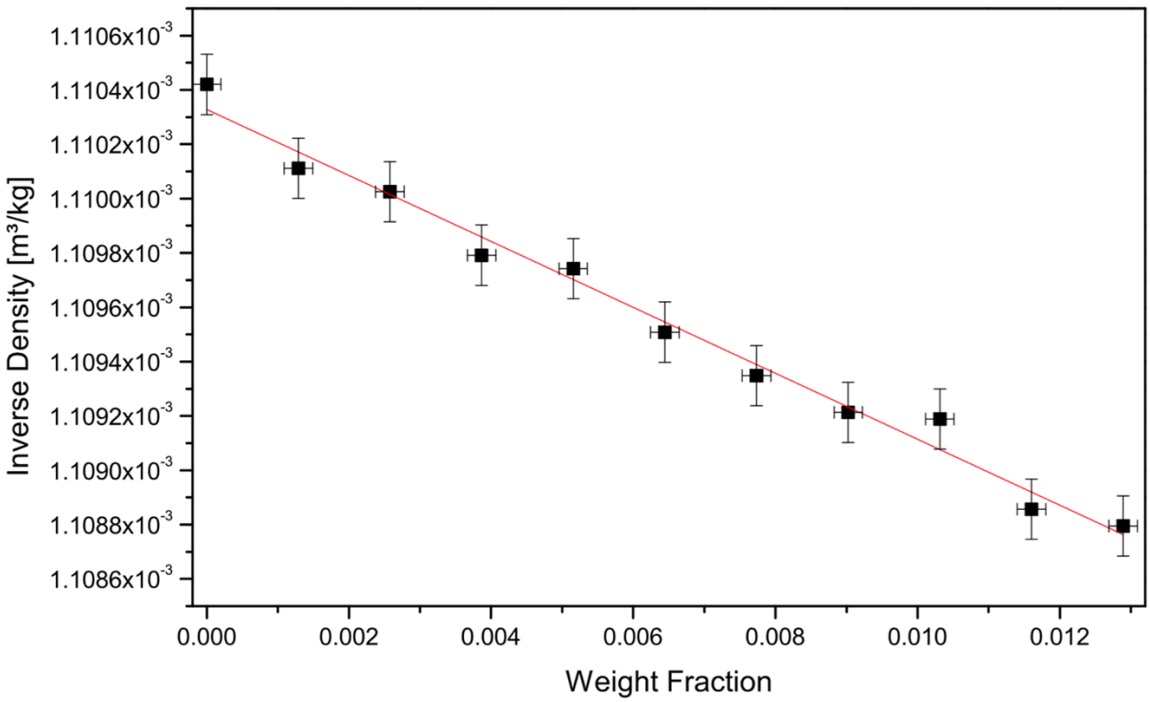

Figure S1.: Plot of the inverse density of the solution of anisole in ethyl acetate versus the weight fraction of anisole at 293 K along with the linear fit of the data.

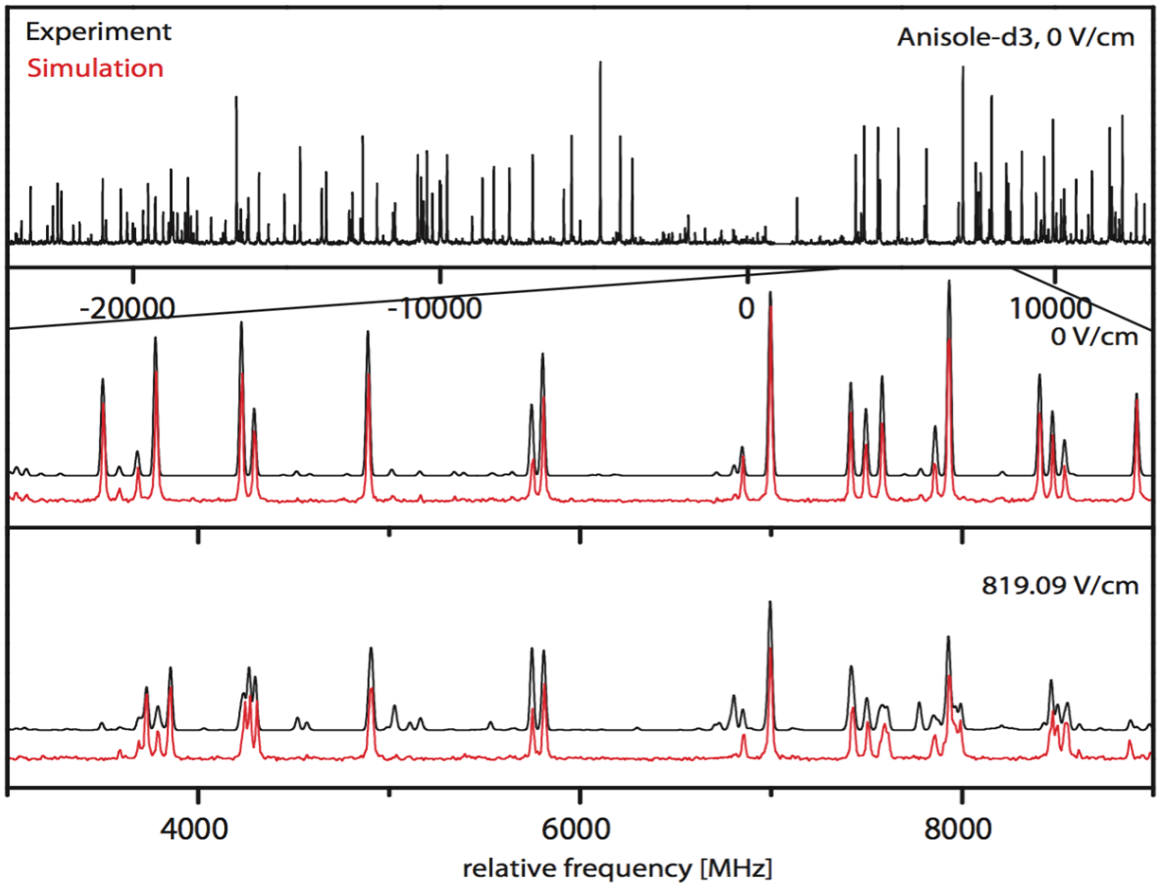

Figure S2.: Rotationally resolved electronic Stark spectrum had been obtained before of d3-anisole at $36\,387.31\,\mathrm{cm}^{-1}$. The field free spectrum had been obtained before by Pasquini et al. [88].

Table S1.: Measured density of the solution of anisole in ethyl acetate versus the weight fraction between 0 and 0.013 of the solute between $258\,\mathrm{K}$ and $348\,\mathrm{K}$. The densities are given as $\mathrm{kg\,m^{-3}}$.

Content available at: http://dx.doi.org/10.25838/d5p-23 or https://researchdata.hhu.de/handle/entry/94

Table S2.: Absorption spectra (in wavenumber) of anisole in ethyl acetate between $258\,\mathrm{K}$ and $348\,\mathrm{K}$ in steps of $5\,\mathrm{K}$.

Content available at: http://dx.doi.org/10.25838/d5p-24 or https://researchdata.hhu.de/handle/entry/95

Table S3.: Emission spectra (in wavenumber) of anisole in ethyl acetate between $258\,\mathrm{K}$ and $348\,\mathrm{K}$ in steps of $5\,\mathrm{K}$.

Content available at: http://dx.doi.org/10.25838/d5p-25 or https://researchdata.hhu.de/handle/entry/96

Table S4.: Linearized laser induced fluroescence Stark spectrum of anisole at an electric field strength of $819.09\,\mathrm{V\,cm^{-1}}$. The first column gives the relative frequeny in $1\,\mathrm{MHz}$ increment, the second column the relative intensities.

Content available at: http://dx.doi.org/10.25838/d5p-26 or https://researchdata.hhu.de/handle/entry/97

Table S5.: Cartesian coordinates of anisole S_0 in Bohr units from the CC2/cc-pVTZ calculations using the Turbomole program package [89–93].

C	0.29514957	0.00251005	0.09552629
C	0.36325862	0.00279133	2.71969272
C	2.68805953	0.00175078	3.98506250
C	4.94040276	0.00032928	2.60276573
C	4.83942652	-0.00012598	-0.03836629
C	2.53570432	0.00098059	-1.30547147
O	2.55346006	0.00236519	6.56185082
H	4.90204262	0.00169625	7.86565457
H	-1.35088692	0.00375032	3.83282143
H	6.75429875	-0.00026448	3.53610674
H	6.58995725	-0.00133602	-1.09559467
H	2.47933655	0.00050984	-3.34751819
H	4.43356120	0.00226577	9.86196638
H	6.00524213	-1.68222636	7.41458968
H	6.00654007	1.68459697	7.41394908
H	-1.51284126	0.00335154	-0.85942358

Table S6.: Cartesian coordinates of anisole S_1 in Bohr units from the CC2/cc-pVTZ calculations using the Turbomole program package [89–93].

C	0.20805155	0.00235130	0.05644450
C	0.29346900	0.00279969	2.76223243
C	2.69816034	0.00182905	3.96742708
C	5.04323249	0.00030120	2.61427622
C	4.91727699	-0.00013485	-0.08356094
C	2.51814961	0.00094956	-1.30692729
O	2.57899068	0.00253942	6.51833936
C	4.91378926	0.00168473	7.89861695
H	-1.38115088	0.00386696	3.92743255
H	6.83592273	-0.00036947	3.57985896
H	6.62977115	-0.00119659	-1.19338397
H	2.46278741	0.00068919	-3.35167403
H	4.37382036	0.00240575	9.87495599
H	6.00247092	-1.68671623	7.45610529
H	6.00414126	1.68880893	7.45534136
H	-1.57617111	0.00313640	-0.93187272

2. Supporting information for chapter 12

Table S7.: SCS-CC2/cc-pVTZ calculated optimized S_0 cartesian coordinates of 1-methylindole (in bohr).

1	c	-5.40477826679479	0.55143802184467	0.29255105238947
2	c	-5.34435046180607	3.21949407947868	0.26114713372917
3	c	-3.06891593692146	4.53137515958348	0.28803584074052
4	c	-0.84233313121419	3.09743079794065	0.34752628172751
5	n	1.63853859756549	3.88785702929054	0.38471290457824
6	c	3.17781344378156	1.77751553842162	0.43925831761388
7	c	1.73282166852620	-0.38391351381939	0.43836897585480
8	c	-0.85676479182853	0.41112804388966	0.37995424631428
9	c	-3.19252851006684	-0.85941668213731	0.35144578134369
10	h	-7.21347709120135	-0.40327405277303	0.27009464002006
11	h	-7.10354254749112	4.26209378476606	0.21525286306177
12	h	-3.03097987517697	6.57681865180210	0.26375780865801
13	h	5.20325632990741	2.00233320127860	0.47463967039074
14	h	2.44248967806868	-2.29183459078242	0.47501751620100
15	h	-3.26384805529746	-2.90474716085273	0.37501931049866
16	c	2.46448779577372	6.49720539424156	0.36764659161649
17	h	1.74463117265022	7.49922314812075	2.01903305587412
18	h	4.51873742460522	6.53908061165066	0.40800044175703
19	h	1.81133048645669	7.45640566648464	-1.33608629311977

Table S8.: SCS-CC2/cc-pVTZ calculated optimized S_1 cartesian coordinates of 1-methylindole (in bohr).

1	c	-5.42189388961080	0.57605033253065	0.29393332794056
2	c	-5.40350235788584	3.26518881916225	0.26271831474245
3	c	-3.05640026387274	4.61334804057749	0.29015241365269
4	c	-0.84364532195645	3.13123934100954	0.34908427155257
5	n	1.62029483388590	3.87682897076673	0.38619640645600
6	c	3.25871862556937	1.74163060481865	0.43827801315102
7	c	1.76975239575037	-0.40079512525586	0.43628288867103
8	c	-0.82540187231387	0.37274280494854	0.38105073571627
9	c	-3.16162633777963	-0.92044437675082	0.35285132584416
10	h	-7.22602248262410	-0.38950845920268	0.27202490087921
11	h	-7.17366457314548	4.28165285195563	0.21780369877020
12	h	-2.99194186064319	6.65505206509769	0.26597644955178
13	h	5.27426256561893	2.00771983910387	0.47284630706438
14	h	2.45826806138663	-2.31842120306728	0.47077147988118
15	h	-3.26601901018558	-2.96066189147036	0.37418158863917
16	c	2.44202822836210	6.48691939059480	0.36617598710629
17	h	1.67900667037501	7.48113821219550	2.00373464247841
18	h	4.49427817390976	6.54218878234212	0.43101447109670
19	h	1.78609634469600	7.42434412907233	-1.34970108394439

Table S9.: SCS-CC2/cc-pVTZ calculated optimized S_2 cartesian coordinates of 1-methylindole (in bohr).

1	c	-5.40481017881080	0.55146973511015	0.29339855346387
2	c	-5.34439784972876	3.21953506522780	0.26310561856296
3	c	-3.06897800085831	4.53141989236399	0.29017544761054
4	c	-0.84236353203005	3.09748963041725	0.34886253294695
5	n	1.63851912093689	3.88787065519937	0.38655652283116
6	c	3.17780893289050	1.77748559760339	0.43860357994878
7	c	1.73281722958428	-0.38393240922719	0.43669106218320
8	c	-0.85678836310148	0.41116943681233	0.37958801759006
9	c	-3.19254090228958	-0.85937697880110	0.35109480013533
10	h	-7.21350499926378	-0.40324209978012	0.27094844538993
11	h	-7.10361833248510	4.26211447584647	0.21782777211768
12	h	-3.03108316787463	6.57686996081286	0.26646496258716
13	h	5.20326110937413	2.00226029088255	0.47374842692100
14	h	2.44251441501324	-2.29186026210040	0.47240741471542
15	h	-3.26383641785980	-2.90472123408990	0.37364494456862
16	c	2.46458922815824	6.49716547132920	0.36629628478009
17	h	1.73370727146611	7.50382173669826	2.00993173155928
18	h	4.51851230999513	6.53918630498716	0.42056621877207
19	h	1.82278005642023	7.45148785913670	-1.34453619743441

3. Supporting information for chapter 14

The Electronic Supporting Information contains:

- The modification path for equations 14.6, 14.7, 14.9, 14.10 and 7.7 of the main paper.
- The Cartesian coordinates of the CC2/cc-pVTZ optimized structure of **1a**.
- The full absorption spectrum of 2-[(4-Methoxyphenyl)ethynyl]-3-(1-methyl-1*H*-indol-3-yl)-quinoxaline in ethyl acetate.
- Wavenumber of the absorption maxima versus solvent polarity function of Bilot-Kawski.
- Wavenumber of the emission maxima versus solvent polarity function of Bilot-Kawski.
- Difference of the wavenumber at the maxima positions versus solvent polarity function of Lippert-Mataga.

Modification of the equations

Equations 14.6 and 14.7 of the main paper were modified from the original sources [1, 2] both by introducing the temperature dependence of the absorption and emission wavnumbers, the refractive index and permittivity as well as substituting the Onsager radius with the real cavity volume, which also moves the volume inside of the solvent polarity function. Original

and modified equations are given in equations S1 and S2, respectively. In the same manner, equations 14.9 and 14.10 of the main paper were modified starting from the source [6], the original and modified equations are shown in equations S3 and S4.

$$\begin{aligned} \tilde{\nu}_A - \tilde{\nu}_F &= -\frac{2\left(\mu_e - \mu_g\right)^2}{4\pi\varepsilon_0 hca^3} \cdot F_{LM} + const. \\ F_{LM} &= \frac{\varepsilon - 1}{2\varepsilon + 1} - \frac{n^2 - 1}{2n^2 + 1} \end{aligned} \tag{S1}$$

$$\begin{aligned} \tilde{\nu}_A(T) - \tilde{\nu}_F(T) &= -\frac{2\left(\mu_e - \mu_g\right)^2}{3\varepsilon_0 hc} \cdot F_{LM}(T) + const. \\ F_{LM}(T) &= \frac{1}{V(T)} \cdot \left[\frac{\varepsilon(T) - 1}{2\varepsilon(T) + 1} - \frac{n(T)^2 - 1}{2n(T)^2 + 1}\right] \end{aligned} \tag{S2}$$

$$\begin{aligned} \tilde{\nu}_A + \tilde{\nu}_F &= -\frac{2\left(\mu_e^2 - \mu_g^2\right)}{4\pi\varepsilon_0 hca^3} \cdot F_{BK} + const. \\ F_{BK} &= \frac{2n^2 + 1}{n^2 + 2} \cdot \left(\frac{\varepsilon - 1}{\varepsilon + 1} - \frac{n^2 - 1}{n^2 + 2}\right) + \frac{3\left(n^4 - 1\right)}{\left(n^2 + 2\right)^2} \end{aligned} \tag{S3}$$

$$\begin{aligned} \tilde{\nu}_A(T) + \tilde{\nu}_F(T) &= -\frac{2\left(\mu_e^2 - \mu_g^2\right)}{3\varepsilon_0 hc} \cdot F_{BK}(T) + const. \\ F_{BK}(T) &= \frac{1}{V(T)} \cdot \left[\frac{2n(T)^2 + 1}{n(T)^2 + 2} \cdot \left(\frac{\varepsilon(T) - 1}{\varepsilon(T) + 1} - \frac{n(T)^2 - 1}{n(T)^2 + 2}\right) + \frac{3\left(n(T)^4 - 1\right)}{\left(n(T)^2 + 2\right)^2}\right] \end{aligned} \tag{S4}$$

Equation 7.7 was modified from the original source [7] by including the dependence on the temperature and the restriction to the Bilot-Kawski solvent polarity function. Original and modified equations are given in equations S5 and S6.

$$\tilde{\nu}_{A/E} = \tilde{\nu}^0_{A/E} - \frac{2\mu_{g/e}\left(\mu_e - \mu_g\right)}{3\varepsilon_0 hc} \cdot F_i \tag{S5}$$

$$\tilde{\nu}_{A/E}(T) = \tilde{\nu}^{0}_{A/E}(T) - \frac{2\mu_{g/e}\,(\mu_e - \mu_g)}{3\varepsilon_0 hc} \cdot F_{BK}(T) \tag{S6}$$

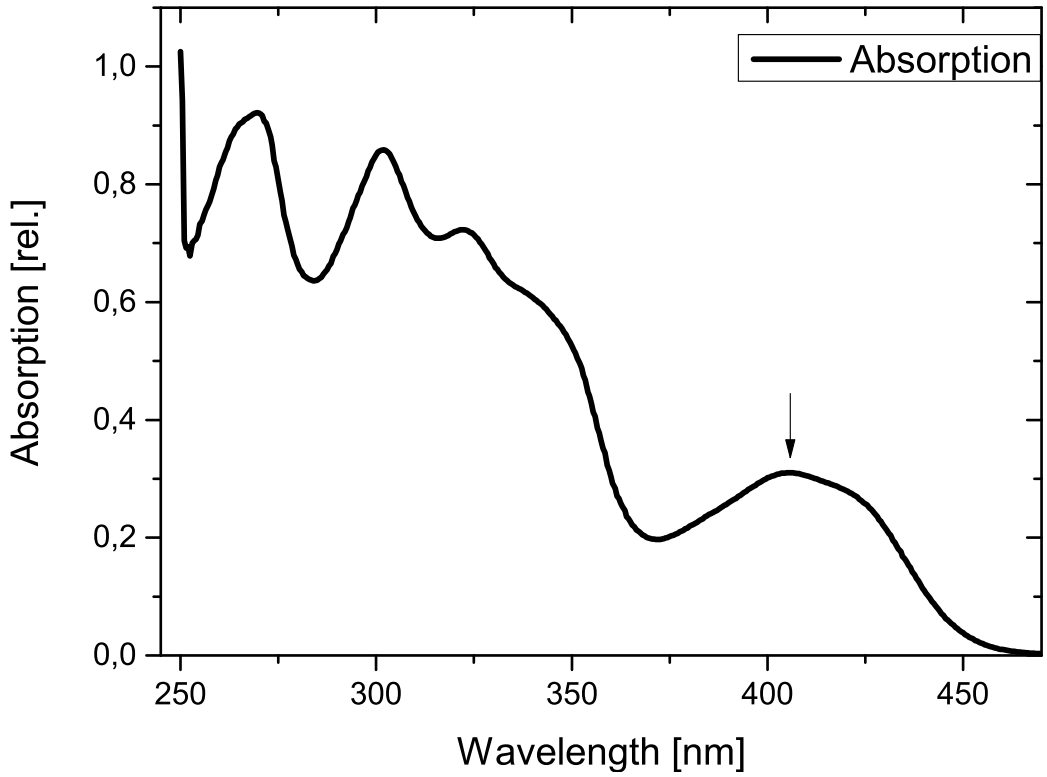

Figure S3.: Full absorption spectrum of **1a**, dissolved in EA. The arrow shows the excitation wavelength for the emission spectrum.

Table S10.: Cartesian coordinates of the S_0-state CC2/cc-pVTZ optimized structure of **1a** in Bohr units.

	X	Y	Z
C	-0.80162523864196	-2.75188063660328	-1.05521808623810
C	1.54253700070270	-2.63772727202942	-0.97954110920860
C	4.23935804931105	-2.33848460788244	-0.86085411414848
C	5.28711963084482	-0.04317128520621	0.07102977744104
C	7.90553354155227	0.26999632035820	0.19905375383801
C	9.55151901871380	-1.68647400276322	-0.59456378296859
O	12.07544056614145	-1.16001247413695	-0.38038028760854
C	13.78352105281251	-3.09772103928477	-1.16996442520508
C	8.53298440500645	-3.97142287951589	-1.52302498145537
C	5.89256526217923	-4.28020669823459	-1.64905391959141
C	-3.52031569856863	-2.70382009327084	-0.96326709262439
N	-4.78061237934411	-4.68223339976533	-1.91892394128325
C	-7.35873172931868	-4.64210128288848	-1.58920193355569
C	-8.82298713532459	-6.68373074927792	-2.57898350483024
C	-11.42286312352811	-6.73747064354684	-2.19962449703165
C	-12.64777498633866	-4.76441442862374	-0.81739768036684
C	-11.25906254144073	-2.75596876714181	0.15587139513968
C	-8.58886882686238	-2.65295724601793	-0.22417070630052
N	-7.27382608611786	-0.60131760207052	0.69122226254138
C	-4.77888372822308	-0.58749173854777	0.27412599726034
C	-3.32884921348421	1.58336844710056	1.24812710175815
C	-3.69482936937319	2.62908252173944	3.63821106776812
N	-2.05163506172542	4.62358148834777	4.02009950510677
C	-0.60344134799149	4.94327426203948	1.85199733244307
C	1.29270855012705	6.75310096162631	1.33805586234498
C	2.38933380757454	6.70911025872659	-1.07375381269006
C	1.59970793952165	4.92545179566161	-2.92605809656191
C	-0.26341835862771	3.12126012164378	-2.39646719150126
C	-1.36648736443009	3.07750191010997	0.04834584264962
C	-1.81141836146904	6.11562047147766	6.32010317926393
H	4.02419152209286	1.48212324125032	0.67355584029368
H	8.73977167330676	2.02759954240038	0.90661331305345
H	15.68807080933793	-2.32697804236133	-0.85735966450820
H	13.53793691989665	-3.55061411712744	-3.19551942004362
H	13.53981568515437	-4.83653129803295	-0.03615143792241
H	9.75049573715093	-5.51826232242065	-2.15114569806554
H	5.10370153571694	-6.05435670491417	-2.37042397262639
H	-7.82788190131638	-8.17532706841898	-3.61478784626140
H	-12.54681549206295	-8.30456507492320	-2.95737362921411
H	-14.69885734464125	-4.83802024629464	-0.53193470521538
H	-12.14820181333699	-1.20926818555070	1.20748112367775
H	-5.01785092164754	2.04665649705689	5.11105337722809
H	1.87299308392636	8.15274754453265	2.75136630928541
H	3.86470303543885	8.08529112809593	-1.54648141798949
H	2.47409149699736	4.96497679806266	-4.80397174247384
H	-0.85187420502836	1.76440383078798	-3.84432962022157
H	0.08393630221856	5.87644478436285	7.16076632118820
H	-3.24479532271644	5.47146004765354	7.68330703875040
H	-2.12557029014725	8.13762821135321	5.91254895498131

Table S11.: Cartesian coordinates of the S_1-state SCS-CC2/cc-pVTZ optimized structure of **1a** in Bohr units.

	X	Y	Z
C	-0.53293268370040	-2.54866357439544	-0.97795113654319
C	1.82863480633287	-2.64816076168838	-0.99825371670604
C	4.52809105400491	-2.57862235318765	-0.96833590182704
C	5.82955790809145	-0.59961186303959	0.31814294871050
C	8.46801630535701	-0.50952362522265	0.33213272165782
C	9.90166704322855	-2.38713261639604	-0.92735284817403
o	12.47084073278010	-2.10176241871146	-0.78098136060925
C	13.96363788532727	-3.98257954923449	-2.01727270420418
C	8.64164635909921	-4.36398053009247	-2.20477593762198
C	5.98392559844579	-4.44576159044554	-2.22058077918929
C	-3.21217333800658	-2.46647780374029	-0.96648612063650
N	-4.46290690527652	-4.55082137241666	-2.02724007126095
C	-6.99408840787469	-4.61975961212226	-1.50311415768101
C	-8.45802300738875	-6.63952274871563	-2.51627620482303
C	-11.04206598086688	-6.87178416178520	-1.96198672524812
C	-12.28119606094179	-5.08246312484979	-0.37504622473832
C	-10.91434001545822	-3.04429577126120	0.62059372679085
C	-8.28890770051359	-2.73933186123196	0.09059301354296
N	-7.06094723053949	-0.66817940625450	1.03861599857897
C	-4.52902270806711	-0.51230846764352	0.37182266575252
C	-3.39692330499830	1.82792168423240	1.20633225139224
C	-4.49209991383472	3.18620228316691	3.26049500355226
N	-3.13217336035379	5.29921702856302	3.76578734020054
C	-1.12752641219163	5.48361284350285	2.02356300068494
C	0.67252938372098	7.41648674454341	1.78859006291117
C	2.39129679621093	7.21544106438569	-0.23446705591941
C	2.25511971787084	5.17354473789888	-1.95900699775362
C	0.44772650623258	3.24282071767344	-1.68952574122002
C	-1.24483886253318	3.34267480915082	0.38078683378627
C	-3.64501315121917	7.12856819234831	5.76905713960041
H	4.73496061246810	0.85563085000302	1.30408405598818
H	9.48470037480529	1.00133052160536	1.31781344997738
H	15.94129210969161	-3.43709859694531	-1.68402474754226
H	13.58845382029694	-4.02361329045998	-4.07312673000445
H	13.61781214628028	-5.88007542763660	-1.21204185949646
H	9.68929784650814	-5.84614512531985	-3.19336183711878
H	5.01292334033147	-5.98008371576334	-3.21732964153052
H	-7.47754862434647	-8.01484539643629	-3.71610957728641
H	-12.11855615386745	-8.45371822119272	-2.76125871691196
H	-14.29749232050325	-5.29586304379255	0.05220681169793
H	-11.81291299359920	-1.61569427955722	1.82442258778776
H	-6.15949707066878	2.65408794274467	4.35015132328630
H	0.73276220859309	9.02643021803486	3.08961659119467
H	3.83448064943801	8.67932306991300	-0.49037668197413
H	3.58585042634175	5.09428674369972	-3.54389815224688
H	0.35405478685085	1.69654089798406	-3.05399731572180
H	-2.02233221716297	7.22813713169321	7.07376137913563
H	-5.33677859775483	6.51265903041531	6.80835772904264
H	-3.98442261262213	9.01111407551550	4.94025934701914

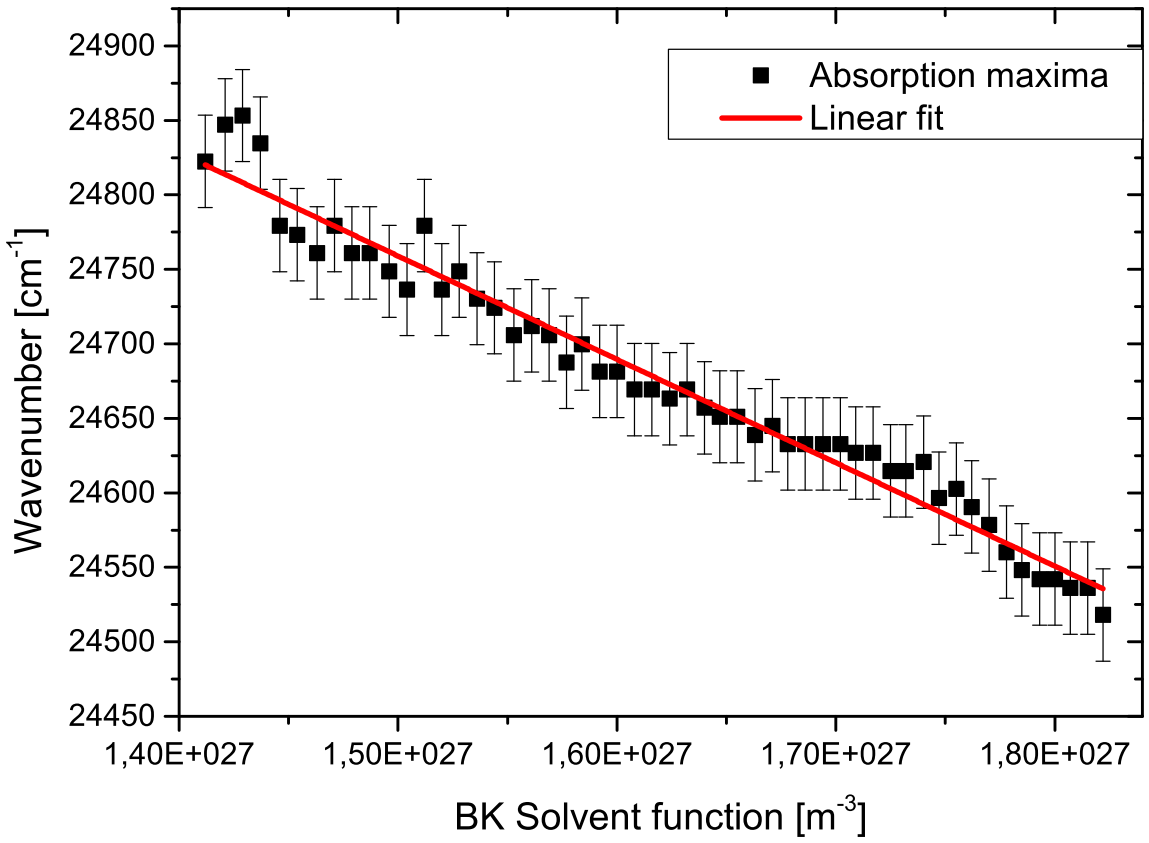

Figure S4.: Wavenumber of the absorption maxima versus solvent polarity function of Bilot-Kawski

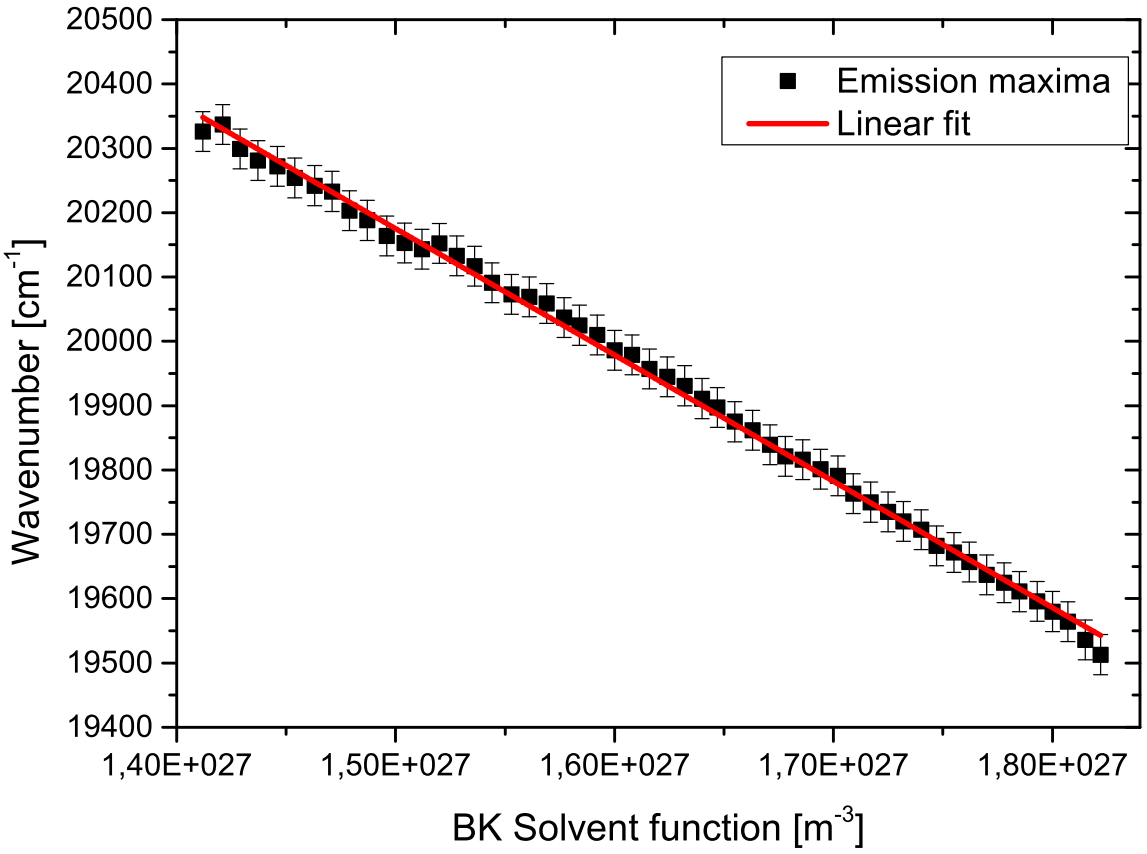

Figure S5.: Wavenumber of the emission maxima versus solvent polarity function of Bilot-Kawski

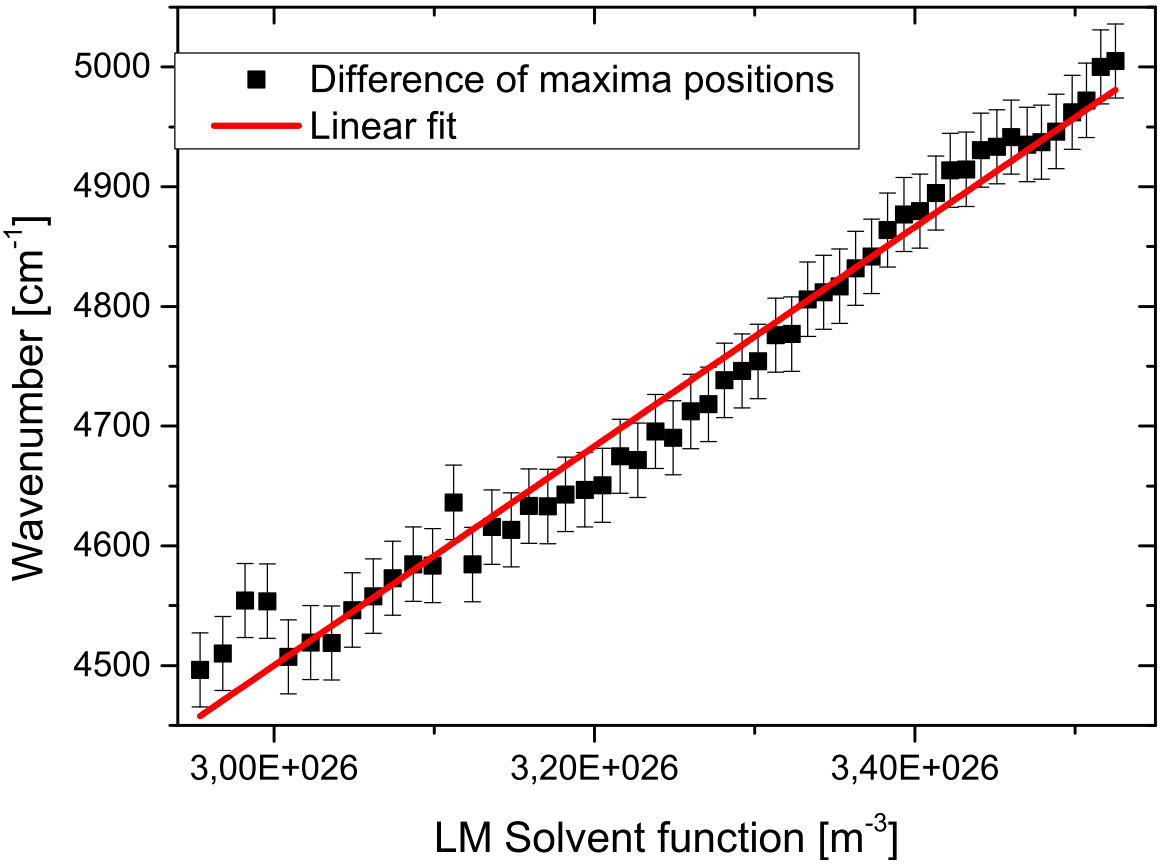

Figure S6.: Difference of the wavenumber at the maxima positions versus solvent polarity function of Lippert-Mataga